



Norwegian University
of Life Sciences

Master's Thesis 2016 30stp
Department of Mathematical Sciences and Technology

Soil-structure interaction modelling for an offshore wind turbine with monopile foundation

Steffen Aasen
Environmental physics and renewable energy

Preface

This thesis constitutes the final work of my master thesis written at NMBU, at the department of mathematical sciences and technology. The work has been done during the spring semester of 2016.

The thesis investigates soil-structure interaction models for offshore wind turbines, with monopile foundation design. It has been contributing to the research project REDWIN, administrated by NGI (Norwegian Geotechnical Institute). Information about the REDWIN project will be given in the introduction chapter for this thesis.

The reader is assumed to be familiar with structural engineering, and especially the finite element method formulation. Analysis within the frequency domain, by use of the fast fourier transform, is also assumed to be familiar to the reader.

Special thanks is given to my main supervisor at NMBU, Tor Anders Nygaard, who has provided helpful and relevant supervision throughout the process of writing this thesis. By opening his network, this thesis has gotten valuable input also from other researchers. I would also like to thank Marit Irene Kvittum at NMBU for giving helpful supervision, and for providing python-scripts that has been used in this thesis.

Special thanks is also given to researchers at NGI, especially Ph.D. candidate Ana Page, who has given valuable help on the geotechnical aspects of the thesis. By taking part in discussing results throughout the project, and giving helpful advice, her contribution has been of high significance. Appreciated feedback and advice has also been given by Kristoffer Skjolden Skau and Jörgen Johansson.

I am also grateful to my co-student Eirik Langeland Knudsen for providing helpful input and discussions throughout the process of this work.

Oslo, May 12, 2016

Steffen Aasen

Abstract

The last decade, there has been an increased use of offshore sites for harvesting wind energy. With a more complex environment than onshore, leading to higher energy prices, cost reductions becomes important for the industry.

With this in mind, the REDWIN research project has been initiated, supported by the Norwegian Research Council ENERGIX program. The goal of the program is to reduce cost in offshore wind by integrated structural and geotechnical design. This thesis contributes to this project by investigating the influence on fatigue damage and maximum moments on an OWT, for different soil-structure interaction models. The models has been applied on the NREL 5MW monopile wind turbine.

To investigate the effect of soil damping, three different soil-structure interaction models has been investigated. The reference model has a stiffness matrix at the mudline, according to that developed by Passon (2006) for the Offshore Code Comparison Collaboration 3 (Jonkman and Musial, 2010). The second model uses the same stiffness matrix, with a rotational dashpot damper, to account for soil damping. The third model has been developed by NGI (Norwegian Geotechnical Institute) for the REDWIND project, and is a kinematic hardening soil model.

The accumulated fatigue damage on the OWT structure is reduced by 11% at the mudline, when applying a rotational dashpot damper to account for soil damping. At the tower root, the reduction of fatigue damage is 16%. With the kinematic hardening model, the reduction of fatigue damage is 3% at the mudline, and 7% at the tower root. Both models are seen relative to the reference model, with no soil damping. The results show that damping has a significant effect on fatigue damage for a bottom fixed offshore wind turbine. The difference between the models, are due to different damping characteristics, and implies that a dashpot damper tend to over-estimate soil damping.

Nomenclature

| | |
|--------------|---|
| $\{\Phi\}$ | Modal vector |
| θ_p | Plastic angular displacement (Model C) |
| ν_s | Poisson ratio of the soil |
| σ_i^* | Slipping stress for kinematic hardening model |
| C | Damping matrix |
| c | Damping coefficient |
| d | Diameter of pile |
| D | Damping factor |
| D' | Accumulated fatigue damage |
| E | Elastic modulus |
| E_h | Hysteretic loss per load cycle |
| E_p' | Maximum potential energy for hysteretic loop |
| f^* | Yield surface function (Model C) |
| f | Load frequency |
| g | Plastic potential function (Model C) |
| G^* | Equivalent soil shear modulus |
| G_s | Soil shear modulus |
| H | Horizontal force |
| I | Area moment of inertia |
| K | Stiffness matrix |
| k | Stiffness coefficient |
| m | Rate of change of soil shear modulus |
| M | Mass matrix |

| | |
|-----------|--|
| m' | Negative slope of S-N curve |
| N | Number of cycles before failure |
| p | Short for 'per revolution' of rotor |
| P_x | Axial load on pile |
| R | Radius of foundation footing (Model C) |
| U | Wind speed |
| u | Displacement along inertial x-axis |
| u_p | Plastic displacement along x-axis (Model C) |
| U_w | Velocity of water |
| V | Vertical force |
| V_{0m} | Peak value of force along x-axis (Model C) |
| W | Distributed load along pile |
| w | Displacement along inertial z-axis |
| w_p | Plastic displacement along z-axis (Model C) |
| w_{pm} | Peak value of vertical plastic deformation (Model C) |
| ζ | Wind shear exponent |
| γ' | Effective unit weight of soil |
| θ | Rotation about y-axis in inertial axis system |
| ω | Angular frequency |
| ϕ | Angle of friction of soil |

List of acronyms and abbreviations

| | |
|------|--|
| DNV | Det Norske Veritas |
| EWEA | European Wind Energy Association |
| IEA | International Energy Agency |
| IFE | Institute for Energy Technology |
| NGI | Norwegian Geotechnical Institute |
| NMBU | Norwegian University of Life Sciences |
| NREL | National Renewable Energy Laboratory |
| NTNU | Norwegian University of Science and Technology |
| OC3 | Offshore Code Comparison Collaboration 3 |
| OWT | Offshore Wind Turbine |
| SWL | Still water line |
| ULS | Ultimate limit state |

Inertial axis system in thesis

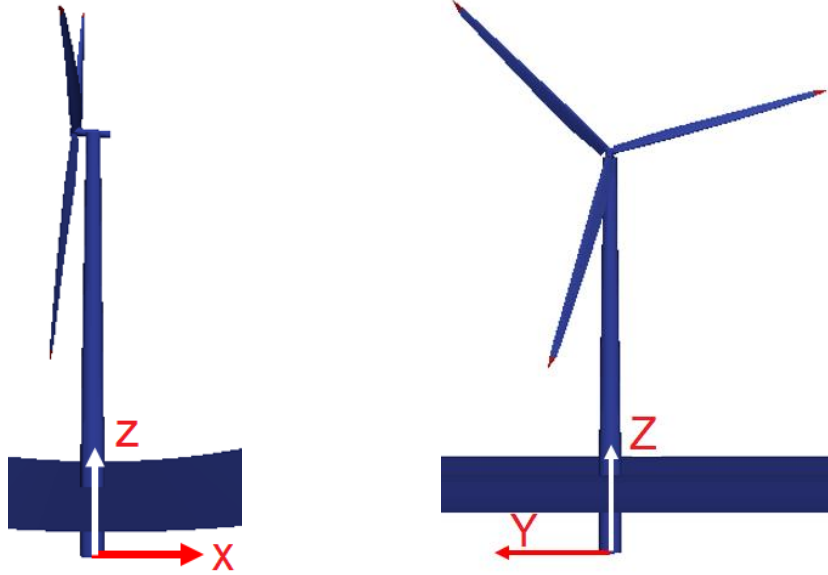


Table of Contents

| | | |
|----------|---|----|
| 1 | Introduction | 1 |
| 1.1 | Background | 1 |
| 1.2 | Previous research | 3 |
| 1.3 | Foundation design in shallow waters | 2 |
| 1.4 | Project description and goals | 4 |
| 1.5 | Structure of thesis | 5 |
| 2 | Loads in the offshore environment | 7 |
| 2.1 | Aerodynamic loads | 7 |
| 2.2 | Hydrodynamic loads | 9 |
| 3 | Soil-structure interaction models | 11 |
| 3.1 | Linear foundation models | 11 |
| 3.1.1 | Stiffness matrix by effective fixity length | 12 |
| 3.1.2 | Stiffness matrix by uncoupled springs | 12 |
| 3.1.3 | Coupled stiffness matrix from a reference model | 13 |
| 3.1.4 | Stiffness matrix from Randolph's continuum model | 13 |
| 3.1.5 | Inclusion of linear soil damping, with a damping matrix | 14 |
| 3.2 | Nonlinear foundation models | 15 |
| 3.2.1 | P-Y curves for laterally loaded piles | 15 |
| 3.2.2 | Model C | 17 |
| 3.2.3 | Kinematic hardening model | 20 |
| 3.3 | Soil damping formulation by viscous damper | 22 |
| 4 | Eigen frequencies and fatigue damage | 23 |
| 4.1 | Eigen frequency of OWT structures | 23 |
| 4.2 | Fatigue damage calculations by S-N curves | 25 |
| 5 | Methodology | 27 |
| 5.1 | The simulation tool 3DFloat | 27 |
| 5.2 | Verifying the NREL 5MW monopile in 3DFloat | 30 |
| 5.3 | Methodology for fatigue damage calculations | 31 |
| 5.4 | Environmental conditions for simulations | 33 |
| 5.5 | Soil profile | 34 |
| 5.6 | Implemented soil models | 36 |

| | | |
|-----------|---|-----------|
| 5.6.1 | Model 1..... | 36 |
| 5.6.2 | Model 2..... | 37 |
| 5.6.3 | Model 3..... | 37 |
| 5.7 | Simulations run in 3DFloat | 40 |
| 6 | Modelling and verification of turbine design..... | 41 |
| 6.1 | The NREL 5MW monopile in 3DFloat..... | 41 |
| 6.2 | Eigen frequency analysis..... | 43 |
| 7 | Results and discussion..... | 47 |
| 7.1 | Model characteristics..... | 48 |
| 7.1.1 | Free vibration tests | 48 |
| 7.1.2 | Fast fourier transform on idling cases | 49 |
| 7.2 | Fatigue damage and maximum moment at different locations..... | 50 |
| 7.2.1 | Pile at mudline..... | 50 |
| 7.2.2 | Tower root | 55 |
| 7.2.3 | Tower top | 57 |
| 7.2.4 | Blade root | 59 |
| 7.3 | Results with updated stiffness of Model 3..... | 61 |
| 7.3.1 | Free vibration test with updated Model 3..... | 61 |
| 7.3.2 | Pile at mudline with updated Model 3 stiffness | 62 |
| 7.3.3 | Tower root with updated Model 3 stiffness..... | 64 |
| 7.4 | Summary of results..... | 65 |
| 8 | Final discussion..... | 67 |
| 8.1 | Main findings | 67 |
| 8.2 | Uncertainties and weaknesses of the study..... | 67 |
| 8.3 | Suggestions for further work | 68 |
| 9 | References | 69 |
| 10 | Appendix | 73 |
| 10.1 | Rainflow counting algorithm and fatigue damage calculations | 73 |
| 10.2 | Stress calculations at cylindrical circumference..... | 77 |
| 10.3 | 3DFloat input file | 80 |

List of figures

| | |
|--|----|
| Figure 1.1: World electricity generation and projection from offshore wind (International Energy Agency, 2014) | 1 |
| Figure 1.2: Common designs for bottom fixed OWT's. Figure after Subhamoy (2014). | 2 |
| Figure 2.1: Loads on a bottom fixed offshore wind turbine. Figure from www.ovi-lab.be. | 7 |
| Figure 2.2: Wind speed fluctuation spectrum. Freely after Vorpahl et al. (2012). | 7 |
| Figure 2.3: Wind profile according to power law. | 8 |
| Figure 2.4: Spectrum of ocean waves. After Munk (1950). | 9 |
| Figure 2.5: Jonwap spectrum from Jonkman (2007). | 10 |
| Figure 3.1: Forces and moments at the mudline. | 12 |
| Figure 3.2: Apparent fixity length model | 12 |
| Figure 3.3: Uncoupled springs model | 12 |
| Figure 3.4: Example of a reference model of the soil, to make stiffness coefficients. Figure from Page and Skau (2016). | 13 |
| Figure 3.5: P-Y curves for piles. Figure from Reese and Wang (2006). | 15 |
| Figure 3.6: a) Model C reference system. Figure from Cassidy (1999). b) Spudcan foundation. Figure from Hu et al. (2014). | 17 |
| Figure 3.7: Yield surface in Model C. Figure from Nguyen-Sy (2005) after Cassidy (1999). | 18 |
| Figure 3.8: Illustration of the plastic potential function. Figure from Nguyen-Sy (2005) after Cassidy (1999). | 19 |
| Figure 3.9: Load-displacement curve for: a) p-y curve b) Model with hysteretic behavior c) Kinematic hardening model. | 20 |
| Figure 3.10: Parallel-series and series-parallel approach. Freely after Iwan (1967). | 21 |
| Figure 3.11: Hysteretic energy and maximum potential energy, for a single degree of freedom system. | 22 |
| Figure 4.1: 1p and 3p frequency relative to structure eigen frequencies. | 23 |
| Figure 4.2: Typical shape of S-N curve. | 25 |
| Figure 5.1: Process diagram for working with 3DFloat | 27 |
| Figure 5.2: Turbulence box in 3DFloat. | 28 |
| Figure 5.3: Interaction between components in 3DFloat. | 29 |
| Figure 5.4: Procedure for design verification of 3DFloat model. | 30 |
| Figure 5.5: Positions for fatigue damage calculations. | 31 |
| Figure 5.6: Positions around circumference for fatigue calculation a) pile at mudline b) blade root . | 32 |
| Figure 5.7: Probability of occurrence for load cases | 33 |
| Figure 5.8: a) Soil properties according to OC3 Phase II (Jonkman and Musial, 2010) b) Finite element representation of the soil volume and pile. Figure from Page and Skau (2016). | 34 |
| Figure 5.9: Horizontal displacement at mudline as response to load. Figure from Page and Skau (2016). | 35 |
| Figure 5.10: Rotation of the pile at mudline as a response to load. Figure from Page and Skau (2016). | 35 |

| | |
|--|----|
| Figure 5.11: Soil-structure interaction models. a) Model 1, b) Model 2, c) Model 3. The figures are simplified by only showing two dimensions. | 36 |
| Figure 5.12: Foundation response of Model 3. a) Response from individual spring. b) Total response is given by parallel coupled springs. Figure from Page and Skau (2016)..... | 38 |
| Figure 5.13: A set of parallel coupled springs gives a fit to the finite element analysis (FEA) of the soil. From from Page and Skau (2016)..... | 39 |
| Figure 6.1: Nacelle in 3DFloat | 42 |
| Figure 6.2: Visualization of selected mode shapes..... | 44 |
| Figure 6.3: Eigen frequencies compared with rotor frequency. | 45 |
| Figure 6.4: Normalized amplitude spectrum of blade root moment (flapwise). | 45 |
| Figure 6.5: Eigen frequencies according to OC3 Phase II (Jonkman and Musial, 2010)..... | 46 |
| Figure 7.1: Free vibration test with 0.1 m tower top displacement. | 48 |
| Figure 7.2: Free vibration test with 0.1 m tower top displacement, zoomed in. | 48 |
| Figure 7.3: Fast fourier transform on mudline moments for load case 1. | 49 |
| Figure 7.4: Fast fourier transform on mudline moments for load case 13. | 49 |
| Figure 7.5: Total accumulated fatigue damage per year at mudline, arranged by soil-structure interaction model. | 50 |
| Figure 7.6: Normalized accumulated fatigue damage by load case at mudline | 51 |
| Figure 7.7: Moment about inertial y-axis at mudline for selected load cases. | 52 |
| Figure 7.8: Damping ratio provided by Model 3, as a function of load level. Figure from Page and Skau (2016) | 52 |
| Figure 7.9: Normalized accumulated fatigue damage by load case at mudline, without probability weight. | 53 |
| Figure 7.10: Maximum moment at mudline arranged after load case. | 54 |
| Figure 7.11: Total accumulated fatigue damage per year at tower root, arranged by soil-structure interaction model. | 55 |
| Figure 7.12: Normalized accumulated fatigue damage by load case at tower root. | 56 |
| Figure 7.13: Maximum moment arranged by load case, at tower root..... | 56 |
| Figure 7.14: Total accumulated fatigue damage per year at tower top, arranged by soil-structure interaction model. | 57 |
| Figure 7.15: Normalized accumulated fatigue damage at tower top, arranged by load case. | 58 |
| Figure 7.16: Maximum moment at tower top, arranged by load case. | 58 |
| Figure 7.17: Total accumulated fatigue damage per year at blade root, arranged by soil-structure interaction model. | 59 |
| Figure 7.18: Normalized accumulated fatigue damage at blade root, arranged after load case. | 60 |
| Figure 7.19: Maximum moment at blade root, arranged after load case..... | 60 |
| Figure 7.20: Free vibration test with new stiffness of Model 3..... | 61 |
| Figure 7.21: Free vibration test with new stiffness of Model 3, zoomed in. | 62 |
| Figure 7.22: Total fatigue damage at mudline per year, with updated Model 3 stiffness. | 62 |
| Figure 7.23: Normalized accumulated fatigue damage at mudline after load case, with new Model 3 parameters. | 63 |
| Figure 7.24: Total fatigue damage at tower root per year, with updated Model 3 stiffness. | 64 |

Figure 7.25: Normalized accumulated fatigue at tower root after load case., with new Model 3 parameters. 64

List of tables

| | |
|---|----|
| Table 4.1: Frequency of cyclic loads on the NREL 5MW wind turbine..... | 23 |
| Table 5.1: Parameters for S-N curves..... | 31 |
| Table 5.2: Load cases for fatigue damage calculations | 33 |
| Table 5.3: Parameters for Model 3 | 39 |
| Table 5.4: Simulations run in 3DFloat | 40 |
| Table 6.1: Properties of the NREL 5 MW baseline wind turbine. Table from Jonkman and Musial (2010). | 41 |
| Table 6.2: Tower and monopile defenition in 3D float | 42 |
| Table 6.3: Eigen frequencies of structure in 3DFloat..... | 43 |
| Table 7.1: Sensitivity to soil-structure interaction model according to position on structure. | 65 |
| Table 7.2: Numerical values for the relative accumulated fatigue damage, according to position on structure..... | 65 |

1 Introduction

1.1 Background

Harvesting wind energy has for decades been a big industry in Northern Europe. Denmark has traditionally been a leader, with electricity from wind turbines accounting for roughly 40% of electricity generation (Energinet.dk, 2016). Especially the last decade, European countries has invested largely in wind turbines, with Germany, Great Britain and Denmark being essential (European Wind Energy Association, 2015). With the recent 2020 climate and energy package from the EU, aiming for 20% of energy consumption coming from renewables by 2020, the recent growth in the wind industry is expected to continue.

As visual impact, noise and other factors are introduced in areas with onshore wind farms, there has been a tendency in Northern Europe to look offshore, to further increase the wind energy potential. This increases the complexity of the wind turbines, but its many benefits are driving the industry. Firstly, the meteorological conditions are better for wind harvesting, where the wind speeds are higher and more stable than onshore. Also bigger wind farms can be installed, as larger areas are accessible offshore. The installations so far have mainly been bottom fixed turbines in the North Sea, where several sites are suitable for bottom fixed wind turbines. In 2012 the world energy generation from offshore wind was 15TWh/y, today (2016) it is around 40TWh/y, and by 2020 it is expected to reach 90TWh/y (International Energy Agency, 2014).

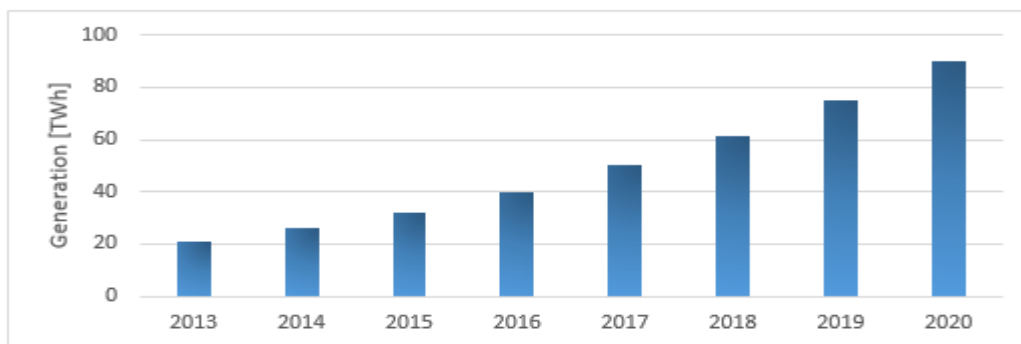


Figure 1.1: World electricity generation and projection from offshore wind (International Energy Agency, 2014)

Additional loads are introduced offshore, compared to the onshore environment. Both average- and peak wind loads are higher, and forces from the ocean, mainly waves and currents, further increase loads on the structure. As a response to this, new analytical tools have been developed for OWT's (Offshore Wind Turbines), to simulate the dynamic behavior of the system under different environmental conditions. Under the OC3 (Offshore Code Comparison Collaboration) and the OC4 project, developed under International Energy Agency Wind, several codes have been compared to verify and validate their accuracy (Robertson et al., 2014). Amongst these codes are 3DFloat, developed by IFE (Norwegian Institute for Energy Technology) and NMBU (Norwegian University of Life Sciences). 3DFloat has mainly been used for floating OWT's, but as projects involving bottom fixed turbines have become relevant, new developments regarding soil-structure interaction have been initiated. This thesis has been part this process, by testing the influence of different soil models in 3DFloat.

To make offshore wind more competitive in energy markets, the REDWIN project (REDucing cost in offshore WIND by integrated structural and geotechnical design) was initiated. The project brings different professional groups together and aims to develop models that describe soil-structure interaction for offshore wind turbines (Institute, 2016). REDWIN is currently led by NGL, partnering with IFE, amongst others. The 3DFloat code, has so far used crude models such as linear springs and dampers, to model soil-structure interactions. For better modelling, more advanced models are being implemented in the code. This thesis takes part in this process by studying and quantifying the effect on turbine behavior.

1.2 Foundation design in shallow waters

The offshore environment differ largely in soil conditions and sea depth, leading to a variety of possible foundation designs. With material- and installation costs being important for the finances of a wind farm, offshore wind turbines have so far been installed in shallow water, as cost generally grows with increasing depth and distance from shore (Myhr et al.,2014). Common foundation designs for bottom fixed turbines is the monopile, gravity foundation, jacket and tripod.

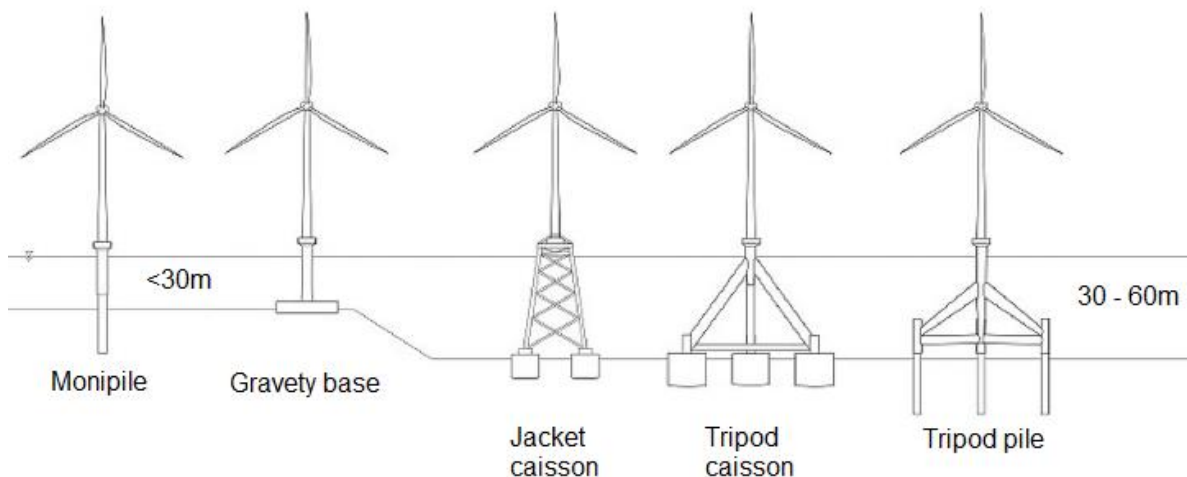


Figure 1.2: Common designs for bottom fixed OWT's. Figure after Subhamoy (2014).

Monopiles are preferred in shallow waters, due to its simple technology and low cost. At depths greater than 30m, the jacket and tripod is regarded as suitable designs, as the monopile foundation meet its limitations. For sites with rocky ground, the gravity base can be a suitable foundation, due to difficulties in interfacing the other designs.

The main function of the foundation is to bring the necessary support for the tower. With a mass of roughly 700 tonnes of the tower-nacelle-hub-rotor system (5MW NREL Turbine), a strong vertical support is required. In extreme weather, the horizontal forces from waves and wind give moments in the order of 10^8 MN at the seabed, creating a need for firm horizontal support from the foundation. With a desired lifetime of roughly 20 years, high standards for the foundation design is necessary.

In this thesis, the monopile foundation has been of interest, as this is the most widespread design, and that of current interest in the REDWIN project.

1.3 Previous research

Several studies have been conducted regarding soil-structure interaction for monopile foundations. The ones regarded most relevant for this thesis, is briefly be presented below.

Zaaijer (2006) studied the influence of different linear soil-structure interaction models for a 3MW OWT, with a monopile foundation. This was quantified by the influence on the first- and second natural frequencies of the structure. He found that an inaccuracy of 4% on the first natural frequency could be expected (with respect to a finite element representation of the soil), with the best performing linear model he tested. The foundation models were also compared with experimental results from real offshore sites, to study how the models reproduced experimental results. Five of the sites he studied corresponded with expectations, but two of the sites gave large unexplained deviations.

Carswell et al. (2014) and Carswell et al. (2015) added damping to the mudline response. Firstly by a horizontal dashpot, and secondly by a rotational dashpot at the mudline. In these studies, the NREL 5MW monopile was used. The results were quantified by average and maximum load- and displacement responses at the mudline. For extreme storm conditions, Carswell et al. (2015) found that the maximum and standard deviation of mudline moment was decreased by 7-9%, with mudline damping introduced to the system.

Yung et al. (2015), compared the p-y curve approach (see Chapter 3.2.1) to a finite element representation of the soil-foundation system, for the NREL 5MW monopile. For the mudline moments, the differences was insignificant, but for the tilt angle at the pile head, the difference was significant (>14%).

Damsgaard et al. (2015) studied the effect of varied soil properties, on fatigue damage equivalent moments (FDEM), on a parked 5MW wind turbine with a monopile foundation. He found that stiffness and damping characteristics significantly affected FDEM for the parked wind turbine. A 50% reduction of the deterministic properties gave a 12% increase in FDEM for the stiffness reduction, and 21% for the damping reduction.

Beuckelaers (2015) introduced a different approach for simulating soil damping, by using a kinematic hardening soil model (see Chapter 3.2.3). By simulating a rotor stop for an OWT with a monopile foundation, he compared results with the p-y curve approach for pile analysis, used by DNV and API standards. It was concluded that the kinematic hardening model, forms a suitable basis for time domain calculations for OWT's.

The studies mentioned above have covered specific loading conditions, which says little of the impact on the OWT in a lifetime perspective. In addition to this, influence on the structure above mudline, has not been given much attention.

With the studies mentioned above as a background, this thesis has used similar soil-structure interaction models, but with a wider range of environmental conditions, and quantification of the impact on fatigue damage and maximum loads, at several locations on the OWT structure. This will give a better understanding of the impact of different soil-structure interaction models in a lifetime perspective.

1.4 Project description and goals

The main goal of this thesis is to study the influence of different soil-structure interaction models on an offshore wind turbine with a monopile foundation. It is a continuation of a semester thesis by the subject author, where an extreme loading case was studied for three different soil models. A weakness of this study, was that the model of main interest, was calibrated outside the load region of main interest. In addition to this, wind and wave conditions was simplified, and few influences on turbine dynamics was investigated. This thesis introduces additional soil-structure interaction models, a new parameterization of current models, a larger range of environmental conditions, and more results for structure influences.

In addition to supervision from Tor Anders Nygaard (main developer of 3Dfloat), frequent contact with NGI has been held, mainly through the REDWIN Phd. Candidate, Ana Page. Special interest on effects from soil damping, has been expressed by geotechnical engineers at NGI. Based on this, effects of soil damping has been of high interest in the thesis. It should be noted that special attention to soil damping came after the literature study on soil-structure interaction models, which the theoretical chapters in this thesis are influenced by.

Based on the description above the thesis has the following goals:

- Perform a literature study on soil-structure interaction models, and present relevant models for OWT modelling.
- Implementation and verification of the NREL 5MW Monopile design in 3DFloat.
- Study the effects of different soil models on the NREL 5MW monopile wind turbine, with a special focus on soil damping.

To quantify the effects of different soil-structure interaction models, maximum loads and fatigue damage is studied, with fatigue damage being that of main interest. Maximum loads are important especially in connection with permanent deformation of the soil, a critical factor to consider in the design phase. Fatigue damage is important for potential costs reduction in the OWT industry. If better soil modelling can improve fatigue damage calculations for OWT's, this has the potential for cost reduction through material savings.

The soil-structure interaction models applied in this thesis are so-called macro element models. This means that the full response of the soil-foundation system, is given at a single point of the OWT structure, normally at the mudline. This approach I widely used in development of soil-structure interaction models. Still, this is contrary to the industry-standard for pile analysis, where the soil response is distributed over the length of the pile (see Chapter 3.2.1). As soil damping is most easily implemented by a macro element model, this approach has been used in this thesis. This is also beneficial with regard to computational burden. This will be further discussed in Chapter 0.

A comparison with the industry standard (p-y curve approach) is planned for, as a continuation of this thesis.

1.5 Structure of thesis

The thesis has a theoretical part, a methodological part, a presentation of results, a discussion and a concluding part. The chapters do not strictly follow this pattern, therefore a brief introduction of the structure of the thesis is given, to better navigate in the text.

Theoretical part

Chapter 2 gives a general presentation of loads in the offshore environment, with a focus on the frequency domain, as this is of high interest in OWT analysis.

Chapter 3 gives a presentation of soil-structure interaction models for OWT's. It gives a general overview of important models, and is a result from a literature study on soil-structure interaction models for OWT's. Only parts of this theory is applied in the thesis.

Chapter 4 presents a theoretical aspect on eigen frequencies and fatigue damage calculations, which will both be used to quantify the influence of different soil-structure interaction models.

Methodological part

Chapter 5 presents the methodologies used in this thesis. This includes:

- A general presentation of the software 3DFloat.
- A presentation of the methodology for verifying the 3DFloat OWT model.
- Specifications regarding fatigue damage calculations.
- Presentation of load cases used in the thesis.
- Presentation of soil profile and soil-structure interaction models investigated in this thesis.
- Presentation of simulations run in 3DFloat

Verification of OWT model

Chapter 6 presents the verification process of the NREL 5MW wind turbine in 3DFloat. It will be tested if the 3DFloat model gives reasonable results, compared with other studies on the same structure, before the model is used for further study.

Results and discussion

Chapter 7 presents influences of different soil-structure interaction models, divided in four subchapters:

- Stiffness and damping characteristics of soil-structure interaction models, from free vibration tests.
- Influence of fatigue damage and maximum moments at selected positions on the OWT.
- Influence on fatigue damage with updated stiffness for one of the soil-structure interaction models.
- Summary of results.

Chapter 8 presents the main findings of the thesis. It also suggests improvements in the methodology used in this thesis, and further studies that that would be a natural continuation of this work.

2 Loads in the offshore environment

As the wind industry has expanded from mainly onshore wind farms, to also include offshore sites, environmental loads on the structure has increased in complexity. With higher wind loads, and hydrodynamic forces introduced, a good description of the subject loads is essential for accurate simulations. In addition to gravitational-, aerodynamic- and hydrodynamic loads, other factors as sea spray, ice impacts, marine growth, scouring and earthquakes influence an OWT (Figure 2.1). As wind and waves are most influential, these will be the focus of this chapter.

As soil-structure interaction is the focus of this thesis, only a brief presentation of aero- and hydrodynamic loads will be presented. The aim is to give the reader a general understanding of these topics, with special attention on the frequency domain. This is of high interest in OWT dynamics, as it is a rotating system, very sensitive to resonance effects.

2.1 Aerodynamic loads

In the frequency spectrum of wind fluctuations, there are mainly three peaks (Figure 2.2). Firstly “The synoptic peak” at around 4 days, due to changing weather, secondly “The diurnal peak” at 12 hours, due to day-/night fluctuations, and thirdly is “The turbulent peak”, at around 1.5 minutes, caused by random fluctuations in wind speed. In structural analysis for monopiles, load periods under five second are of main interest, as this is where the eigen frequencies of the structure is. Load fluctuations in this region, has the potential to cause resonance effects, which greatly influence fatigue life of the structure.

The aerodynamic loads in the frequency region of a few seconds, is mainly caused by aerodynamic effects on the rotor. Two load cycles of high interest is the $1p$ and $3p$ load frequency, with p meaning ‘per revolution’. $1p$ and $3p$ load frequencies are mainly caused by the wind profile at the site, and tower shadowing effects. These effects are briefly described below.

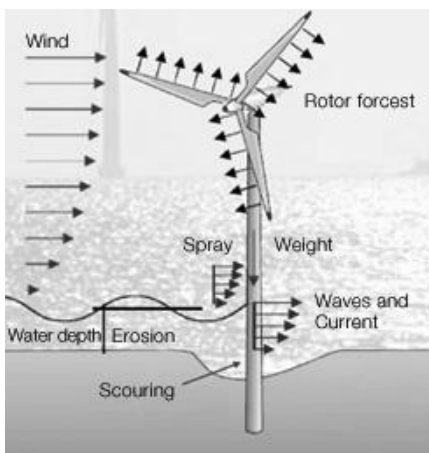


Figure 2.1: Loads on a bottom fixed offshore wind turbine. Figure from www.ovi-lab.be.

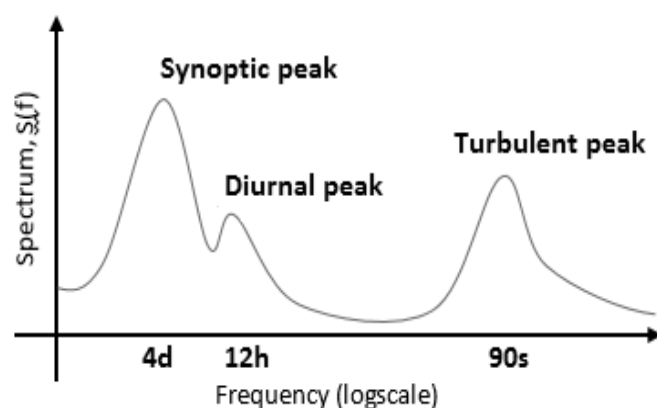


Figure 2.2: Wind speed fluctuation spectrum. Freely after Vorpahl et al. (2012)

The general wind profile

Due to friction at the earth's surface, wind speed tends to decrease close to the ground (or sea surface). As an approximation, a vertical power shear law can be used, to express wind speed as a function of the height:

$$U(z) = U_{ref} \left(\frac{z}{z_{ref}} \right)^\zeta \quad (2.1)$$

, where U is the horizontal wind velocity at height z , U_{ref} is the wind speed at some reference height, z_{ref} , and ζ is the shear exponent. This describes an increasing wind speed with height. This feature of the wind should be carefully considered in wind turbine design, as it introduces cyclic loads on the structure. With a rotational frequency, $1p$, of the turbine, each rotor blade will experience cyclic loads with this frequency, as it passes maximum height once per revolution. An additional load frequency of $3p$ is introduced on the structure, when the turbine has three rotor blades, as blades passes the top three times per revolution. Figure 2.3 gives a plot of the wind profile with a wind speed of 12 m/s, a reference height of 90 m, and a shear exponent of 0.14. As seen in the figure, the blade tip speed varies with roughly 2 m/s for a turbine with hub at 90 m, and a rotor diameter of 120 m.

Tower shadowing

The $3p$ excitation from the blades, is further increased by an effect known as *tower shadowing*. In front of the tower, wind speeds are lower due to aerodynamic effects caused by the tower. This leads to a decrease in wind speed each time a blade passes the tower, significantly increasing $1p$ effect on each blade, and the $3p$ effect on the full structure.

Time domain variations in wind speed

Wind speed will fluctuate in both magnitude and direction. For an overview of wind characteristics in the time domain, the author suggests Vorpahl et al. (2012) for an overview. Long-term variations in wind speed, and turbulence intensity used in this thesis, is presented in Chapter 5.4.

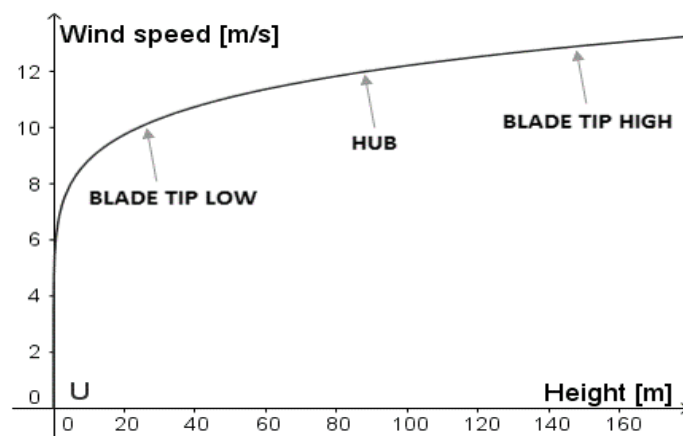


Figure 2.3: Wind profile according to power law.

2.2 Hydrodynamic loads

The hydrodynamic forces on a bottom fixed OWT is mainly due to forces from waves and currents. Water moving relative to an immersed body, impose lift- and drag forces on the body, depending on its shape. For a cylinder with water moving perpendicular to its central axis, the lift force is approximately zero. If the water has an acceleration relative to the cylinder, there are additional inertia forces. Morison's equation gives an approximation for the forces on a body in a flow of water, and is for a cylinder given by:

$$\hat{F} = \frac{1}{2} C_d \rho D |U_w| U_w + C_m \rho A \dot{U}_w \quad (2.2)$$

, where \hat{F} is force per unit length of the member, C_d is the drag coefficient of the member, ρ is the density of water, D is the diameter of the member, U_w is the velocity of the water, C_m is the inertia coefficient, and A is the cross sectional area of the cylinder.

When both the body and fluid is moving relative to a reference point, a relative form of the Morison's equation can be used. For more details on this, the reader is referred to Jonkman (2007). For hydrodynamic forces on wet elements, 3DFloat uses the relative form of Morison's equation.

Waves

Figure 2.4 shows a tentative classification of ocean waves, according to wave period. Ordinary gravity waves are of highest significance, as they have periods of a few seconds, which is in the region of the 1st tower eigen frequencies. The most interesting frequencies for the NREL 5MW Monopile, is around 0,25 hz, or a wave period of 4s, as this is the 1st tower eigen frequencies (see Chapter 6.2). Even though this is within the spectrum of ordinary gravity waves, the majority of waves considered in this thesis has wave periods over 6 seconds, or below 0.17 Hz, leaving most of them outside the resonance zone.

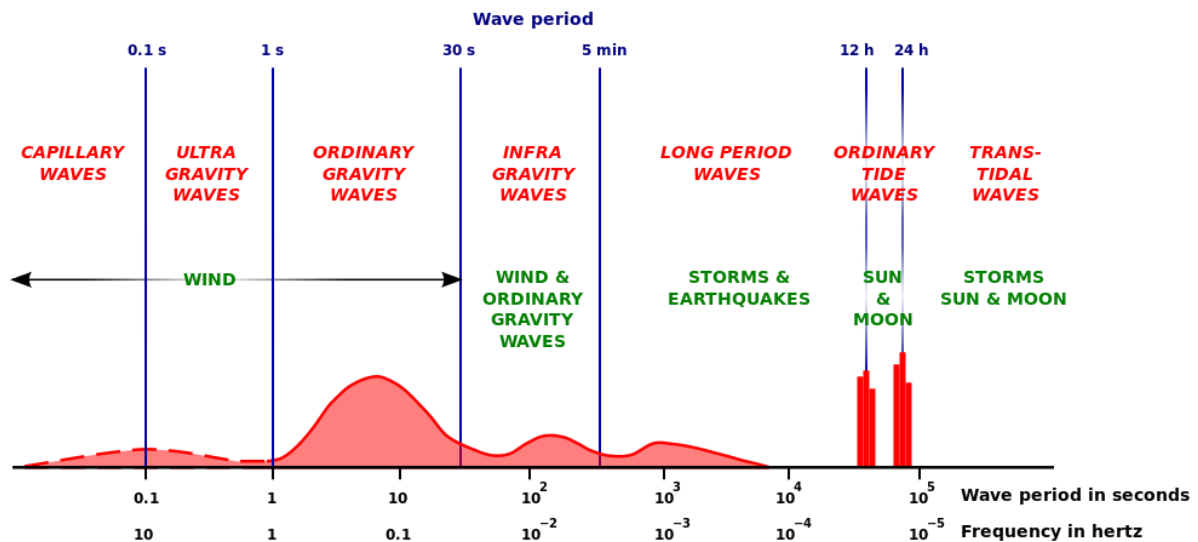


Figure 2.4: Spectrum of ocean waves. After Munk (1950).

Constant wind over a significant time-span make ordinary gravity waves. Wave height and direction is a function of the wind velocity, which over time changes in magnitude and direction. This leads to intersecting wave systems. Together with this, effects of the cost line leads to an irregular wave surface at offshore sites. A significant factor influencing the wave height and shape is sea depth. At deep sites far from shore, waves tends to be relatively high, with long periods. At intermediate and shallow water sites, waves are smaller, with steeper wave crest, and shorter wave periods.

Several modeling techniques for waves exist, with *linear airy theory* being a widespread approach for deep water sites. Airy wave theory, models the sea surface with a sinusoidal shape. For shallow waters, where wave crests often are steeper, higher order models as for example *Stream function wave theory* gives more representative wave modelling. The reader is referred to external sources for more theory concerning this.

To simulate irregular sea states at an offshore site, the Jonswap spectrum is widely used. The Jonswap spectrum gives the wave energy distribution as a function of frequency, as shown in Figure 2.5, here with peak wave frequency at 0.5 rad/s, equivalent to a wave period of 13 s. The gamma factor is used to calibrate the peakedness of the function. An irregular sea state can then be modelled by superposition of regular waves, with wave frequencies according to the Jonswap spectrum. In 3DFloat, an irregular sea state is made from the superposition of airy waves, with frequencies according to the Jonswap spectrum. Superposition of airy waves, generated from the Jonswap spectrum, will be used in this thesis.

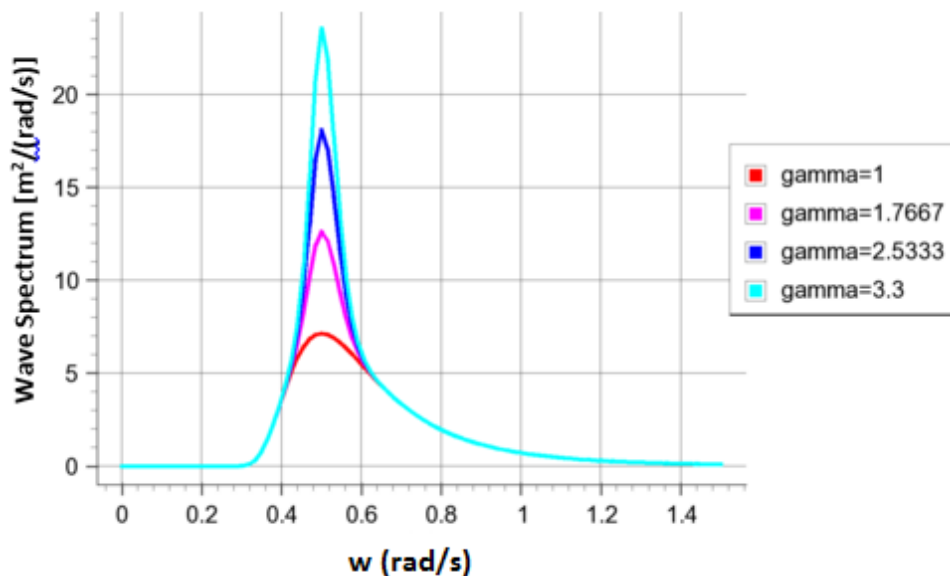


Figure 2.5: Jonswap spectrum from Jonkman (2007)

3 Soil-structure interaction models

Several mechanisms work together to give the loading response from the soil on an offshore foundation. The simplest approach assumes a linear response from the soil, where responding forces from the foundation is linearly dependent on displacement of the foundation. The soil stiffness can be determined from for example monotonic load tests. For small displacements, the soil response can be approximated by a linear model, but for larger displacements, nonlinearities and possibly soil deformations, can be significant. Linear models also neglect soil damping effects, which also impact the dynamics of the system. In addition to this, soil properties can change over time due to for example scour (erosion of soil due to flowing water).

In this chapter, different soil-structure interaction models will be presented, as a presentation of a literature study on the topic. The monopile foundation will be the main focus, but also soil-structure interaction models for other offshore foundation structures will be presented, as their mathematical formulations can be translated to the monopile foundation. This presentation will start with the simplest models, formulated by a stiffness matrix at the mudline. Several approaches exist for determining stiffness coefficients, and an overview of these will be given. As nonlinear effects should be considered for more accurate models, especially for high loads, a section with nonlinear models will follow.

As this section is the presentation of a literature study, not all the models is necessary to read, for understanding this thesis. Especially Model C, and the P-y curve approach in Chapter 3.2 has little relevance for understanding the results presented in this thesis. Mathematical formulations of Chapter 3.2 is also of higher complexity, therefore the reader should be familiar with soil-structure interaction formulations.

3.1 Linear foundation models

The models presented in this section are from the studies by Zaaier (2006) and Passon (2006), on foundation models for offshore wind turbines. The models are two-dimensional, and take only one of the horizontal dimensions into consideration. In an OWT perspective, this means that side-to-side movement of the tower is not considered. Linear models have an advantage, due to their low computational burden.

This class of models is expressed by a stiffness matrix at the mudline. The stiffness matrix represents the response from the soil, given at a single point at the mudline. The response from the soil, F , given at the mudline will be approximated by:

$$F = \begin{bmatrix} H \\ M \\ V \end{bmatrix} = \begin{bmatrix} k_{uu} & k_{u\theta} & 0 \\ k_{\theta u} & k_{\theta\theta} & 0 \\ 0 & 0 & k_w \end{bmatrix} \begin{bmatrix} u \\ \theta \\ w \end{bmatrix} \quad (3.1)$$

, where u is horizontal displacement, w is vertical displacement, and θ is the angular displacement. V , M , and H is their respective forces and moments. The different k 's are corresponding stiffness coefficients. The stiffness matrix approach is easily implemented into a finite element analysis program, as the stiffness matrix can be added to the node at the mudline. Finding the stiffness coefficients for equation (3.1) has several approaches, and will be presented next.

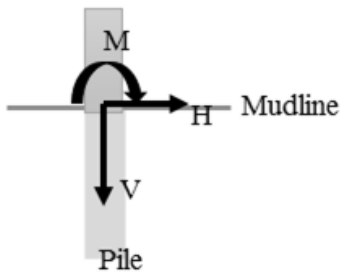


Figure 3.1: Forces and moments at the mudline

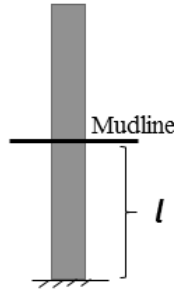


Figure 3.2: Apparent fixity length model

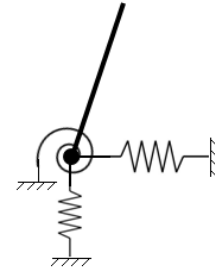


Figure 3.3: Uncoupled springs model

3.1.1 Stiffness matrix by effective fixity length

This model replaces the soil with an extended pile length, constrained at a length, l , under the mudline as shown in Figure 3.2. The extended pile length will in this way represent the soil response, as the pile is free to move at the mudline node. A pile penetration of four times the pile diameter, gives the best results in the studies by (Zaaijer, 2006). Other papers suggests a pile length from 3.3 to 8 times the pile diameter, depending on soil conditions (Kühn, 1995). With a given pile length, the stiffness matrix at the mudline can be expressed by:

$$K = \frac{3EI}{l^3} \begin{bmatrix} 6 & -3l & 0 \\ -3l & 2l^2 & 0 \\ 0 & 0 & \frac{Al^2}{2I} \end{bmatrix} \quad (3.2)$$

, with E being the E-modulus of the pile, A being the cross sectional area of the pile, and I being the area moment of inertia of the pile.

3.1.2 Stiffness matrix by uncoupled springs

The stiffness of the soil-pile system, can be expressed as a set of uncoupled springs at the mudline as in Figure 3.3. An uncoupled model, has stiffness coefficients only on the matrix diagonal, meaning that the different degrees of freedom have no impact on each other. Stiffness coefficients of the springs can be determined by static analyses from a reference model, for example a finite element model of the soil-structure system. Given the displacements for a representative load case at the mudline, the spring stiffness's can be found by solving:

$$\begin{bmatrix} H \\ M \\ V \end{bmatrix} = \begin{bmatrix} k_{uu} & 0 & 0 \\ 0 & k_{\theta\theta} & 0 \\ 0 & 0 & k_w \end{bmatrix} \begin{bmatrix} u \\ \theta \\ w \end{bmatrix} \quad (3.3)$$

, with the stiffness coefficients being the unknowns.

3.1.3 Coupled stiffness matrix from a reference model

In a coupled model, the stiffness matrix has additional coefficients, compared with an uncoupled model. In this way, the different degrees of freedom have impact on each other. From the studies by Zaaijer (2006), this proves to give a better representation of the soil response. By applying different load combinations on a reference model, a coupled stiffness matrix can be obtained. From two lateral load cases and one axial load case, the stiffness matrix can be determined. A solution of the following equation is suggested by Zaaijer (2006) to obtain the stiffness coefficients:

$$\begin{bmatrix} F_1 \\ M_1 \\ F_2 \\ F_3 \end{bmatrix} = \begin{bmatrix} x_1 & \theta_1 & 0 & 0 \\ 0 & x_1 & \theta_1 & 0 \\ x_2 & \theta_2 & 0 & 0 \\ 0 & 0 & 0 & k_z \end{bmatrix} \begin{bmatrix} k_{xx} \\ k_{x\theta} \\ k_{\theta\theta} \\ k_z \end{bmatrix} \quad (3.4)$$

A full finite element model of the soil volume and the foundation, can for example be used as a reference model, as in Figure 3.4.

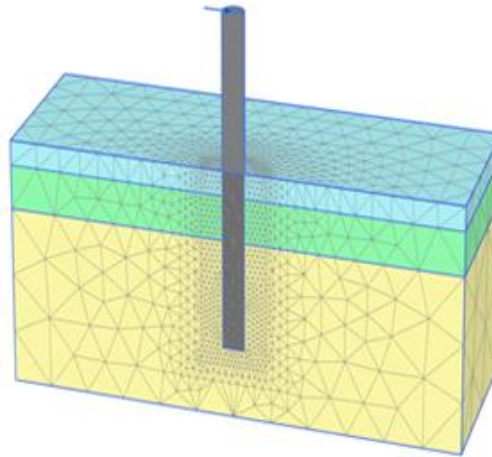


Figure 3.4: Example of a reference model of the soil, to make stiffness coefficients. Figure from Page and Skau (2016).

3.1.4 Stiffness matrix from Randolph's continuum model

This approach builds on the results from analyzing flexible piles response to lateral loading. Randolph (1981) suggested an equivalent shear modulus of the soil to be:

$$G^* = G_s \left(1 + \frac{3\nu_s}{4}\right) \quad (3.5)$$

, where G_s is the shear modulus of the soil and ν_s is the Poisson's ratio of the soil. According to his analyses, a pile in an elastic continuum would behave as an infinite long pile with shear modulus G^* , when

$$\frac{l}{d} \geq \left(\frac{E_p}{G^*}\right)^{\frac{2}{7}} \quad (3.6)$$

Here l is the length of the pile, d is the outer diameter of the pile, and E_p is the effective Young's Modulus of the pile. Assuming the vertical degree of freedom is constrained, and with a linearly increasing soil

shear modulus, the elements of the stiffness matrix at the mudline is according to Randolph (1981), given by:

$$k_{uu} = 4.52 \cdot m^* \cdot r_0^2 \cdot \left(\frac{E_p}{m^* r_0} \right)^{\frac{1}{3}} \quad (3.7)$$

$$k_{u\theta} = k_{\theta u} = -2.40 m^* r_0^3 \left[\frac{E_p}{m^* r_0} \right]^{\frac{5}{9}} \quad (3.8)$$

$$k_{\theta\theta} = 2.16 m^* r_0^4 \left[\frac{E_p}{m^* r_0} \right]^{\frac{7}{9}} \quad (3.9)$$

, where r_0 is the radius of the pile, and

$$E_p = \frac{EI}{\frac{1}{64}\pi D^4} \text{ and } m^* = m \cdot \left(1 + \frac{3}{4}\nu \right) \quad (3.10)$$

, with m being the rate of change of the soil shear modulus, which can be obtained from a linear fit to the actual soil properties of the relevant site. The vertical degree of freedom is constrained.

3.1.5 Inclusion of linear soil damping, with a damping matrix

In addition to the stiffness matrix implemented at the mudline, a damping matrix can be added, to account for energy dissipation in the soil. The dynamics at the mudline node, will then be expressed by:

$$\begin{bmatrix} H \\ M \\ V \end{bmatrix} = \begin{bmatrix} k_{uu} & k_{u\theta} & 0 \\ k_{\theta u} & k_{\theta\theta} & 0 \\ 0 & 0 & k_w \end{bmatrix} \begin{bmatrix} u \\ \theta \\ w \end{bmatrix} + \begin{bmatrix} c_{uu} & c_{u\theta} & 0 \\ c_{\theta u} & c_{\theta\theta} & 0 \\ 0 & 0 & c_w \end{bmatrix} \begin{bmatrix} \dot{u} \\ \dot{\theta} \\ \dot{w} \end{bmatrix} \quad (3.11)$$

, where the different c 's are damping coefficients. A procedure for finding representative damping coefficients is presented in Chapter 3.3.

3.2 Nonlinear foundation models

In this section, a selection of nonlinear models for soil-structure interaction will be presented. For small load amplitudes, a linear response can be a good approximation, but for higher loads, nonlinear effects are expected to increase in magnitude. Extreme loads can lead to permanent deformation of the soil, and effects such as stiffening/softening of the soil around the foundation over time, is relevant to account for, as it can influence eigen frequencies of the full OWT structure.

The first model presented, representing the soil with so called *p-y curves*, is a common approach for analyzing piles in the offshore industry (Pradhan, 2012). An advantage of this approach, is that it models the actual behavior of pile under the mudline. The other models presented are macro element models, where the full response of the foundation is given in a single point at the mudline.

3.2.1 P-Y curves for laterally loaded piles

The p-y curve method is the most common approach for analyzing piles in the offshore industry. It has been developed during several decades, with the contribution from Matlock and Reese (1960), and Matlock (1970), being essential. The method is recommended by API (American Petroleum Institute, 2000) for designing offshore platforms with pile foundations, and by DNV (Det Norske Veritas, 2014) for offshore wind turbine design (mainly for ULS analysis). Due to its widespread usage, several procedures are developed for obtaining p-y curves, both with various soil properties and loading conditions.

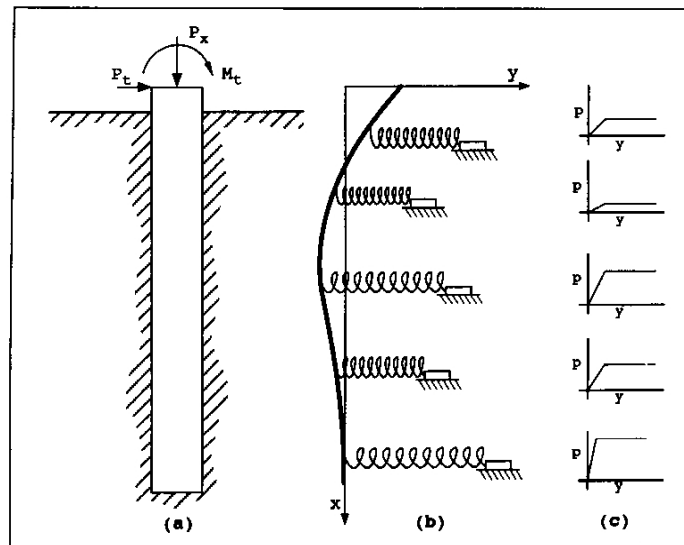


Figure 3.5: P-Y curves for piles. Figure from Reese and Wang (2006).

The method applies a set of springs along the pile as shown in Figure 3.5. The standard beam column equation is applied to give the response of the pile, with the springs representing the soil resistance. The equation is according to Reese and Wang (2006) given by:

$$\frac{d^2}{dx^2} \left(E_p I_p \frac{d^2 y}{dx^2} \right) + P_x \left(\frac{d^2 y}{dx^2} \right) - p(y) - W = 0 \quad (3.12)$$

, where P_x is the axial load on the pile, y is the lateral deflection of pile along the length of the pile, p is the soil resistance per unit length, W is the distributed load along the length of the pile, E_p is the elastic modulus of the pile and I_p is the area moment of inertia of the pile. In a finite element analysis of the structure, p-y curves can be attached to nodal points along the pile foundation.

Determining p-y curves

Depending on the soil properties, several methods exist for determining the p-y curves. Semi-empirical solutions has been suggested for elastic springs, with stiffness as a function of depth. Matlock and Reese (1960) gives expressions where the soil stiffness vary with depth in a power- or polynomial form.

DNV (Det Norske Veritas, 2014) suggests semi-empirical methods for determining p-y curves for clay and sand, both for static and cyclic loading. API (American Petroleum Institute, 2000) suggest the same routines.

Alternatively, p-y curves can be extracted from numerical analysis of the soil-structure interaction. A finite element model of the soil volume, as given in Figure 3.4, can be used to obtain p-y curves at different depths.

An experimental test would best represent soil p-y characteristic at the relevant site, as the methods above can vary significantly in the resulting p-y curves. Pradhan (2012) compared p-y curves obtained from API standards, with p-y curves from FEM modelling in the software PLAXIS 3D. For large pile diameters, the two approaches gave significant deviations. Pradhan (2012) argues that this is due to the pile behaving more and more like a rigid pile as the pile diameter increase. API standards are based on piles with relatively small diameter, giving them more flexible properties.

3.2.2 Model C

The following model is primarily developed for shallow offshore foundations, specifically the spudcan foundation (Figure 3.6b). It is included in this thesis as an example of a mathematical formulation that accounts for plasticity effects of the soil, hardening of the soil and yield behavior. With experimental results for a monopile, the parameters of Model C could be fitted to account for monopile behavior.

Model C was developed by Cassidy (1999) for analyzing jack-up structures subjected to random waves, based on a series of loading test performed by Gottardi and Houlsby (1995). It is a macro element model for a spudcan footing on dense sand, where the response from the foundation is given in a single point connected to the superstructure. The model gives vertical-, rotational- and horizontal responses from the soil, as a function of the respective displacements of the footing. Figure 3.6a gives a basic overview of displacements due to applied loads for the foundation.

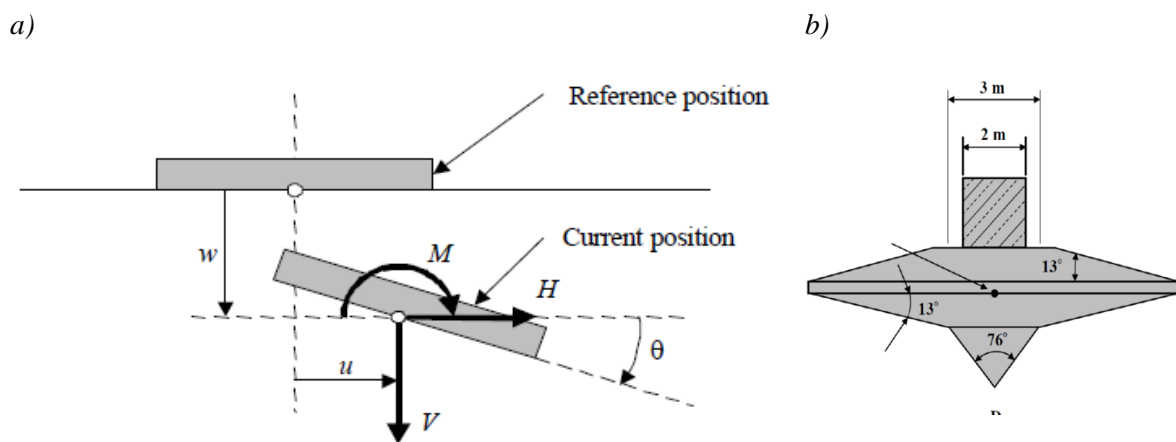


Figure 3.6: a) Model C reference system. Figure from Cassidy (1999). b) Spudcan foundation. Figure from Hu et al. (2014)

The most important mathematical formulations of the model are:

- The yield surface, which defines the plastic and elastic load regions for the model.
- An elastic response function, to represent displacement increments in the elastic load region.
- A flow rule, to represent plastic displacement increments in the plastic load region.
- A hardening rule, defining the size of the yield surface. The size of the yield function is a function of vertical plastic displacement, and does not depend on the horizontal- and rotational displacements.

Briefly summarized the model uses the yield surface to determine whether there is a plastic or elastic response from the foundation. Elastic responses are given by linear coefficients, and plastic responses are given by the flow rule. The size of the yield surface is a function of the vertical plastic deformation, with their relation given by the hardening rule. A description of the yield surface, elastic response function, flow rule and hardening rule will be given below.

Yield surface

A simplified form of the yield surface applied in model C is given by:

$$f^* = \left(\frac{h}{h_0}\right)^2 + \left(\frac{m}{m_0}\right)^2 - 16v^2(1-v)^2 = 0 \quad (3.13)$$

, where $h = \frac{H}{V_0}$, $m = \frac{M}{2RV_0}$, $v = \frac{V}{V_0}$. R is the radius of the subject footing and V_0 is a parameter that defines the size of the yield surface, given by equation (3.16). As shown in Figure 3.7, the yield surface takes the shape of rugby ball. For load cases inside the yield surface, the models gives a linear response to displacements. On the yield surface, the response is given by the flow rule.

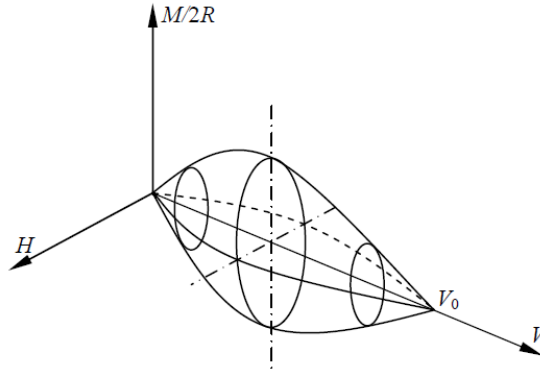


Figure 3.7: Yield surface in Model C. Figure from Nguyen-Sy (2005) after Cassidy (1999).

Elastic response function

The relation between incremental loads (dV , dM , dH) and increment displacements (dw , $d\theta$, du), is for the elastic case given by:

$$\begin{bmatrix} dV \\ 0.5R^{-1} dM \\ dH \end{bmatrix} = 2RG \begin{bmatrix} k_v & 0 & 0 \\ 0 & k_m & k_c \\ 0 & k_c & k_h \end{bmatrix} \begin{bmatrix} dw_e \\ 2Rd\theta_e \\ du_e \end{bmatrix} \quad (3.14)$$

, where R is the radius of the footing, G is a representative shear modulus and the different k 's are dimensionless constants.

Flow rule

The flow rule for plasticity in Model C is given by:

$$\begin{bmatrix} dw_p \\ d\theta_p \\ du_p \end{bmatrix} = \Lambda \begin{bmatrix} \frac{dg}{dV} \\ \frac{dg}{dM} \\ \frac{dg}{dH} \end{bmatrix} \quad (3.15)$$

, where p denotes plastic displacements, Λ is a non-negative scalar, and g is a plastic potential function, similar to the yield function. Often the yield function, f , would be used in place of g , but to better represent experimental data, the plastic potential function g is introduced. For a detailed description of the plastic potential function, g , the reader is referred to Cassidy (1999). In a geometric interpretation of the flow rule, the direction of the increment displacement vector is normal to the surface of the plastic potential function as in Figure 3.8.

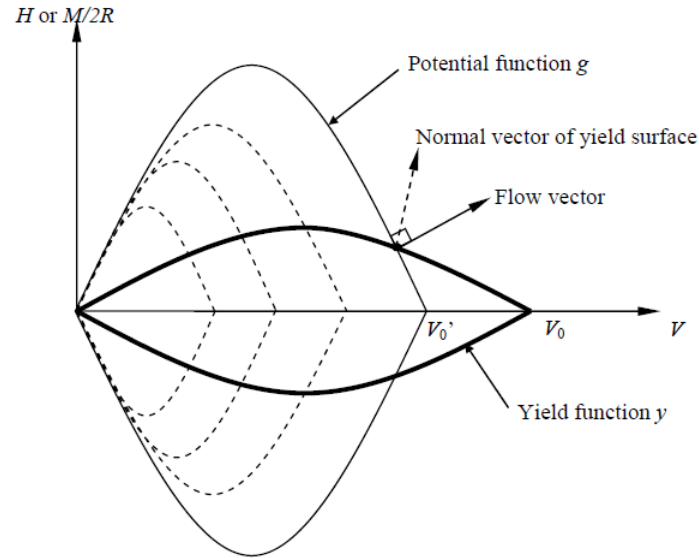


Figure 3.8: Illustration of the plastic potential function. Figure from Nguyen-Sy (2005) after Cassidy (1999).

Hardening rule

The hardening rule defines how the size of the yield surface change, as a function of plastic deformation in the vertical direction, given by w_p . The hardening rule is a fit to experimental data, and is given by:

$$V_0 = \frac{k w_p}{1 + \left(\frac{k w_{pm}}{V_{0m}} - 2 \right) \left(\frac{w_p}{w_{pm}} \right) + \left(\frac{w_p}{w_{pm}} \right)^2} \quad (3.16)$$

, where k is an initial plastic stiffness, V_{0m} is the peak value of V_0 , and w_{pm} is the corresponding plastic deformation at this peak value. Relevant to note is that the vertical plastic deformation, w_p , is the only variable of the function. From Equation (3.13) it can be seen how the yield surface change as the parameter v , is a function of V_0 .

Evaluation of the model

The capability of the Model C has been evaluated by Houlsby and Cassidy (2002). This was done by comparing numerical results from the model, to a set of data from tests reported by Gottardi and Houlsby (1995). Results showed high accuracy for the soil conditions of this experiment.

3.2.3 Kinematic hardening model

A kinematic hardening soil model simulates both yield behavior and hysteretic damping from the soil. By following a different load-displacement curve for loading and unloading, hysteretic damping is introduced to the system. By also allowing the yield point to move, yield behavior is accounted for.

In the p-y curve approach, each p-y curve follows the same elastic curve for loading and unloading. This is illustrated in Figure 3.9a. The p-y curves models the non-linear behavior of the soil, but effects such as damping and yield behavior is ignored.

The soil damping effect also influences the structure, as energy is taken out from the OWT system. The effects of soil damping on a monopile OWT, was studied by Carswell et.al. (2014). Especially in extreme conditions, the damping effect considerably affected the dynamics of the structure. With soil damping included, maximum moment at the mudline was reduced by 7-9% according to the study.

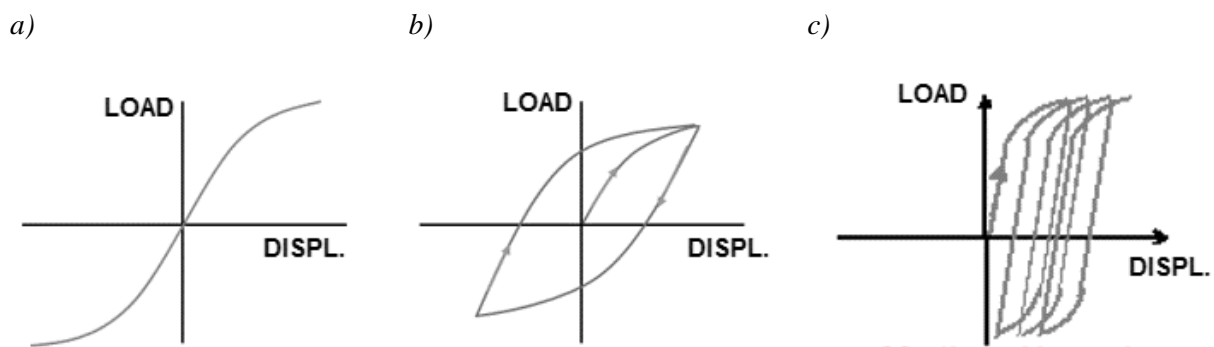


Figure 3.9: Load-displacement curve for: a) p-y curve b) Model with hysteretic behavior c) Kinematic hardening model.

Figure 3.9b shows a load-displacement curve of a kinematic hardening model as a response to cyclic loading. The area within the hysteresis loops, represents energy absorbed by the soil, which gives a damping effect. In a kinematic hardening model, the yield surface remains the same in shape, but translates in stress space. For a 1D model this can lead to behavior as given in Figure 3.9c.

Mathematical formulation by Iwan (1967)

Motivated to make a mathematical formulation of cyclic systems with hysteretic behavior, Iwan (1967) formulated a class of models to describe the behavior of composite systems. This formulation has in some cases been adapted to OWT soil-structure interaction modelling, as for example in the study by Beuckelaers (2015). A similar approach is also adapted in this thesis (Model 3 – see Chapter 5.6.3).

In this formulation, the Bauschinger effect was essential in the model formulation. The Bauschinger effect states that plastic yield in a material increases the yield strength in direction of plastic flow, and reduces yield strength in the opposite direction. The formulation by Iwan (1967) applies a set of elastic elements, and slip elements to represent the system behavior. The elements are organized in a parallel-series or series-parallel configuration as in Figure 3.10.

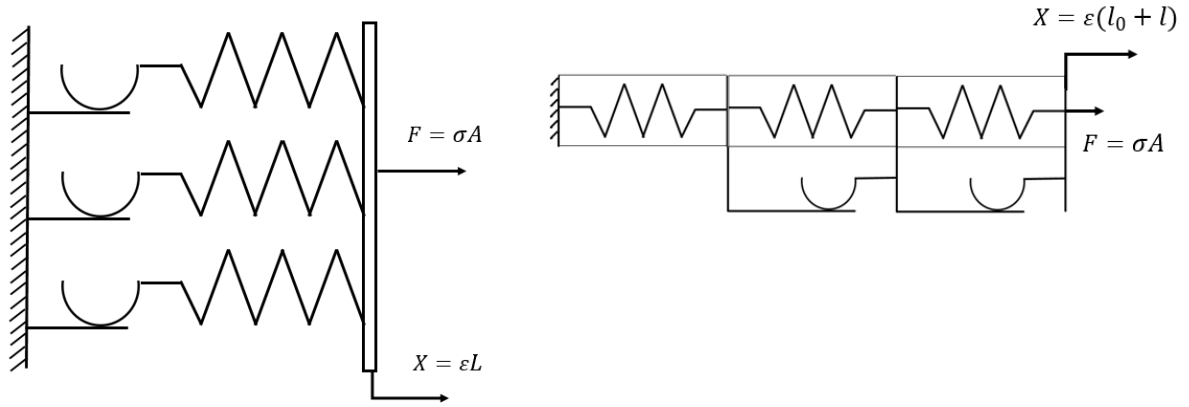


Figure 3.10: Parallel-series and series-parallel approach. Freely after Iwan (1967).

In Iwan (1967), each spring element is assigned an representative area A_i , with an elastic modulus E_i , and critical slipping stress for each slip element, σ_i^* . The loading behavior of the parallel-series model is then represented by:

$$\sigma = \frac{F}{A} = \sum_{i=1}^n \frac{E_i}{N} \epsilon + \sum_{i=n+1}^N \frac{\sigma_i^*}{N}$$

, where the summation from 1 to n includes all elements which remain elastic after loading to a strain, ϵ , and the summation from $n+1$ to N includes all elements that have slipped or yielded. A similar approach is adapted in this thesis for Model 3 (Chapter 5.6.3).

For the mathematical formulation for the series-parallel model, the reader is referred to Iwan (1967).

3.3 Soil damping formulation by viscous damper

Soil damping in OWT analysis refers to the absorption of energy by the soil, from the OWT system. There are two main forms of soil damping; hysteretic material damping, and radiation damping. The radiation damping is due to geometric dissipation of waves, and the hysteretic material damping, due to hysteretic effects in the soil. Geometric dissipation is regarded negligible for frequencies under 1Hz, and since this is the main frequency domain for OWT's, hysteretic material damping is of main interest (Carswell et. al, 2015).

Except from the soil model that includes a viscous damping through a damping matrix, only model C and the kinematic hardening model introduce soil damping. In these models, energy is absorbed by the soil when yield behavior occurs. Chapter 3.1.5 briefly introduces how soil damping can be implemented through a damping matrix. An approach to find a representative damping coefficient is given below. One of the soil models in this thesis introduces damping based on this approach (see Model 2 – Chapter 5.6.2).

For a soil-structure interaction model to represent soil damping, the right amount of energy should be absorbed by the soil for each load cycle. The hysteretic loss per cycle is has the notation E_h . For a single degree of freedom system, with a linear spring and a dashpot damper, the hysteretic curve can look as in Figure 3.11, with the hysteretic energy loss being the area inside the hysteretic loop. The maximum potential energy is has the notation E_p' . The damping provided by the system can be quantified by the damping factor D , given by:

$$D = \frac{1}{4\pi} \cdot \frac{E_h}{E_p'} \quad (3.17)$$

Knowing the hysteretic damping energy loss of a system, an equivalent horizontal (or rotational) viscous damper can be introduced, representing the damping of the system. The viscous damping coefficient can according to Chopra (2007) be represented by:

$$c = \frac{E_h}{2u^2\pi^2 f} \quad (3.18)$$

, where u is the horizontal displacement of the system, and f is the load frequency. Following this, the damping value will be representative for a given frequency and displacement level.

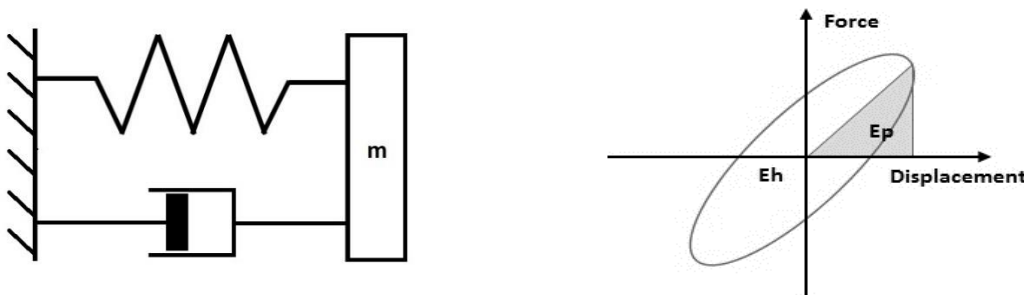


Figure 3.11: Hysteretic energy and maximum potential energy, for a single degree of freedom system.

4 Eigen frequencies and fatigue damage

As eigen frequencies is a central topic in OWT analysis, a brief introduction of this topic will be given below. The aim is to give the reader a general background, as this is a central topic of discussion through the thesis.

Fatigue damage calculations has been used to quantify the effect of different soil-structure interaction models in the thesis. A brief theoretical presentation of fatigue damage calculation by S-N curves, will be given in this chapter. A more specific description of S-N curves and coefficients used in this thesis, will be given in Chapter 5.3.

4.1 Eigen frequency of OWT structures

A detailed analysis in the frequency domain is essential in OWT design. Both wind and wave loads appear cyclic on the wind turbine, possibly leading to resonance effects. Resonance effects fatigue life of the structure, and can influence optimal behavior for the OWT system. The frequency of some cyclic loads experienced by the structure is presented in Table 4.1.

Table 4.1: Frequency of cyclic loads on the NREL 5MW wind turbine

| | | Frequency | Period |
|-----------|--|--------------------------------------|--|
| Wind | - Synoptic peak (weather change) - Turbulent peak | 3×10^{-6} $\sim 10^{-2}$ | 4 days 90 s |
| Waves | - Tidal waves - Ordinary gravity waves peak | $\sim 10^{-5}$ ~ 0.1 | 12 h, 24 h 10 s |
| Rotor 1p | - cut in - rated | 0.12 0.20 | 8.7 s 5.0 s |
| Rotor 3p | - cut in - rated | 0.35 0.61 | 2.9 s 1.7 s |
| Generator | - cut in - rated | 11.2 19.6 | 5.1×10^{-2} s 9.0×10^{-2} s |

For OWT's with monopile foundation, the $1p$ and $3p$ frequencies are often of highest significance, as they are in the region of the eigen frequencies of the structure. To avoid resonance, the system is designed to have eigen frequencies below, between or above $1p$ and $3p$, as seen in Figure 4.1. Chapter 6.2 gives the lowest eigen frequencies of the 5MW NREL monopile, which is from 0.25-2 Hz. This is near the $1p$ and $3p$ frequency, and is therefore given extra attention.

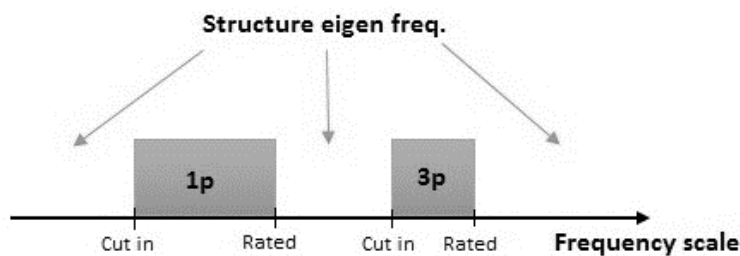


Figure 4.1: $1p$ and $3p$ frequency relative to structure eigen frequencies.

Finding eigen frequencies of the structure

The dynamic equation for an elastic system with linear damping can be expressed by the system equation of motion given by:

$$[M]\{\ddot{d}\} + [C]\{\dot{d}\} + [K]\{d\} = \{F(t)\} \quad (4.1)$$

[M] is the system mass matrix, [C] is the system damping matrix, [K] is the system stiffness matrix, $\{d\}$ is the displacement vector of the system, and $\{F(t)\}$ an external time varying force acting on the system. For free undamped vibrations, the damping and external forces of the system is set to zero, giving:

$$[M]\{\ddot{d}\} + [K]\{d\} = \{0\} \quad (4.2)$$

To find the natural frequencies of the system, the displacement vector is assumed to be according to:

$$\{d\} = \{\phi\}e^{i\omega t} = \{\phi\}(\cos(\omega t) + i \sin(\omega t)) \quad (4.3)$$

By derivation of equation (4.3), and substitution, equation (4.1) can be reduced to:

$$[[K] - \omega^2[M]]\{\phi\} = \{0\} \quad (4.4)$$

This equation has a nontrivial solution only when $|[K] - \omega^2[M]| = 0$. This system will have a number of solutions for the Eigen frequencies, ω , equal to the dimensions of the mass and stiffness matrices. This system can be solved in 3DFloat, giving the eigen frequencies of the subject system.

4.2 Fatigue damage calculations by S-N curves

Due to cyclic loading, materials has a tendency to weaken, which over time leads to potential failure. The study of fatigue is a critical design factor in OWT design, as it determines the lifetime of the structural components. According to DNV-standards, the lifetime should be over 20 years (Det Norske Veritas, 2014). As described in chapter 4.1, the majority of loads in the offshore environment is cyclic, thereby causing fatigue in the OWT structure.

A widely used approach for fatigue analysis is by the use of S-N curves. The S-N curve approach gives the number of stress cycles before failure for a given stress range. Figure 4.2 gives a typical shape of a S-N curve. As seen, the number of cycles before failure decrease rapidly for high stress ranges. Note that the horizontal axis is logarithmic.

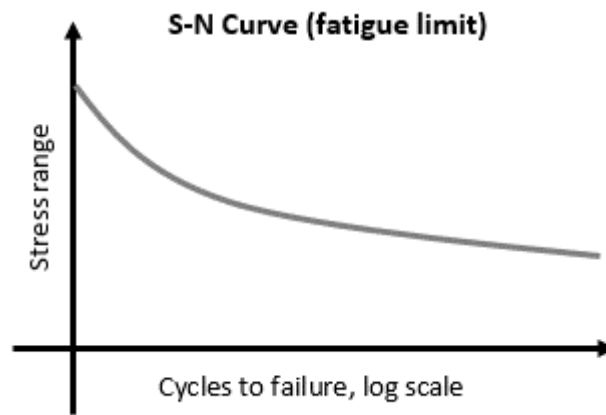


Figure 4.2: Typical shape of S-N curve

Due to changing environmental conditions, the stress range varies much in the offshore environment. To use the S-N approach for a variety of stress ranges, one can assume linear cumulative damage, meaning that one stress cycle in a given stress range, with a corresponding N cycles to failure, contributes $1/N$ to failure. This is known as the Palmir-Miner rule, mathematically expressed as:

$$D' = \sum_{i=1}^k \frac{n_i}{N_i} \quad (4.5)$$

Here all stress cycles are collected in k number of stress blocks. D' is the accumulated fatigue damage (failure when $D'=1$), n_i is the number of stress cycles in block i , and N_i is the number for cycles before failure for stress block i .

The approach given above is suggested by DNV for fatigue damage calculations for OWT's (Det Norske Veritas, 2014).

5 Methodology

This chapter will present the methodology used in this thesis. It includes the following subchapters:

1. A presentation of the software 3DFloat
2. Methodology for verification of the NREL 5MW Monopile in 3DFloat
3. Methodology for fatigue damage calculations
4. Presentation of environmental conditions used in simulations
5. Presentation of the soil profile used in the thesis
6. Presentation of the different soil-structure interaction models applied in thesis
7. Presentation of the simulations performed in 3DFloat

5.1 The simulation tool 3DFloat

3DFloat is a hydro-aero-servo-elastic simulation tool to represent the dynamic behavior of offshore wind turbines. This means it takes loads from the ocean and wind, responses from the control system, and elastic material behavior, into consideration as the dynamics of the system is calculated. The structure is modelled by a finite element representation, giving the elastic behavior of the subject system. It has been developed by IFE and NMBU since 2006 and has been part of the IEA offshore comparison task OC3 and OC4. The code written in FORTRAN90, with linear algebra additions from LAPACK (3DFloat manual, 2009).

The program has a command line interphase. The models are implemented through an input file, where all input commands are given. The input file gives the user control of environmental conditions as waves, currents and winds. The full structure is also defined here, including floater, mooring lines, tower, nacelle and blade properties. A control system for the rotor, and generator characteristics can also be defined. When making the input file, a set of sensors is set, that stores data of selected variables to files. 3DFloat comes with tools to make plots of relevant data, and 3d-simulations of the system in the time domain.

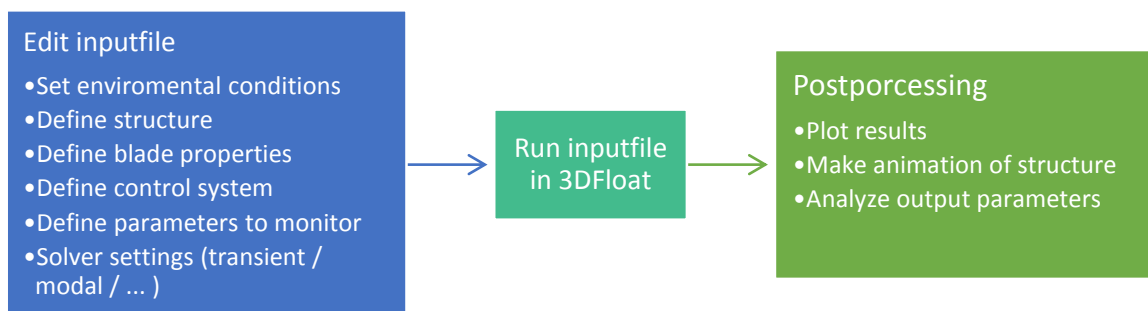


Figure 5.1: Process diagram for working with 3DFloat

A brief description of how the structure, environmental conditions and control system is modelled, follows on the below.

Structure

The structure is modeled by two-node Euler-Bernoulli beams. Each node has six degrees of freedom, three in translation and three in rotation. A general nonlinear finite element model framework is the core of the 3DFloat model, where computational nodes is interconnected with elements. Blade element properties with tabulated drag coefficients are read from input file to properly simulate aerodynamic forces on the rotor.

Aerodynamics

For aerodynamic loads, both constant and turbulent winds can be defined. The wind speed and direction can also be varied during simulations. As wind is generally increasing with height, wind speed at a reference height is defined, together with a wind shear exponent. To simulate turbulence, a turbulence box can be applied. The turbulence box contains data with wind speed and direction. The turbulence box is ‘dragged’ pass the rotor during simulation, as seen in Figure 5.2.

Aerodynamic loads on the rotor is calculated from unsteady blade element/momentum theory, with extension for dynamic inflow and yaw errors.

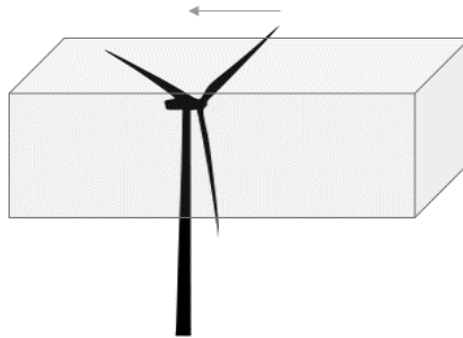


Figure 5.2: Turbulence box in 3DFloat.

Hydrodynamics

The wave kinematics for regular waves includes first order Airy waves, and stream function up to order 12. Irregular waves are represented by first or second order Airy waves. Since the classical Airy wave theory neglects the instantaneous wave surface, various options are implemented to allow integration of the loads to the instantaneous water surface, such as the “extrapolated” and “Wheeler stretching” approaches.

Control system

The control system is for a variable speed rotor. The pitch angle is fixed below rated speed. Above rated speed a PI-controller is used to control rotation speed and power generation. Alternatively, a control system developed for the IEA OC3 project can be implemented.

Figure 5.3 presents the components in 3DFloat, and the interaction between them. The platform and mooring lines boxes are de-emphasized, as they are not relevant for this thesis.

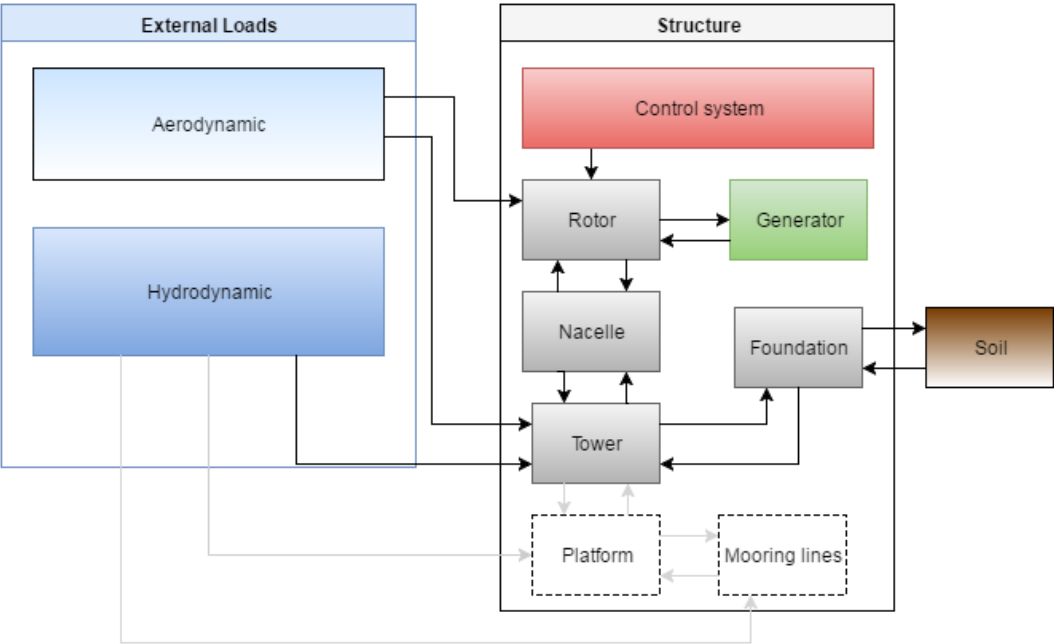


Figure 5.3: Interaction between components in 3DFloat.

5.2 Verifying the NREL 5MW monopile in 3DFloat

For reliable results, a verification of the structure above seabed has been conducted. This is to ensure that 3DFloat gives representative behavior, before new soil-structure interaction models are tested. A comparison with results from OC3 Phase II was therefore done. The structural eigen frequencies has been used as a basis for comparison, as this will give an indication of the full structural dynamics.

A special attention on resonance effects has been central, as that would be detrimental to fatigue life. As the $3p$ frequency is close to some of the blade modes, much attention has been given to resonance in this frequency region.

Figure 5.4 presents the procedure used to verify the 3DFloat model:

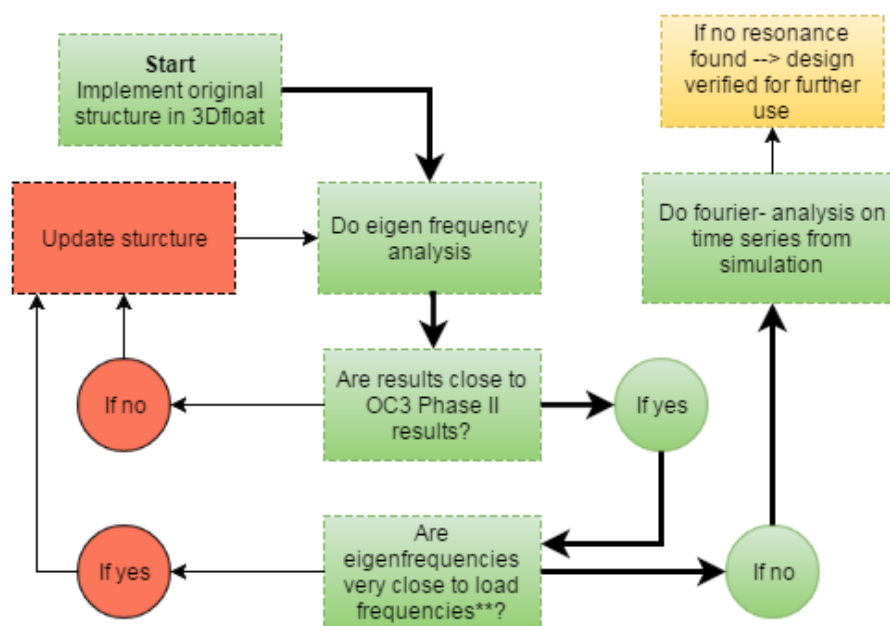


Figure 5.4: Procedure for design verification of 3DFloat model.

**very close: less than 5% difference

As eigen frequencies are checked against both OC3 Phase II results, and load frequencies, the main emphasis has been on avoiding resonance with load frequencies. It has been regarded more important to avoid resonance, even though this gives eigen frequencies slightly above or below OC3 Phase II results.

The structure is mainly updated by changing the nacelle properties. As explained in Chapter 6.1, the nacelle is modelled by cylindrical elements. The material properties of the nacelle was varied, so that eigen frequencies are in the desired region.

The verification process is documented in chapter 6, as this has been a significant part of the work in this thesis.

5.3 Methodology for fatigue damage calculations

The fatigue damage calculations uses the S-N curve approach, with the Palmer-Miner rule as described in chapter 4.2. The Rainflow-counting algorithm is used to count stress cycles. This is according to standards from DNV (Det Norske Veritas, 2014). S-N curves for air are used, even though some of the positions for fatigue damage calculation are exposed to sea water. This will give misleading absolute values for positions exposed to water, but as relative values are of main interest in this thesis, this has not been considered. S-N curve F3 for air, from table 7-14 in the DNV standard DNV-OS-J101 (Det Norske Veritas, 2014) are used in the fatigue calculations, and are according to:

$$\log_{10} N = \log_{10} a - m' \log_{10} \left(\Delta\sigma \left(\frac{t}{t_{ref}} \right)^k \right) \quad (5.1)$$

, where N are the number of stress cycles before failure at stress range $\Delta\sigma$, m' is the negative slope of the $\log N$ - $\log S$ curve, $\log_{10} a$ is the intercept of the $\log N$ axis, t_{ref} is a reference thickness, t is the thickness through which the potential fatigue crack will grow, and k is a thickness exponent. The S-N curve has different parameters, depending on the number of stress cycles. Parameter values used in this thesis are given in Table 5.1.

Table 5.1: Parameters for S-N curves

| | $N < 10^7$ | $N > 10^7$ |
|---------------|------------|------------|
| $\log_{10} a$ | 11.546 | 14.576 |
| m' | 3.0 | 5.0 |
| k | 0.25 | 0.25 |
| t_{ref} | 25mm | 25mm |

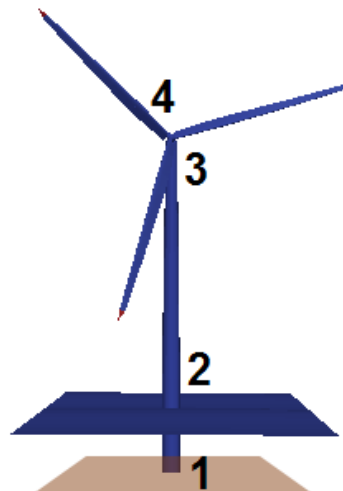


Figure 5.5: Positions for fatigue damage calculations

Simulation time in this thesis has been 1800 seconds. Results have been extrapolated to find the accumulated fatigue damage per year. When extrapolating data, some stress cycles will enter the high cycle region ($N > 10^7$), but this has not been accounted for. This will in some cases underestimate the accumulated fatigue damage in this thesis.

Four positions on the wind turbine are selected for fatigue damage calculations:

1. Pile at mudline
2. Tower root (10 m over still water line)
3. Tower top
4. Blade root

Output data from 3DFloat, with forces and moments in elements of interest, is used to calculate stress at the circumference of the cylindrical elements. A python script has been used for this purpose, also calculating fatigue damage for positions of interest. The scripts are based on python functions written and provided by Marit Irene Kvittem, working at DNV and NMBU. Python scripts used in the thesis can be found in the the appendix.

Positions for fatigue damage calculations

Fatigue damage is calculated based on stress amplitudes. For the pile and tower, stress levels are calculated for eight positions around the circumference of interest. For the blade root, a finer resolution had been used, with 16 points for stress calculations.

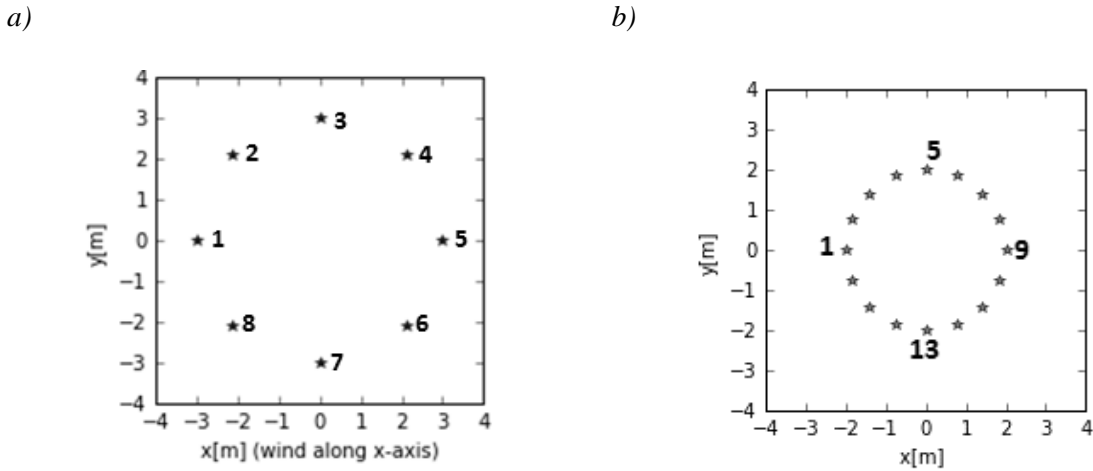


Figure 5.6: Positions around circumference for fatigue calculation a) pile at mudline b) blade root

In the inertial axis system, with an angle γ , being zero along the negative x-axis, and increasing moving against the clock, the stress levels at the different positions are found by:

$$\sigma = -\frac{F_z}{A} + \frac{M_y}{I_y} r \cos(\gamma) - \frac{M_x}{I_x} r \sin(\gamma) \quad (5.2)$$

$$\tau = \frac{M_z}{I_p} r + \frac{2F_y}{A} \cos(\gamma) - \frac{2F_x}{A} \sin(\gamma) \quad (5.3)$$

, with σ being the axial stress, and τ being the shear stress at given location at the cylinder circumference. A is the area of the cylinder wall at a given cross section, I_x and I_y are area moments of inertia, and I_p is the polar moment of inertia. All forces and moments are given relative to a node at the center of the cylindrical elements.

The positions with the highest fatigue damage are presented in the results. This has been at position 1 (Figure 5.6a) for the tower and pile, but variable for the blade root.

5.4 Environmental conditions for simulations

The environmental conditions for fatigue damage calculations are according to that of the Upwind Design Basis for a shallow water site (Fisher et al, 2010, p.70). The different load cases, with its corresponding wave and wind conditions, are presented in Table 5.2. Probability of occurrence for the different load cases are visualized in Figure 5.7.

Table 5.2: Load cases for fatigue damage calculations

| Load case | Wind Speed [m/s] | Turbulence intensity [%] | Wave height [m] | Peak Wave period [s] | Probability of occurrence [-] |
|-----------|------------------|--------------------------|-----------------|----------------------|-------------------------------|
| 1 | 2 | 29.2 | 1.07 | 6.03 | 0.0671 |
| 2 | 4 | 20.4 | 1.10 | 5.88 | 0.08911 |
| 3 | 6 | 17.5 | 1.18 | 5.76 | 0.14048 |
| 4 | 8 | 16.0 | 1.31 | 5.67 | 0.13923 |
| 5 | 10 | 15.2 | 1.48 | 5.74 | 0.14654 |
| 6 | 12 | 14.6 | 1.70 | 5.88 | 0.14272 |
| 7 | 14 | 14.2 | 1.91 | 6.07 | 0.08381 |
| 8 | 16 | 13.9 | 2.19 | 6.37 | 0.08316 |
| 9 | 18 | 13.6 | 2.47 | 6.71 | 0.04186 |
| 10 | 20 | 13.4 | 2.76 | 6.99 | 0.03480 |
| 11 | 22 | 13.3 | 3.09 | 7.40 | 0.01535 |
| 12 | 24 | 13.1 | 3.42 | 7.80 | 0.00974 |
| 13 | 26 | 12.0 | 3.76 | 8.14 | 0.00510 |
| 14 | 28 | 11.9 | 4.17 | 8.49 | 0.00202 |
| 15 | 30 | 11.8 | 4.46 | 8.86 | 0.00096 |

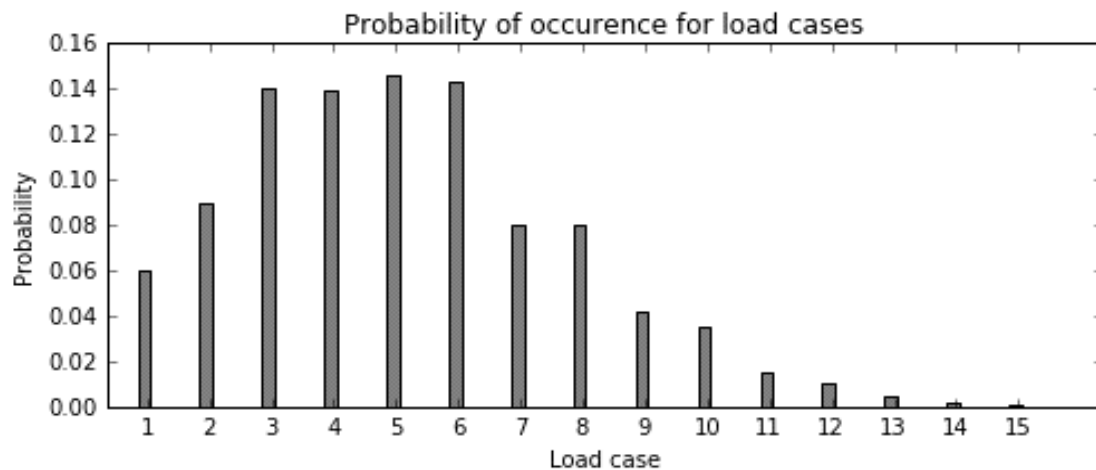


Figure 5.7: Probability of occurrence for load cases

Unidirectional irregular airy wave components has been generated in 3DFloat according to the Jonswap spectrum, with a gamma factor of 2.87. Peak wave period, and wave height is according to Table 5.2. Airy wave components has been used, as this is the available option in 3DFloat for making irregular waves.

Turbulence is read from files containing wind data, produced by the turbulence generator (Mann 64bit turbulence generator) provided by the hawc2 OWT simulation project, accessible at their web pages (www.hawc2.dk). A separate turbulence file is made for each load case.

5.5 Soil profile

The soil profile will be given according to OC3 Phase II. It is defined to give realistic soil properties, while still giving a noticeable impact on the system (Jonkman and Musial, 2010). It consists of three layers with different effective unit weight, γ' , and friction angle, ϕ . The soil properties is illustrated in Figure 5.8a, where the soil becomes stronger with depth.

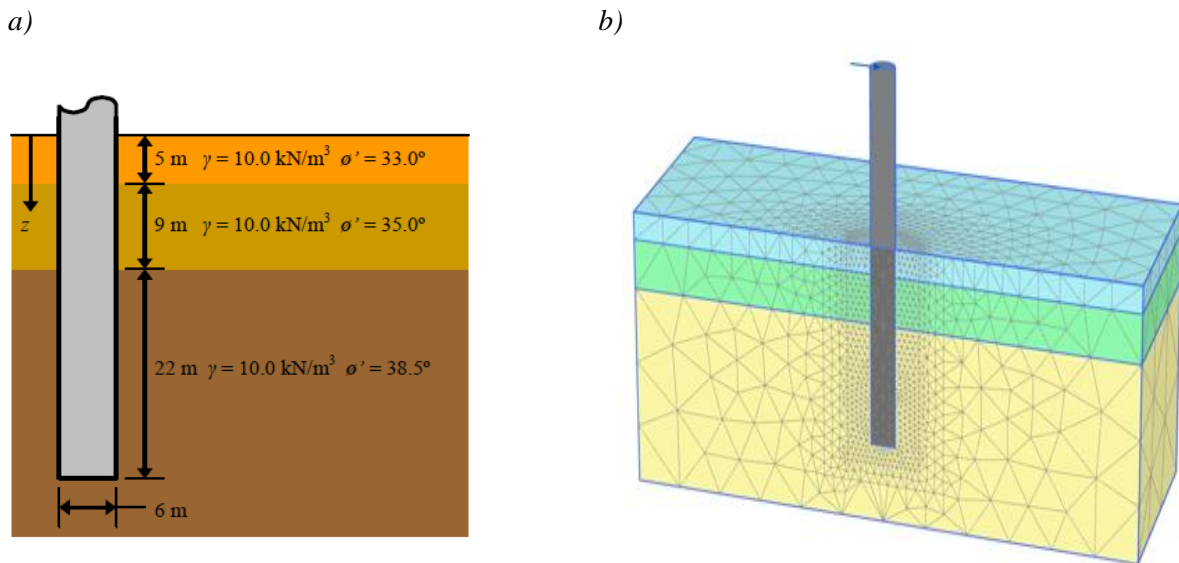


Figure 5.8: a) Soil properties according to OC3 Phase II (Jonkman and Musial, 2010) b) Finite element representation of the soil volume and pile. Figure from Page and Skau (2016).

Based on the soil profile above, Page and Skau (2016) have generated load-displacement curves for the OC3 monopile. These curves has been used in the parametrization of soil-structure interaction model 3, described in Chapter 5.6.3. A finite element model of the soil-structure system was set up, as illustrated in Figure 5.8b. A horizontal load was applied 20.0 m above the seabed. Load-displacements curves according to Page and Skau (2016) are given in Figure 5.9 and Figure 5.10.

The figures also indicates the load level and displacements that was used in the report by Passon (2006), where he generates stiffness coefficients for the mudline. Passon (2006), used the same soil profile, but a p-y curve approach to model the soil response.

Passon's (2006) results are relevant, as they are used to formulate one of the soil-structure interaction models in this thesis (Model 2, Chapter 5.6.2)

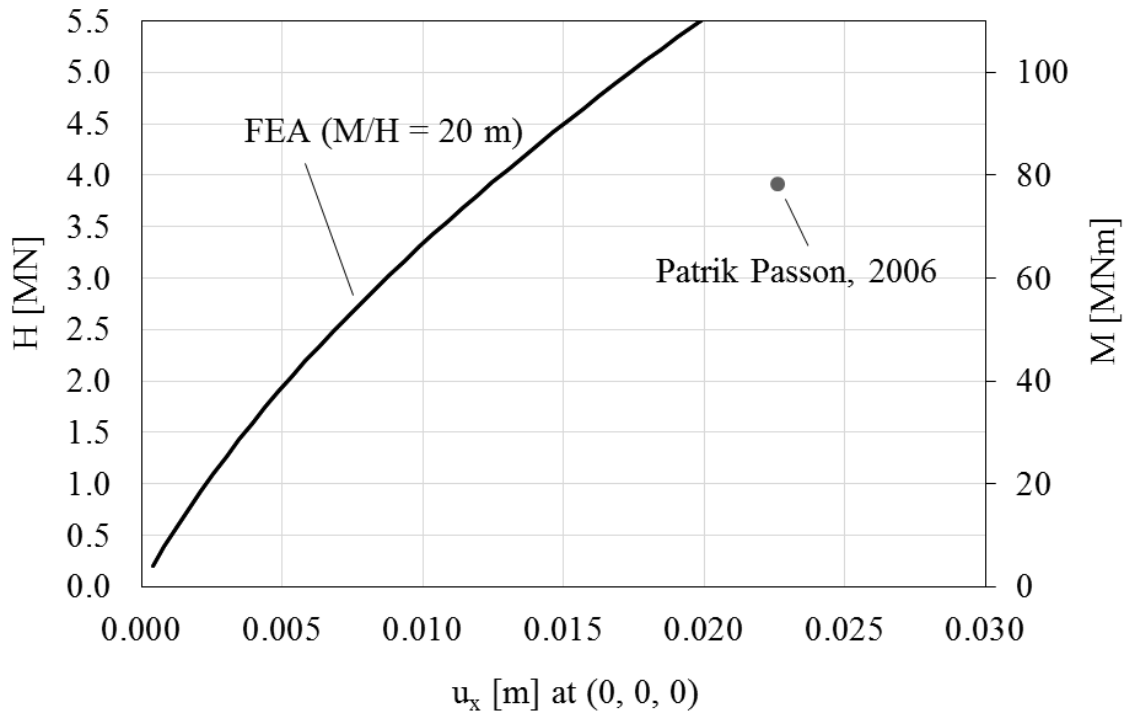


Figure 5.9: Horizontal displacement at mudline as response to load. Figure from Page and Skau (2016).

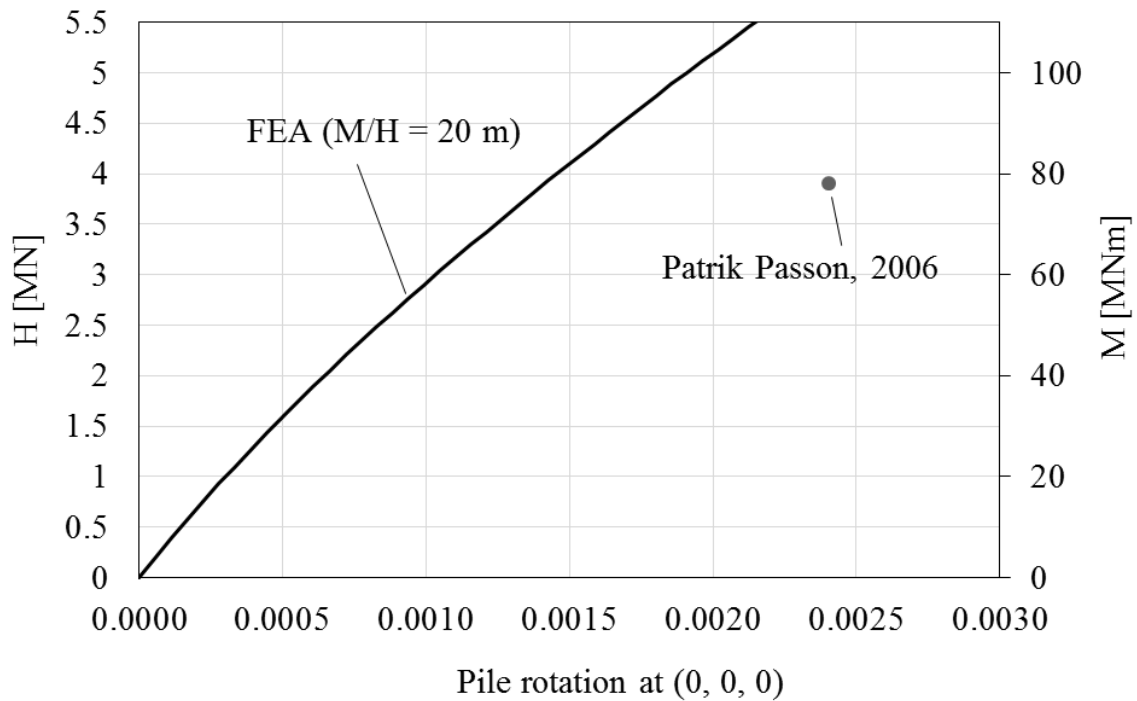


Figure 5.10: Rotation of the pile at mudline as a response to load. Figure from Page and Skau (2016).

5.6 Implemented soil models

Three different soil-structure interaction models are considered in this thesis. The reference model is represented by a stiffness matrix at the mudline, derived for the OC3 comparison exercise (Passon, 2006). The second model has a stiffness matrix with and a rotational dashpot damper at the mudline, as described in Chapter 3.3. The third model is a kinematic hardening model (see Chapter 3.2.3), recently implemented to 3DFloat. This model is developed by NGI as a part of the REDWIN project. The models will be referred to as Model 1, Model 2 and Model 3. A detailed description of all soil-structure interaction models, will be given in the following subchapters.

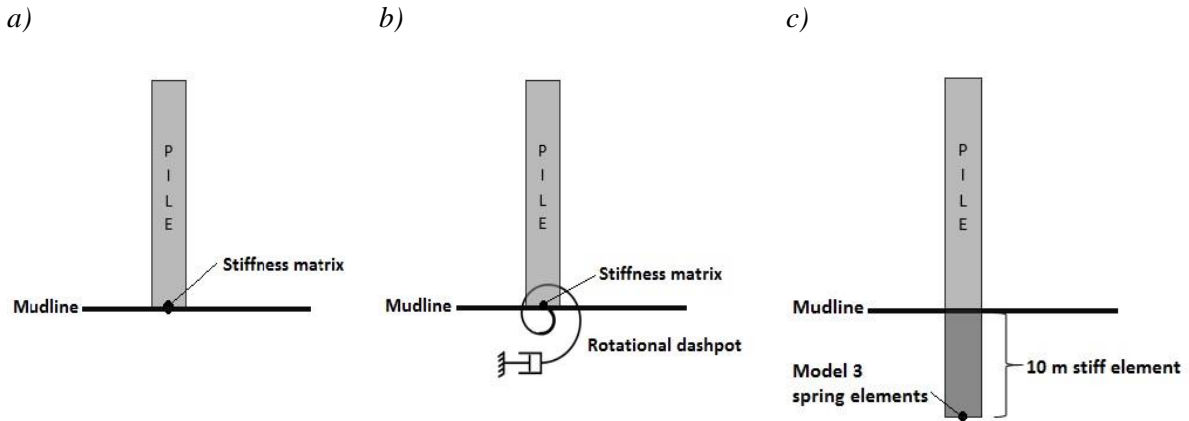


Figure 5.11: Soil-structure interaction models. a) Model 1, b) Model 2, c) Model 3. The figures are simplified by only showing two dimensions.

5.6.1 Model 1

Model 1 is a linear foundation model, developed by Passon (2006). The soil and pile response, is modelled by a stiffness matrix at the mudline node, as described in Chapter 3.1. The stiffness matrix is derived from results from pile analysis, with the software LPILE 4.0, and a soil profile according to that of OC3 Phase II. The reader is referred to Passon (2006) for more details on the reference model used to attain the stiffness coefficients. The model was developed for a two dimensional system, ignoring side-to-side movement of the tower. In 3DFloat, the horizontal- and rotational stiffness in the inertial x-z-plane has been used also for the y-z plane. The stiffness matrix at the mudline is given by:

$$\begin{bmatrix} k_{xx} & 0 & 0 & 0 & k_{x\beta} & 0 \\ 0 & k_{yy} & 0 & k_{y\alpha} & 0 & 0 \\ 0 & 0 & 0 & 0 & 0 & 0 \\ 0 & k_{\alpha y} & 0 & k_{\alpha\alpha} & 0 & 0 \\ k_{\beta x} & 0 & 0 & 0 & k_{\beta\beta} & 0 \\ 0 & 0 & 0 & 0 & 0 & 0 \end{bmatrix} \quad \begin{aligned} k_{xx} &= k_{yy} = 2.57481 \cdot 10^9 \text{ [N/m]} \\ k_{\alpha\alpha} &= k_{\beta\beta} = 2.62912 \cdot 10^{11} \text{ [Nm/rad]} \\ k_{x\beta} &= k_{\beta x} = -2.25325 \cdot 10^{10} \text{ [N/rad], [N]} \\ k_{y\alpha} &= k_{\alpha y} = 2.25325 \cdot 10^{10} \text{ [N/rad], [N]} \end{aligned}$$

, where x and y represent displacement in the horizontal plane, and α and β are rotations around the corresponding axis.

5.6.2 Model 2

This model uses the stiffness matrix from Model 1, with inclusion of rotational dashpot dampers. According to Carswell et al. (2015), it is argued that a rotational dashpot will represent soil damping better than a horizontal dashpot, as moment typically dominate the mudline loading for OWT monopiles. This approach has been adapted in this thesis, with rotational dashpots coefficients according to:

$$c_{\theta\theta} = c_{\beta\beta} = 9.34 \times 10^8 \text{ Nms/rad}$$

, where α and β are rotations around the horizontal axes at mudline. Unfortunately, the author was not able to attain hysteretic energy dissipation values for the soil profile of OC3. As an alternative approach, damping coefficients according to Carswell et al. (2015) has been used. In this study (Carswell, 2015), the hysteretic energy loss of the soil is retrieved by using the soil modelling software INFIDEL, developed by NGL. A rotational dashpot coefficient has been calculated according to the approach described in Chapter 3.3. For the soil profile and load level in Carswell (2015), this corresponded to a foundation damping factor (D) of 0.79%.

In 3DFloat simulations, the soil-damping coefficients has been constant throughout all 15 load cases, which does not represent realistic damping behavior. Soil damping is expected to increase, with higher load levels. As two different soil damping coefficients is provided in Carswell et al. (2015), a choice was made to use the damping coefficient generated from mudline displacements that correspond best with the load levels from 3DFloat simulations.

In Carswell et al. (2015), a different soil profile was used than that of OC3 Phase II. As the aim has been to study the influence of varied soil damping, rather than finding the correct soil damping for the given profile, the approach described above has been regarded the best alternative available for finding a damping coefficient, within the limitations of this thesis.

5.6.3 Model 3

Model 3 is a kinematic hardening model, as described in 3.2.3. The model has been developed by NGL, as part of the REDWIN project, described in the introduction. For a detailed description of the model development, the reader is referred to Page and Skau (2016).

In this approach, foundation response is represented by a set of linear perfectly-plastic springs. Each spring gives an elastic response up to a given load, where the spring yields. Displacements beyond the yield point gives a constant response, given by a yield moment. Unloading in each spring is elastic, giving a hysteretic behavior of the system. This is illustrated in Figure 5.12a. The total response of the system is given from a set of parallel-coupled springs, illustrated in Figure 5.12b. The figures are only conceptual. In 3DFloat, the response from the soil-foundation system, is given by a set of rotational springs connected to a common node ten meters under the mudline.

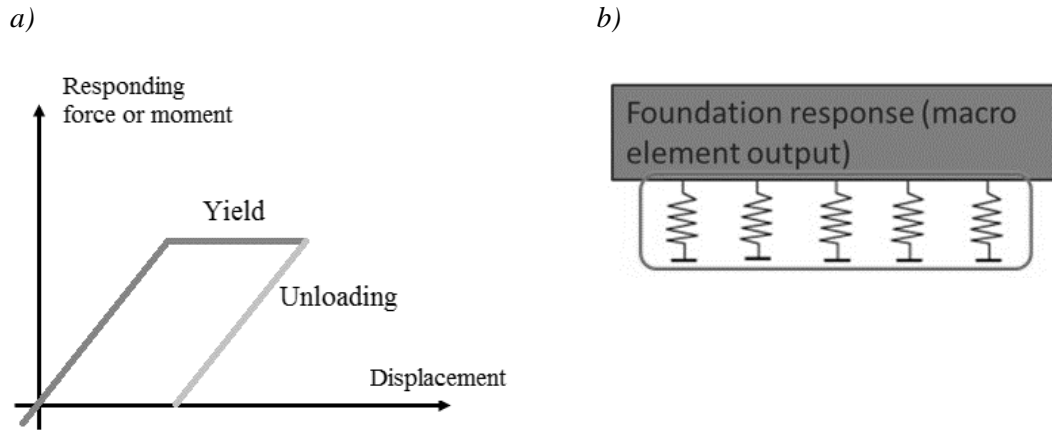


Figure 5.12: Foundation response of Model 3. a) Response from individual spring. b) Total response is given by parallel coupled springs. Figure from Page and Skau (2016).

For the system to represent realistic soil behavior, the set of spring elements has been calibrated according to the load-displacement curves for the soil profile, given in Chapter 5.5. An illustration of how this is done, is given in Figure 5.13. To give both rotation and lateral displacement at the mudline, a set of rotational springs has been attached to a decoupling point 10 m under the mudline. In 3DFloat, this has been solved by attaching a ten meter stiff element from the mudline to the decoupling point.

Two set of spring parameters is given. The first set of springs, has stiffness characteristics according to the loading test performed by Page and Skau (2016), presented in Chapter 5.5. A second set of spring parameters, with initial stiffness similar to that of the stiffness matrix from Passon (2006) has also been generated, so that damping properties of Model 2 and Model 3 can be compared, without stiffness properties determining the results.

**The yield load of spring no. 1 for the was changed by the author of this thesis. This was due to high loads in load case 6, making the turbine fall over. This indicated that the yield load has been underestimated. This will only affect the damping and stiffness characteristics of the model outside the load region of main interest. The old value was $8.741e7$ Nm. A high value was chosen, so that this spring will not give yield behavior.

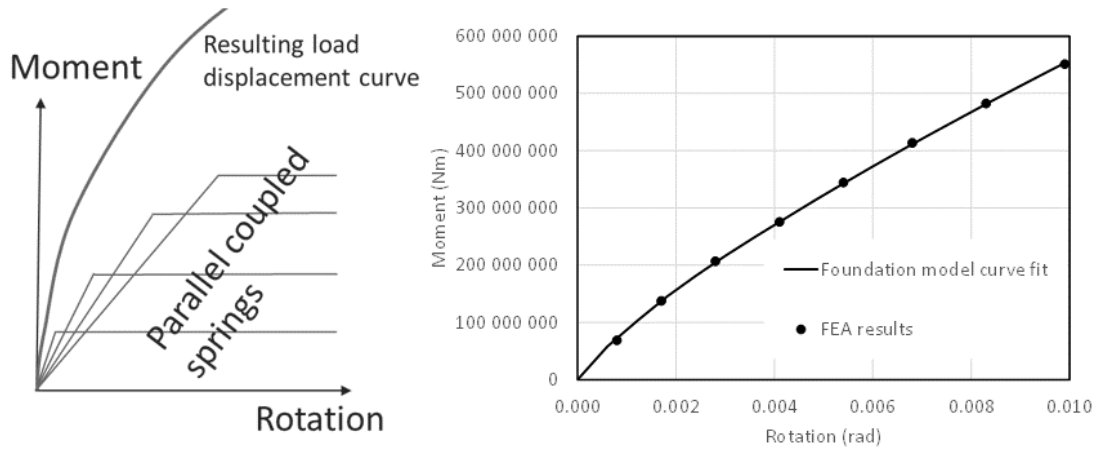


Figure 5.13: A set of parallel coupled springs gives a fit to the finite element analysis (FEA) of the soil. From from Page and Skau (2016).

Table 5.3: Parameters for Model 3

| Spring set 1 | | | Spring set 2 (updated stiffness) | | |
|--------------|--------------------|-------------------|----------------------------------|--------------------|-------------------|
| Spring no. | Stiffness [Nm/rad] | Yield Load [Nm] | Spring no. | Stiffness [Nm/rad] | Yield Load [Nm] |
| 1 | 63.69e9 | 8.741e10** | 1 | 45.00e9 | 8.741e10** |
| 2 | 1.858e9 | 2.253e6 | 2 | 1.858e9 | 2.253e6 |
| 3 | 2.064e9 | 2.181e6 | 3 | 2.064e9 | 2.181e6 |
| 4 | 2.435e9 | 2.205e6 | 4 | 2.435e9 | 2.205e6 |
| 5 | 2.883e9 | 2.192e6 | 5 | 2.883e9 | 2.192e6 |
| 6 | 3.278e9 | 2.033e6 | 6 | 3.278e9 | 2.033e6 |
| 7 | 3.594e9 | 1.749e6 | 7 | 3.594e9 | 1.749e6 |
| 8 | 4.119e9 | 1.477e6 | 8 | 4.119e9 | 1.477e6 |
| 9 | 1.462e9 | 3.469e5 | 9 | 1.462e9 | 3.469e5 |
| 10 | 1.255e9 | 1.478e5 | 10 | 1.255e9 | 1.478e5 |

5.7 Simulations run in 3DFloat

To find the impact of the different soil-structure interaction models, on fatigue damage and maximum moments, the following simulations has been run in 3DFloat:

Table 5.4: Simulations run in 3DFloat

| Soil-structure interaction model | $c_{\theta\theta}$ and $c_{\beta\beta}$ [Nm-s/rad] (only Model 2) | Load cases run | Real time simulation time for each load case [s] |
|----------------------------------|---|----------------|--|
| Model 1 | | 1-15 | 1800 |
| Model 2 (0.5D)** | 4.67e8 | 1-15 | 1800 |
| Model 2 (0.75D)** | 7.005e8 | 1-15 | 1800 |
| Model 2 (1.0D)** | 9.34e8 | 1-15 | 1800 |
| Model 2 (1.25D)** | 11.675e8 | 1-15 | 1800 |
| Model 2 (1.5D)** | 14.01e8 | 1-15 | 1800 |
| Model 3 | | 1-15 | 1800 |
| Model 3, updated stiffness | | 1-15 | 1800 |
| Free vibration tests | | | |
| Model 1 | | | 50s |
| Model 2 (1.0D)** | 9.34e8 | | 50s |
| Model 3 | | | 50s |
| Model 3, updated stiffness | | | 40s |

**The D 's are not related to the damping factor, but only an indication of the magnitude of the damping coefficients used.

The environmental conditions for all load cases are presented in Chapter 5.4.

As it takes some time for the rotor to accumulate momentum, and the generator to start, results are produced from 200s into the simulations.

6 Modelling and verification of turbine design

In this chapter, the structure of the wind turbine and its monopile foundation are presented, with their properties. The implementation in 3DFloat is reviewed, and a verification of the model is done by comparing eigen frequencies, with results from the 3rd offshore code comparison collaboration (OC3 - Jonkman and Musial, 2010). Special attention is given to resonance effects, as that would be detrimental to fatigue life.

6.1 The NREL 5MW monopile in 3DFloat

The NREL 5MW baseline turbine was developed by NREL, and has also been implemented by the European Union Upwind project. It is a utility-scale multimegawatt turbine that should give a representative design for simulation tools. The turbine is an upwind, three-bladed, variable-speed, variable-blade-pitch-to-feather controlled turbine (Jonkman and Musial, 2010). A summary of the turbine properties are given in the table below:

Table 6.1: Properties of the NREL 5 MW baseline wind turbine. Table from Jonkman and Musial (2010).

| | |
|--|------------------------------------|
| Rating | 5 MW |
| Rotor orientation, configuration | Upwind, 3 blades |
| Control | Variable speed, collective pitch |
| Drivetrain | High speed, multiple-stage gearbox |
| Rotor, hub diameter | 126 m, 3 m |
| Hub height | 90 m |
| Cut-in, rated, cut-out wind speed | 3 m/s, 11.4 m/s, 25 m/s |
| Cut-in, rated rotor speed | 6.9 rpm, 12.1 rpm |
| Rated tip speed | 80 m/s |
| Overhang, shaft tilt, precone | 5 m, 5°, 2.5° |
| Rotor mass | 110,000 kg |
| Nacelle mass | 240,000 kg |
| Tower mass | 347,500 kg |
| Coordinate location of overall center of mass (CM) | (-0.2 m, 0.0 m, 64.0 m) |

Monopile and tower

A detailed description of the structural properties of the tower with the monopile foundation is given in Jonkman and Musial (2010). In 3DFloat, two node Euler-Bernoulli beams model the tower and pile foundation. Different sections is defined by two reference nodes that defines the center of the cylinder top and cylinder bottom. For each node, a cylinder diameter and thickness is defined. 3DFloat will then mesh the given cylinder into a chosen number of beam elements, with linearly increasing wall thickness and diameter. Table 6.2 gives the properties of the monopile and the tower according to the 3DFloat implementation. In the reference model, the monopile is not defined under the mudline, as the total soil response is given at the mudline node.

The transition piece, that connects the pile and the tower, has not been given attention in this thesis. The design has been simplified according to OC3 properties of the structure.

Table 6.2: Tower and monopile definition in 3D float

| Section | Length (L), diameter (D), wall thickness (T) | Number of elements |
|----------------------------|---|--------------------|
| Monopile | L:30m, D:6m, T:6cm | 6 |
| Tower - Bottom - Top | L: 77.6m D: 6m, T: 3.5cm D: 3.87m, T: 2.4cm | 20 |

Nacelle and hub

For structural design in 3Dfloat, the nacelle/hub system is modelled with Euler Bernoulli beams. As the tower and monopile use standard structural steel properties, the nacelle stiffness has been chosen to give representative dynamic responses of the structure, compared with OC3 results. The nacelle stiffness has also been calibrated to avoid resonance effects with the $3p$ load frequency. Point masses has been applied to the nacelle to give equivalent center of mass to the NREL 5MW monopile turbine. For a detailed description, the 3DFloat input file has been attached in the appendix.

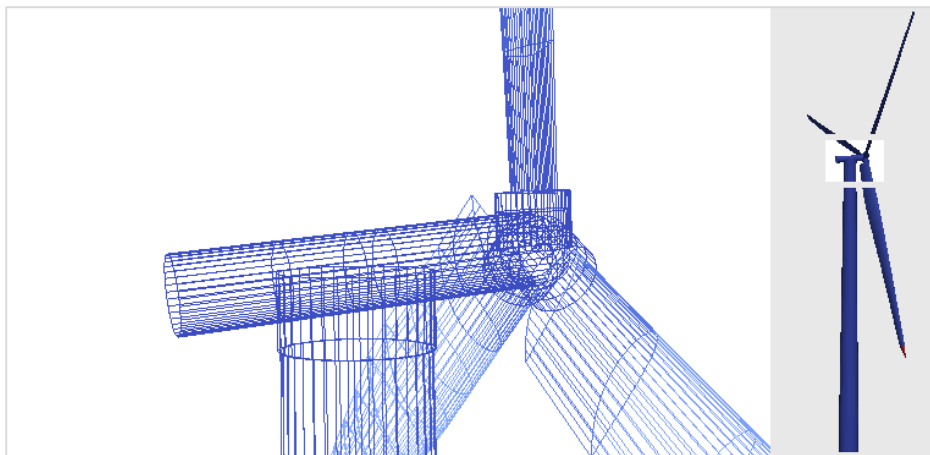


Figure 6.1: Nacelle in 3DFloat

Blade properties and control system

Blades with both structural- and aerodynamic properties are defined in 3DFloat, with structural properties directly given in the input file. Aerodynamic properties are read from data files. A detailed description of both structural- and aerodynamic properties can be found in chapter three in Jonkman et al. (2009). The aerodynamic properties are defined by lift-, drag- and pitching moment coefficients for different angles of attack. A pitch control system from the OC3 project has been used for blade pitch control. (Name: 5mw_floating, Control type: iea_oc3_floating)

Soil-structure interaction model

For the reference system a stiffness matrix has been applied at the mudline. The applied stiffness matrix is according to Passon (2006), but extended to a three dimensional system (Soil-structure interaction model: Model 1).

6.2 Eigen frequency analysis

The aim of this section is to do an eigen frequency analysis of the 3DFloat model of the NREL 5MW wind turbine. This is to verify that eigen frequencies corresponds with other simulations from the OC3 project (Phase II), where several programs were used to analyze the NREL 5MW wind turbine. Special attention will be given to resonance, to make sure fatigue damage will not be significantly influenced, as this parameter will be used to study influence on soil-interaction models. The results from OC3 Phase II can be found in Jonkman et al. (2010).

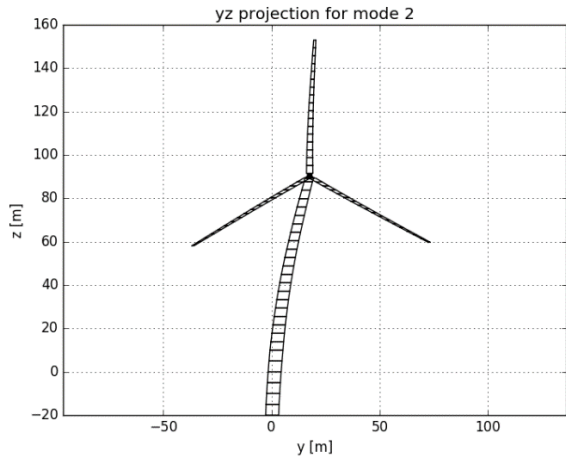
Eigen frequencies and mode shapes

In the OC3 (Phase II) eigen frequency analysis, the structure had a stiffness matrix at the mudline, with gravity and structural damping enabled. Water and air density was set to zero. For Eigen frequency analysis, 3DFloat finds the free undamped vibrations, as described in chapter 4.1. The results from 3DFloat is presented in Table 6.3 and Figure 6.2.

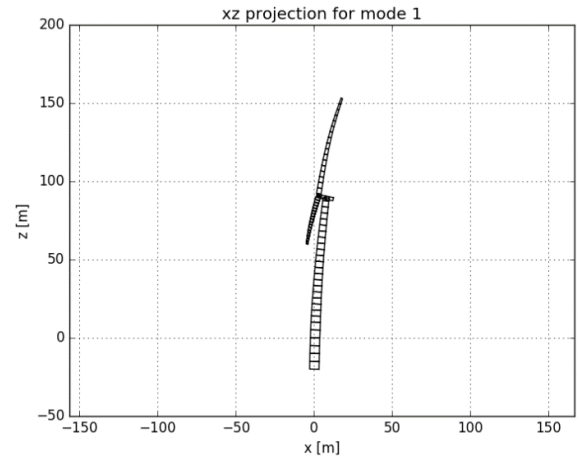
Table 6.3: Eigen frequencies of structure in 3DFloat

| # | Mode shape | Frequency [Hz] |
|----|---|----------------|
| 1 | 1 st Tower Fore-Aft | 0.255 |
| 2 | 1 st Tower Side-To-Side | 0.257 |
| 3 | 1 st blade assymetric flapwise yaw | 0.625 |
| 4 | 1 st blade assymetric flapwise pitch | 0.650 |
| 5 | 1 st blade collective flap | 0.680 |
| 6 | 1 st blade assymetric edgewise yaw | 1.061 |
| 7 | 1 st blade assymetric edgewise pitch | 1.072 |
| 8 | 2 nd Tower Fore-Aft | 1.509 |
| 9 | 2 nd Tower Side-To-Side | 1.579 |
| 10 | 2 nd blade assymetric flapwise yaw | 1,677 |
| 11 | 2 nd blade assymetric flapwise pitch | 1,895 |

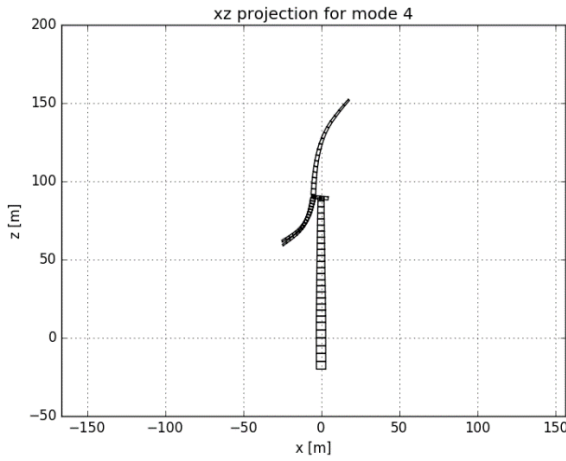
Mode 3, 4 and 5 are highlighted, as they are close the $3p$ frequency, imposed on the structure by the blades. A comparison with OC3 Phase II results, is given at the end of this section.



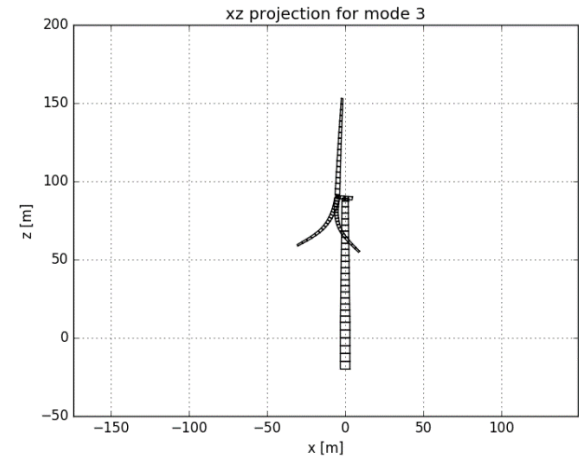
a) 1st tower side-to-side



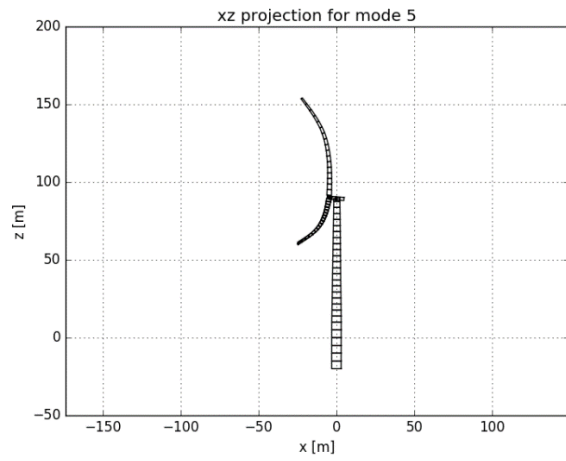
b) 1st tower fore-aft



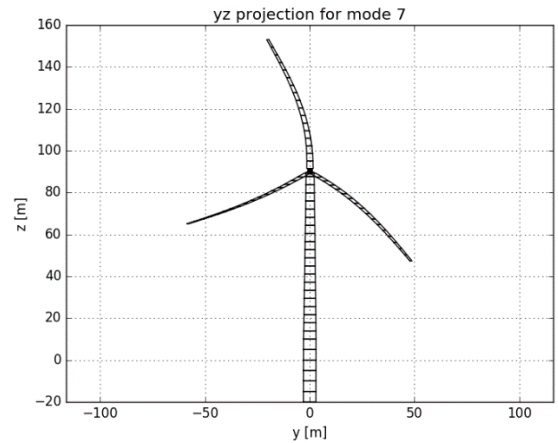
c) 1st blade asymmetric flapwise pitch



d) 1st blade asymmetric flapwise yaw



e) 1st blade collective flap



f) 1st blade asymmetric edgewise pitch

Figure 6.2: Visualization of selected mode shapes

As given in Table 6.1, the cut-in frequency for the rotor is 6.9rpm or 0.12Hz, and the rated rotor speed is 12.1 rpm or 0.20Hz. The equivalent $3p$ will then be at 0.35Hz and 0.61Hz. A visualization of the rotor frequency p and $3p$ with the eigen frequencies of the structure is given in Figure 6.3. It can be seen that mode 3, 4 and 5 are close to $3p$, being over by 3.3%, 7,4% and 12,4%.

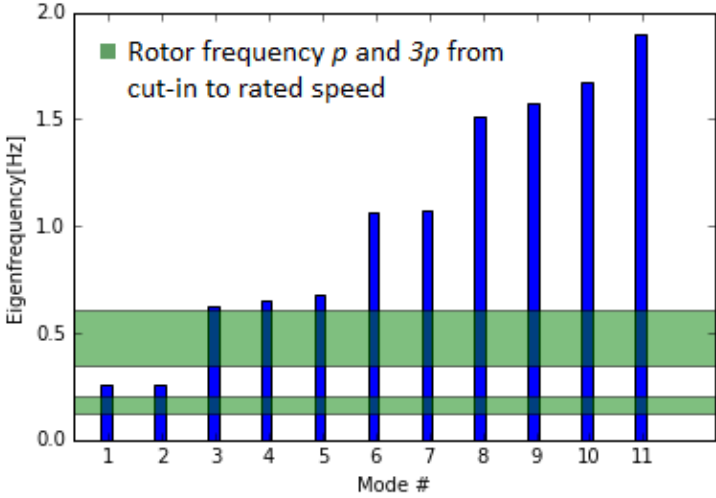


Figure 6.3: Eigen frequencies compared with rotor loads.

Fast fourier transform to look for resonance effects

To see how eigen frequencies influence dynamic simulations, a 3DFloat simulation with irregular waves and turbulent wind was conducted. The mean wind speed was set to 12m/s and the significant wave height to 2m. Simulation time was set to 2000 seconds. A fast fourier transform was done on the blade root moment, to see if there were frequency components around $3p$. Especially the blade root moment in the flapwise direction is of interest, as both mode 3,4 and 5 are flapwise blade modes. The fast fourier transform was done with data from 3DFloat output files, and analyzed with a python script using fast fourier transform from the numpy.fft library.

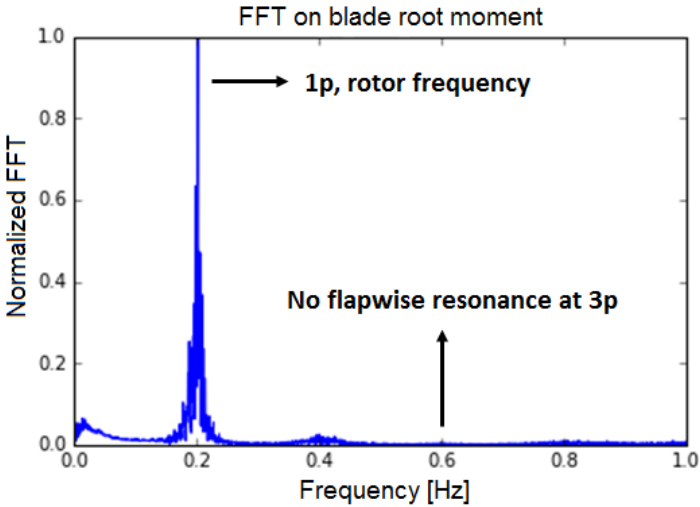


Figure 6.4: Normalized amplitude spectrum of blade root moment (flapwise).

Figure 6.4 shows the normalized amplitude spectrum for the flapwise blade root moment. There is no sign of resonance around $3p$ at 0.61Hz. The $1p$ effect due to blade shadowing and logarithmic wind profile is clearly displayed. The $3p$ load mainly acts on the tower and is only expected to influence individual blades through feedback response from the tower. The results indicates that the feedback response is weak, and therefore do not influence blade dynamics significantly.

Comparison with OC3 Phase II results

The author did not have access to numerical values from other eigen frequency analysis on the given turbine, but a bar plot is provided from OC3 Phase II, as shown in Figure 6.5. Each bar represent results from different simulation software. Only a qualitative comparison with 3DFloat results is conducted.

By comparing Figure 6.5 with Figure 6.3 it can be seen that 1st tower frequencies are roughly at 0.25Hz, 1st blade flapwise frequencies are around 0,6 Hz, 1st blade edgewise frequencies around 1.1 Hz, and 2nd tower- and blade flapwise modes are between 1.5 and 2.0 Hz. 3DFloat results corresponds well with this. Comparison with numerical values would be preferable, but this was not presented in the available reports. Still this indicates that the 3DFloat model gives structural responses similar to what would be expected.

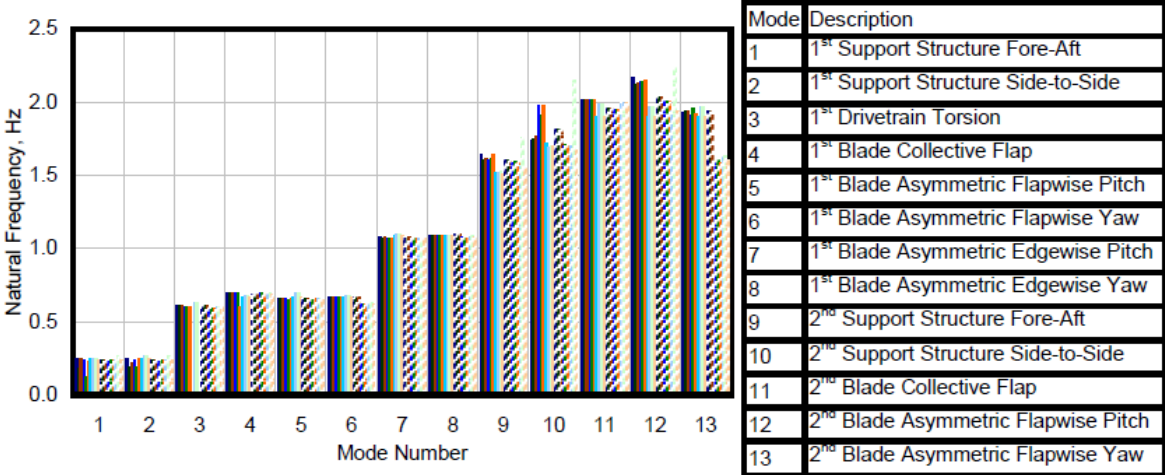


Figure 6.5: Eigen frequencies according to OC3 Phase II (Jonkman and Musial, 2010).

7 Results and discussion

For readability of the thesis, results and discussions are presented interchangeably. Comments and discussions will be placed before the figure that is being discussed. The chapter will be divided in four subchapters:

1. Soil-structure interaction model characteristics.
2. Fatigue damage and maximum moments at different locations of the OWT.
3. Results with updated Model 3 parameters.
4. Summary of results

Section 1, presents results from a free vibration test, and fast fourier transform on two selected load cases, for all three soil-structure interaction models. This has been done to identify damping and stiffness characteristics of the different models.

Section 2, presents the main findings of this thesis. This section presents the impact of the different soil-structure interaction models, on fatigue damage and maximum moments.

Section 3, presents the fatigue damage with updated model parameters for Model 3. As Model 3 reduces fatigue damage significantly compared with model 1, and at the tower root, also compared with model 2, there was an interest towards the end on the project, to find out if this was caused by the stiffness or damping properties of Model 3. With new stiffness, calibrated to match that of Model 2, new simulations were run. Results for the mudline and tower root are presented, with new Model 3 characteristics.

Section 4, presents the main results of this thesis in a condensed form.

7.1 Model characteristics

7.1.1 Free vibration tests

Starting from a tower top displacement of 0.1 m, Figure 7.1 presents the free vibration test. Figure 7.2 presents a zoomed in figure. It can be seen from the free vibration test that Model 3 gives a stiffer behavior relative to Model 1 and 2, as the vibration frequency is higher. Model 1 and 2 shows the same vibration frequency, as it has the same stiffness matrix attached at the mudline. From Figure 7.2 it can be seen that Model 2 has the highest soil damping effect. Model 1, Model 2 and Model 3 have the same structural, aerodynamic and hydrodynamic damping. In addition, Model 2 includes damping by a rotational dashpot, and Model 3, hysteretic damping by the kinematic hardening effects. The damping effect of Model 3 is expected to increase with higher load amplitudes.

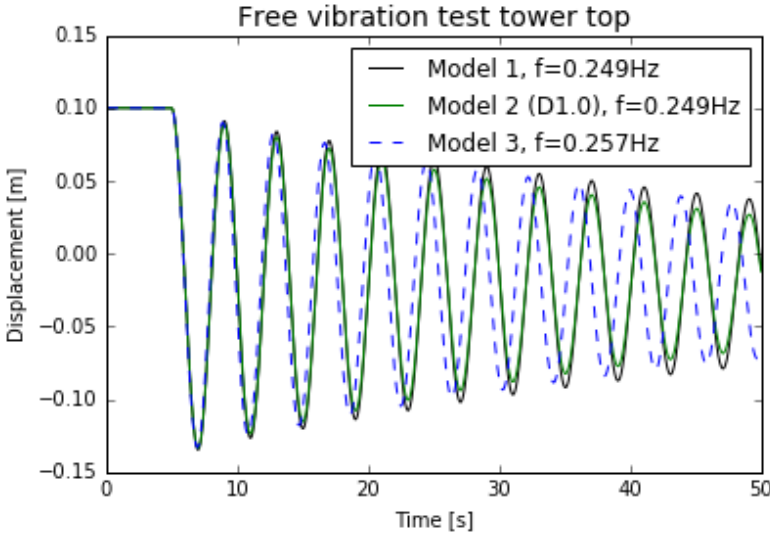


Figure 7.1: Free vibration test with 0.1 m tower top displacement.

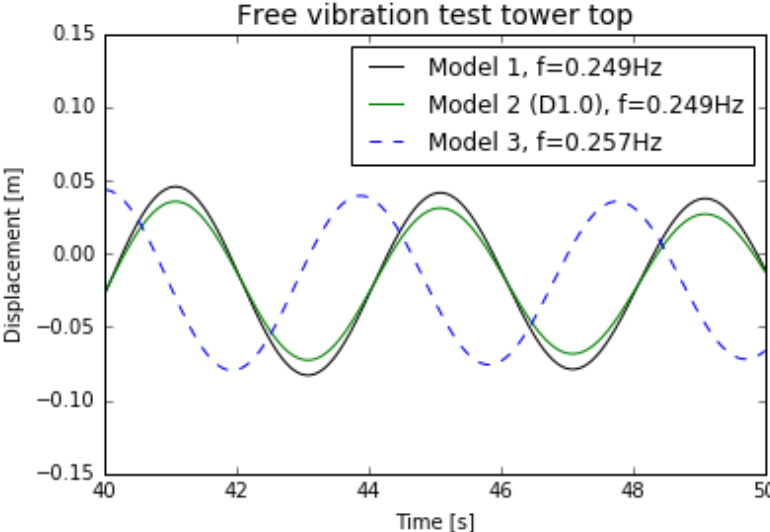


Figure 7.2: Free vibration test with 0.1 m tower top displacement, zoomed in.

7.1.2 Fast fourier transform on idling cases

Figure 7.3 presents the amplitude spectrum from a fast fourier transforms on mudline moments (around inertial y-axis), for load case 1. We see Model 1 and 2 having their main frequency components, just below 0.25Hz, at the 1st tower fore-aft eigen frequency. Model 2 has a reduced amplitude spectrum, due to the modelled viscous soil damping. Model 3 has its main frequency components slightly over 0.25Hz, at the 1st tower fore-aft eigen frequency of Model 3. Here the amplitude spectrum is further reduced.

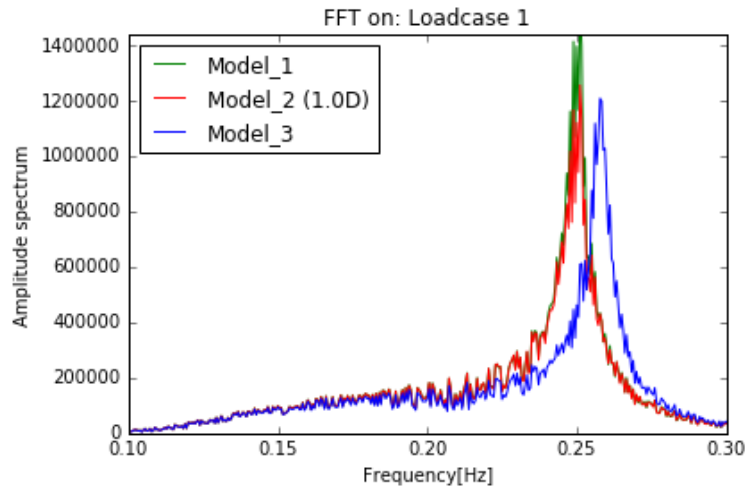


Figure 7.3: Fast fourier transform on mudline moments for load case 1.

Figure 7.4 presents fast fourier transforms on mudline moments (around inertial y-axis), for load case 13. The figure shows the same behavior as for load case 1, but with a higher contribution from lower frequency components. In load case 13, waves are significantly higher, leading to higher load amplitudes for frequencies below 0.25 Hz.

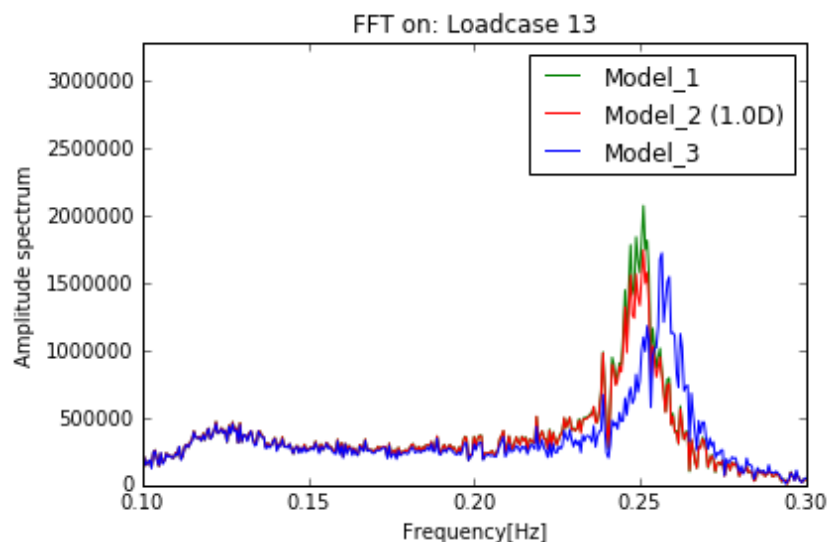


Figure 7.4: Fast fourier transform on mudline moments for load case 13.

7.2 Fatigue damage and maximum moment at different locations

The following results will be present according to positions on the OWT structure, from bottom to top. Results for all three soil-structure interaction models are presented in the same figures, even though there is not an interest of comparison between them in all the figures. For better navigation in the text, a discussion will be placed before the figure of interest, for each position on the OWT structure. In chapter 8, a more general discussion, with the main finding of the thesis, will be presented.

In this section the results it is important to have in mind that load case 1,13,14 and 15 are idling cases, where the rotor blades are pitched out of the wind, with the rotor free to rotate.

7.2.1 Pile at mudline

Total accumulated fatigue damage

Total accumulated fatigue damage summed for all load cases, is given in Figure 7.5. As seen in the figure, the accumulated fatigue damage is clearly decreasing, when soil damping is introduced (Model 2). The decrease in fatigue damage in Model 3, is mainly due to the stiffness characteristics of the model, as can be seen in chapter 7.3.

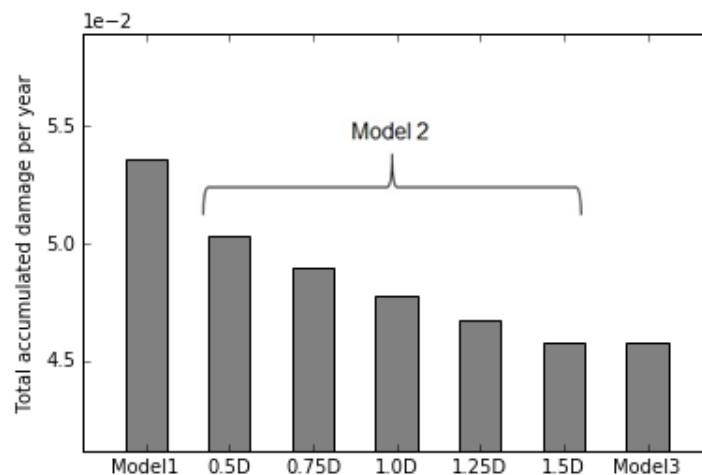


Figure 7.5: Total accumulated fatigue damage per year at mudline, arranged by soil-structure interaction model.

Accumulated fatigue damage arranged by load case

Figure 7.6 presents the relative accumulated fatigue damage by load case. Results are normalized relative to the highest value. Each load case is also probability weighed, according to Table 5.2 (p. 33)

The following trends are evident:

1. Model 1 produces the highest fatigue damage.
2. The fatigue damage in Model 2 decreases, with increasing soil damping.
3. Model 3 gives relatively higher fatigue damage in operational cases (LC 2-12), than in idling cases (LC 1&13-15), compared to Model 2.
4. The soil damping effect is stronger for idling cases, than for operational cases.

Comments on the observed trends:

1. As Model 1 has no soil damping introduced, structural energy is not dissipated in the soil. Logically, this allows for higher displacement- and load amplitudes at the mudline, which leads to higher fatigue damage.
2. The same argumentation as for ‘1.’ holds here, as increased soil damping leads to decreased displacement- and load amplitudes.
3. Model 3 gives damping as a function of load level, whereas damping from model 2 is depending on displacement rate of change. As idling cases bring higher load amplitudes than operational cases, and thereby more damping from Model 3, this explains the differences we see in operational vs. idling cases. Figure 7.8 presents damping as a function of load amplitude from Model 3. Chapter 7.3 shows how the stiffness of Model 3 also has influenced the results.
4. In operational cases, with a rotating rotor, aerodynamic damping gives a high contribution to the total damping of the system. Because of this, soil damping has a smaller relative effect on the full OWT system. In addition to this, load amplitudes are higher for idling cases, due to less aerodynamic damping. Higher load amplitudes increase the damping effect in Model 3. A plot of representative load amplitudes at the mudline is given in Figure 7.7.

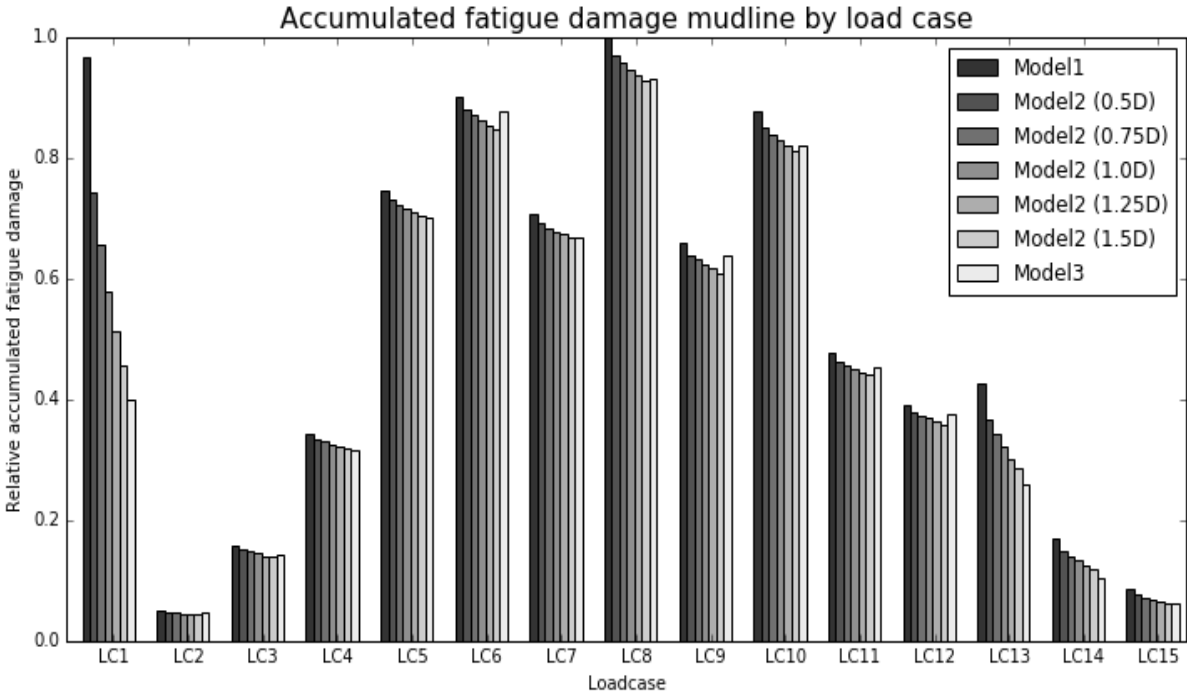


Figure 7.6: Normalized accumulated fatigue damage by load case at mudline

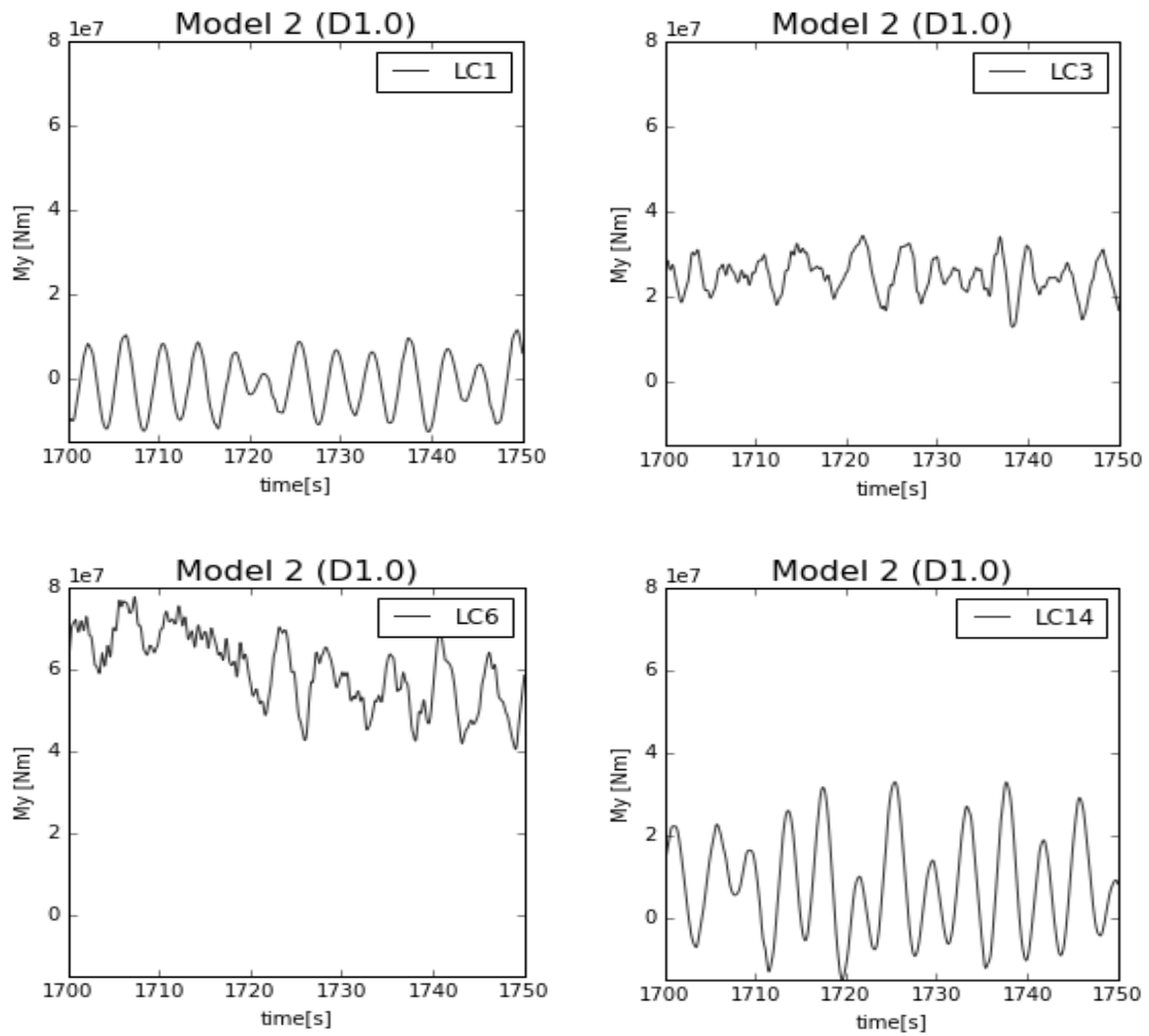


Figure 7.7: Moment about inertial y-axis at mudline for selected load cases.

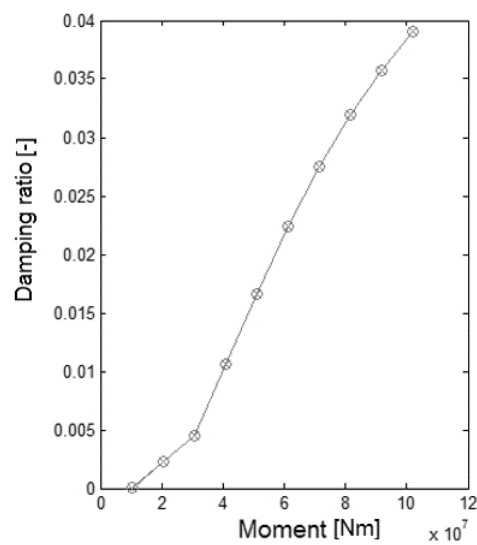


Figure 7.8: Damping ratio provided by Model 3, as a function of load level. Figure from Page and Skau (2016)

Figure 7.9 presents the accumulated fatigue damage, arranged by load case, but contrary to Figure 7.6, this figure is not weighed by probability of occurrence. Each column represents 1600 seconds of real time simulation. As seen in the figure, idling cases (LC 1 & 13-15) give high fatigue damage, compared with operational cases. Load case 1, with little wind (2 m/s) and small wave height (1.07 m), gives fatigue damage at the level of load case 8 and 9, which much harsher environmental conditions, but an operational rotor. This shows the significant effect of aerodynamic damping. Even though absolute values are higher, stress amplitudes at the mudline is strongly reduced by aerodynamic damping. With less aerodynamic damping, soil- and structural damping gives higher influence on fatigue damage, as seen in the figure. Structural damping in this thesis has been at 1%, according to OC3 specifications. It has been questioned if this is underestimated - therefore further studies regarding this is suggested.

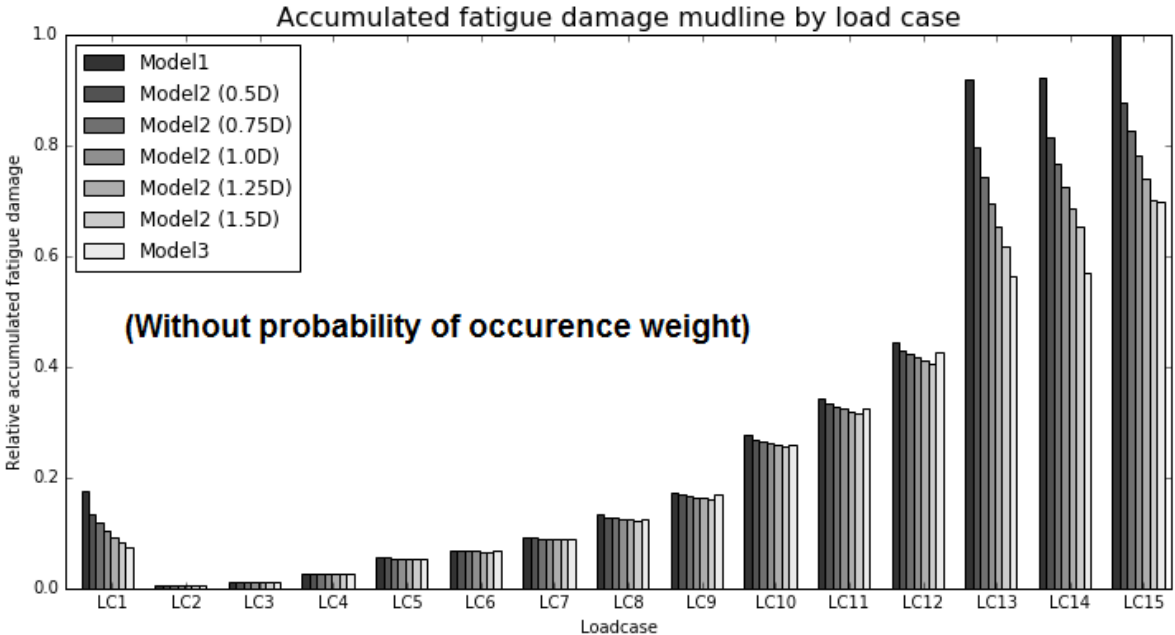


Figure 7.9: Normalized accumulated fatigue damage by load case at mudline, without probability weight.

Maximum moment at mudline

The maximum moment (M_y in inertial axis system) at the mudline, is given in Figure 7.10. For idling cases, we see that maximum moment tend to decrease, with increased soil damping coefficient. As load amplitudes are high for the idling cases, the damping effect becomes evident. In operational cases, soil damping has a smaller effect on maximum loads. It is Important to underline that fatigue damage is a function of load amplitudes, and not absolute values. Even though absolute values are highest for load case 5,6 and 7, load amplitudes are higher for load case 13, 14 and 15.

This highest moment is observed for load case 5. Here the wind speed is just under rated conditions (11.2 m/s). From load case 6-12, the pitch control reduces the maximum moments.

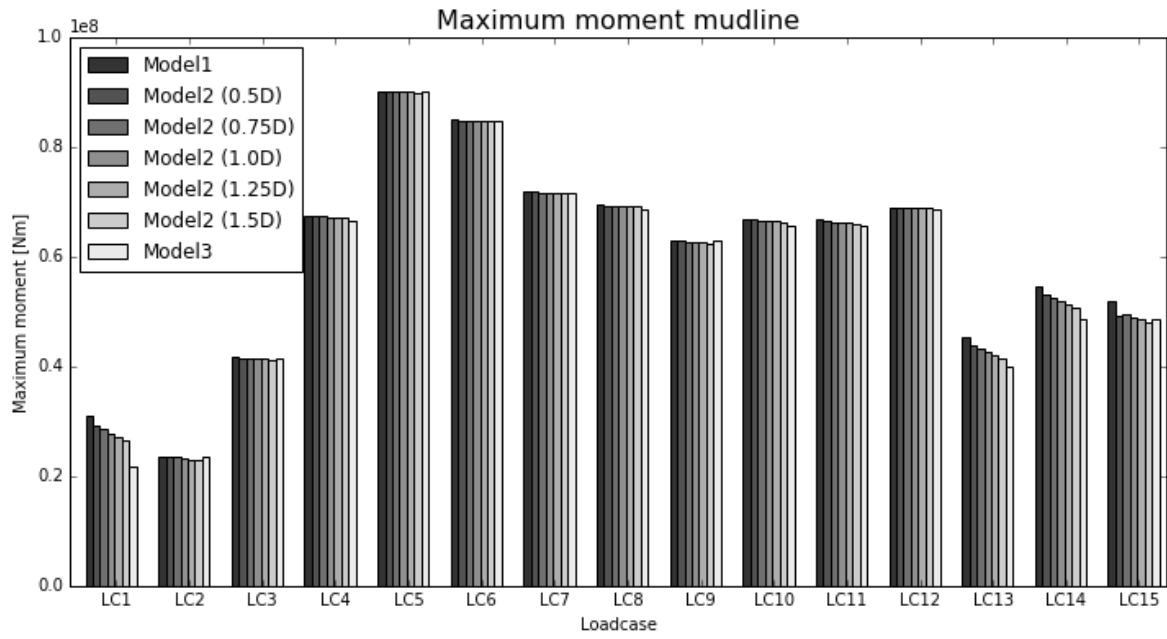


Figure 7.10: Maximum moment at mudline arranged after load case.

7.2.2 Tower root

Total accumulated fatigue damage at the tower root

Total accumulated fatigue damage for all load cases is given in Figure 7.11. As for mudline, the fatigue damage is decreasing, with increased soil damping coefficient. At the tower root we see the same trend as for the mudline, but Model 3 gives an even stronger reduction of fatigue damage. This will be further discussed below.

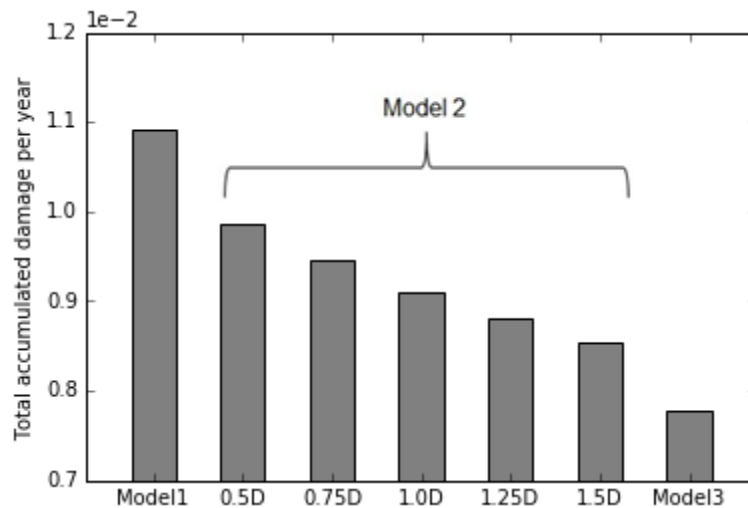


Figure 7.11: Total accumulated fatigue damage per year at tower root, arranged by soil-structure interaction model.

Accumulated fatigue damage at the tower root arranged by load case

Figure 7.12 presents the relative accumulated fatigue damage at the tower root by load case. Results are normalized relative to the highest value. Each load case is also probability weighed, according to Table 5.2 (p. 33).

In general, we see the same trends as for the mudline, with some exceptions.

The exceptions are the following:

1. Load case 1 has a higher relative contribution to the total accumulated fatigue damage.
2. Model 3 gives reduced fatigue damage also for operational cases compared with Model 2 (1.5D). This was mainly seen for idling cases, at the mudline.

Because of time limitation, no in depth analysis has been done on the differences mentioned above. Still the author suggest the following explanation for the observed differences:

In addition to having different damping characteristics compared with Model 2, Model 3 has different stiffness. This is seen in the free vibration analysis in Chapter 7.1, where a higher vibration frequency implies higher system stiffness. This influence the mode shape, and eigen frequencies of the structure, which in turn influence the stress level at the tower root.

Further investigation is needed, to verify the explanation given above.

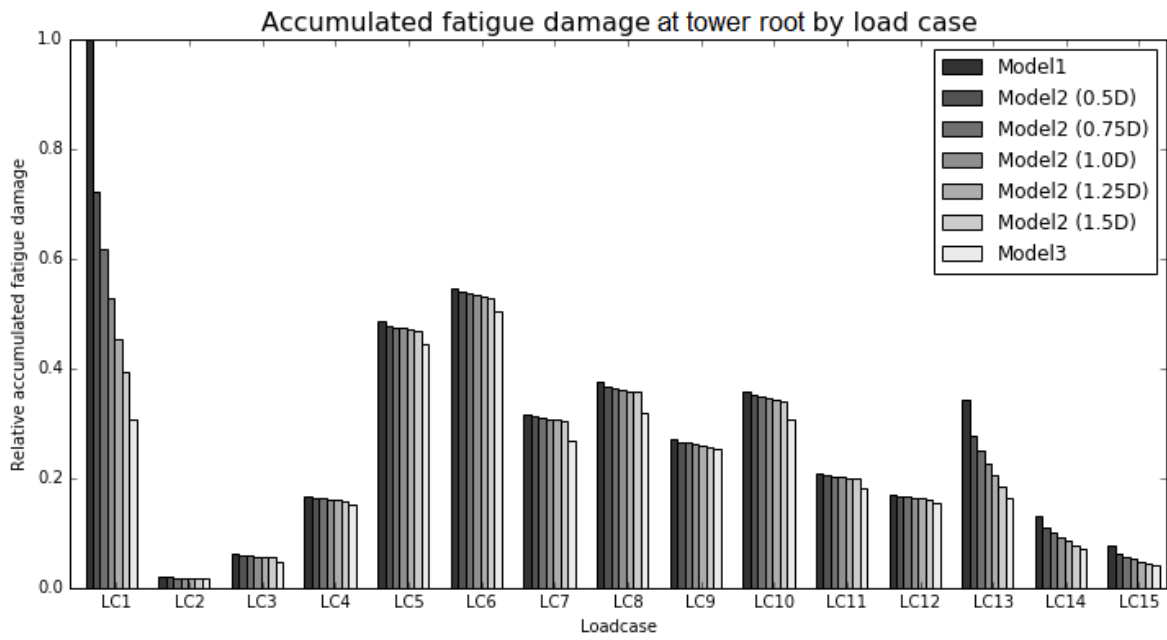


Figure 7.12: Normalized accumulated fatigue damage by load case at tower root.

Maximum moment at tower root

The maximum moment for the tower root is given in Figure 7.13. In general, the maximum moment decreases, with increased soil damping. The same trends is seen as at the mudline.

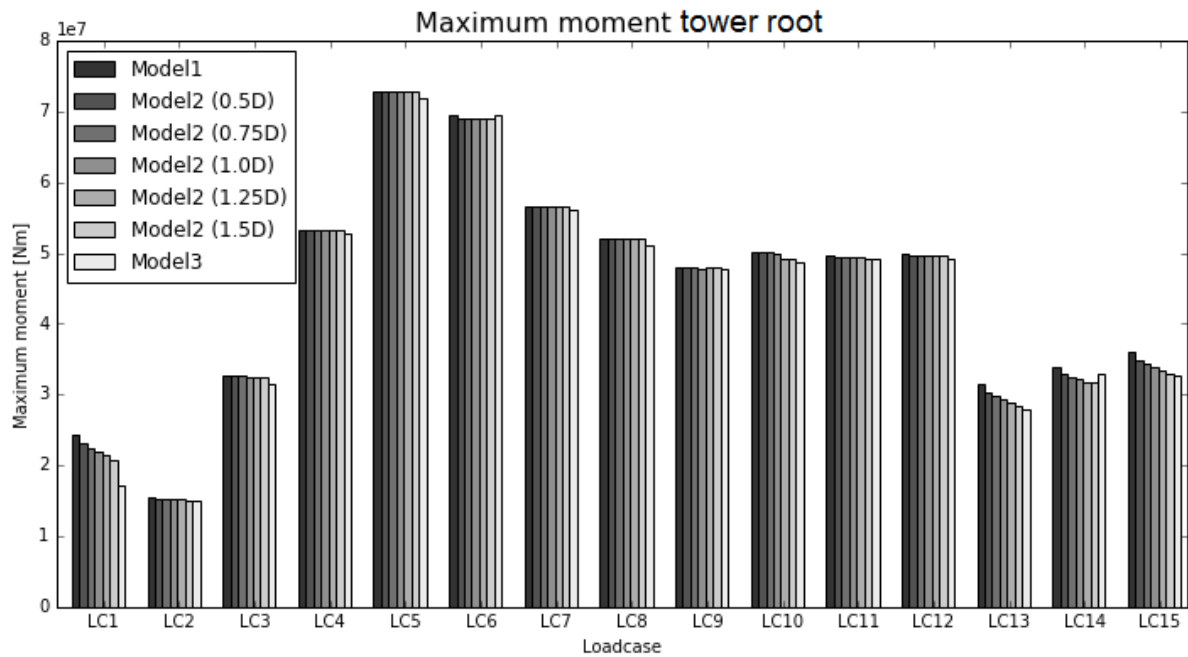


Figure 7.13: Maximum moment arranged by load case, at tower root.

7.2.3 Tower top

Total accumulated fatigue damage

Total accumulated fatigue damage at the tower top, is given in Figure 7.14. As the figure shows, the influence of the different soil-structure interaction models is small. The results indicate that the soil response has little influence on tower top loads. This will be further discussed below.

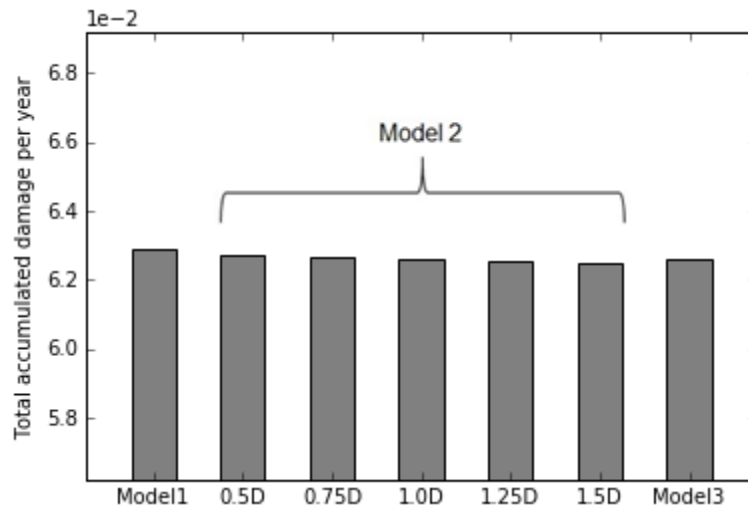


Figure 7.14: Total accumulated fatigue damage per year at tower top, arranged by soil-structure interaction model.

Accumulated fatigue damage arranged by load case at tower top

Figure 7.15 presents the relative accumulated fatigue damage by load case. Results are normalized relative to the highest value. Each load case is also probability weighed, according to Table 5.2 (p. 33).

Soil-structure interaction model gives little influence on fatigue damage at the tower top, as would be expected from Figure 7.14. Still a small reduction can be observed as a function of increase soil damping for Model 2. In the figure, this is visible for load case 6,7 and 9.

At the tower top, rotor dynamics gives the highest load amplitudes and thereby fatigue damage, whereas on the mudline and tower root, tower fore-aft movements, and its resulting bending moments, dominates fatigue damage. As the soil response has much higher influence on tower fore-aft movement, than on rotor dynamics, this explains why we see little influence at the tower top, when varying the soil response.

The argument above, also explains why contributions from idling cases are very low. As the rotor is idle, the $3p$ load cycles caused by the rotating blades, are absent.

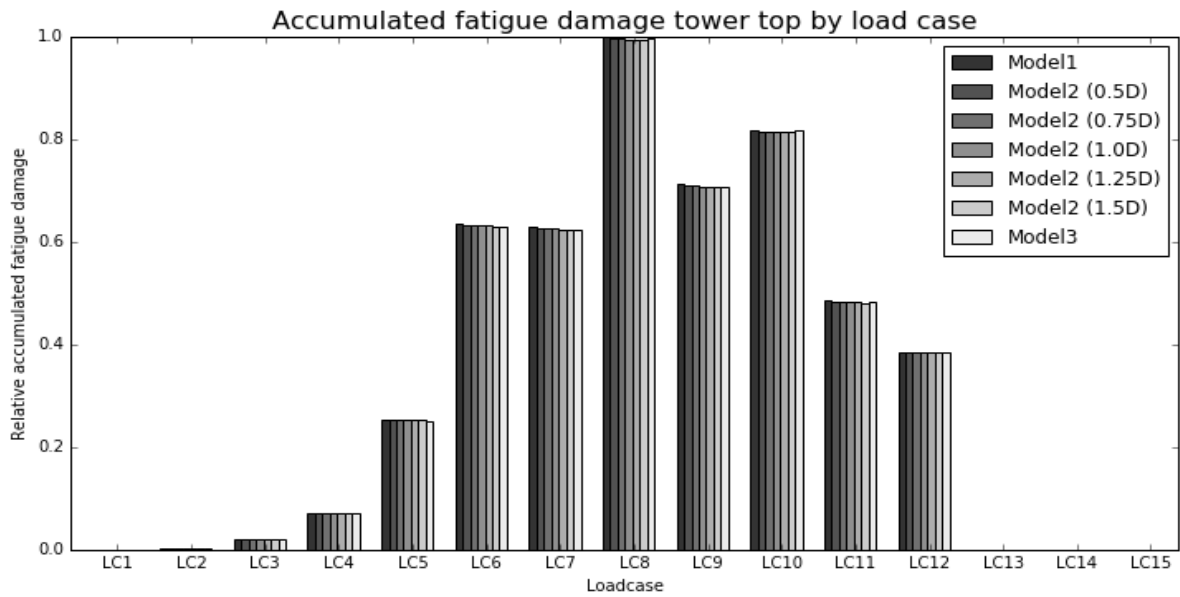


Figure 7.15: Normalized accumulated fatigue damage at tower top, arranged by load case.

Maximum moments at tower top

Maximum moments at the tower top, is given in Figure 7.16. Moment is increasing with wind speed, but little variation is seen with respect to soil damping value. The highest influence is seen for the idling cases, but as they have little influence on fatigue life, the total impact on the system is insignificant. As observed variations is of little significance for fatigue damage, this will not be further discussed.

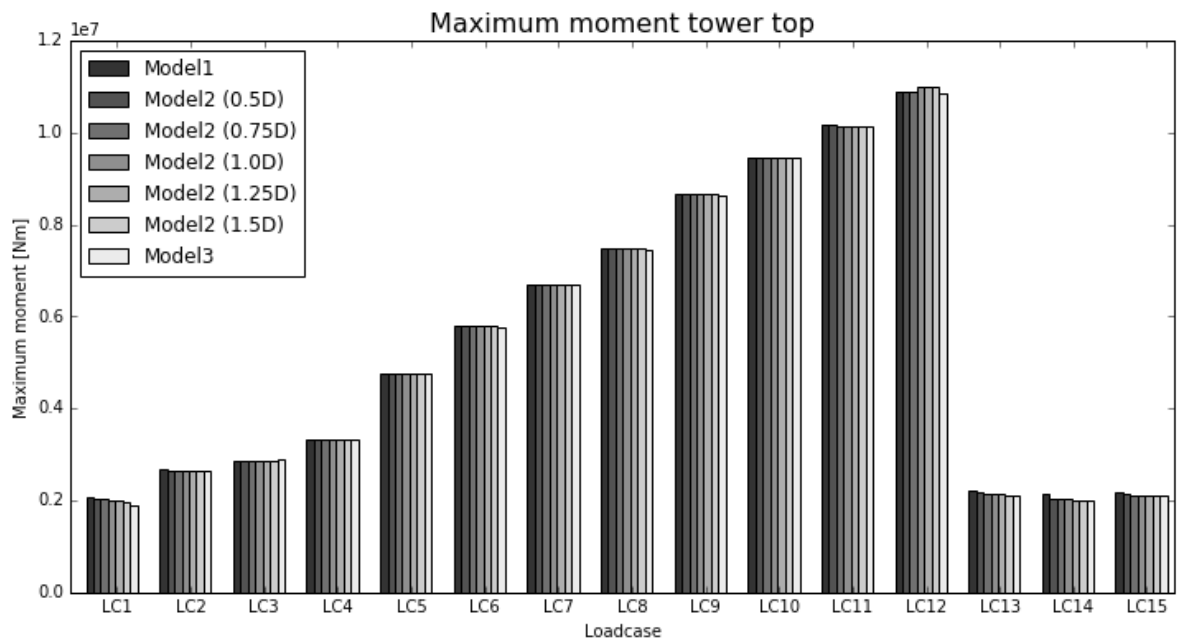


Figure 7.16: Maximum moment at tower top, arranged by load case.

7.2.4 Blade root

Total accumulated fatigue damage at the blade root is given in Figure 7.17. As for the tower top, we see little variation with increased soil damping.

Figure 7.18 presents the relative accumulated fatigue damage by load case. Results are normalized relative to the highest value. Each load case is also probability weighed, according to Table 5.2 (p. 33).

The maximum moment at the blade root is given in Figure 7.19. There is little influence of the soil-structure interaction model. We see the maximum moment being relatively equal for load case 5-12, where blade pitch control regulates the aerodynamic forces on the rotor blades.

As soil-structure interaction model has an insignificant impact on the results, the results for the blade root will not be discussed any further.

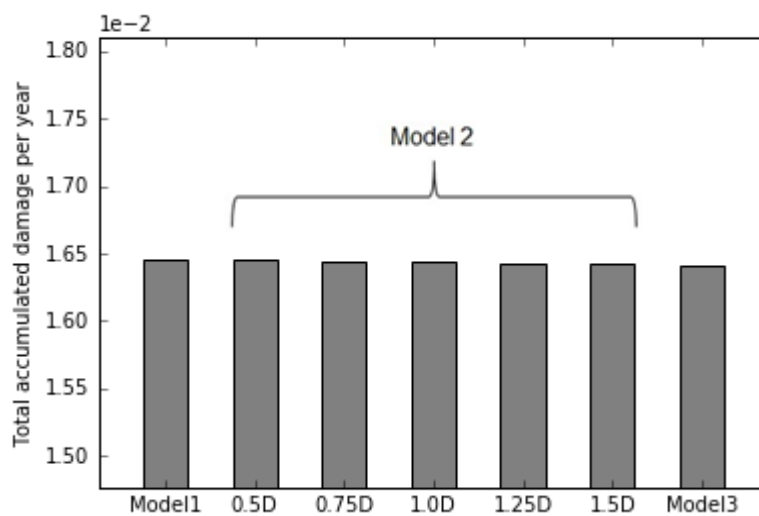


Figure 7.17: Total accumulated fatigue damage per year at blade root, arranged by soil-structure interaction model.

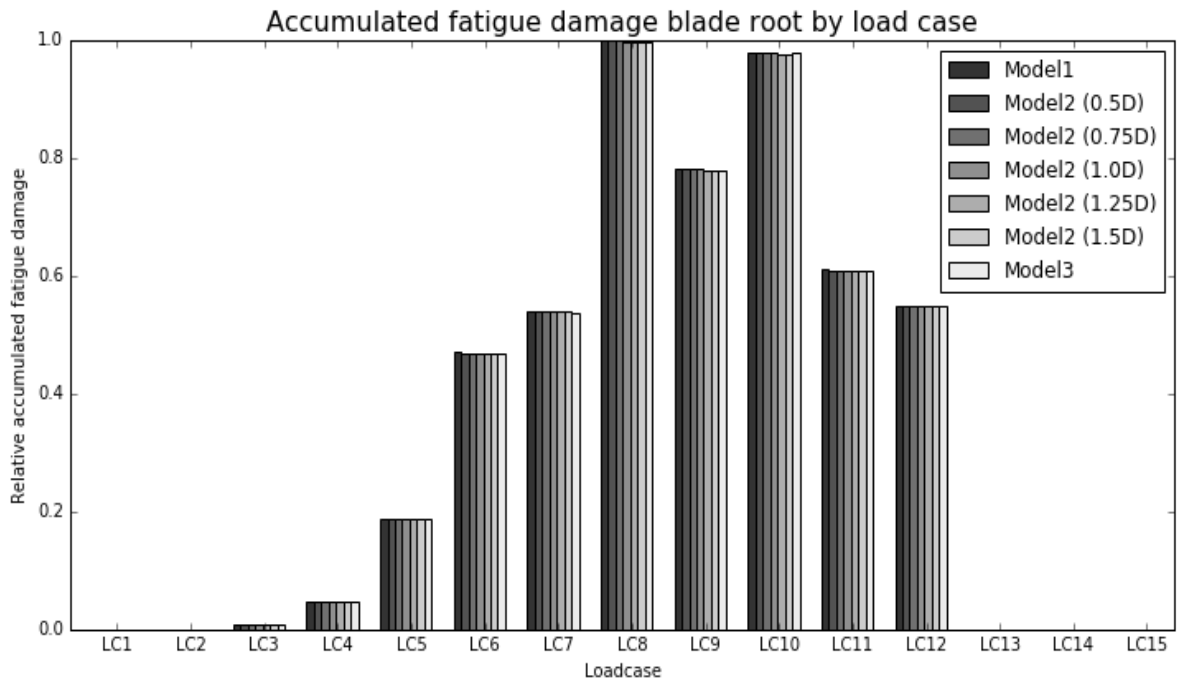


Figure 7.18: Normalized accumulated fatigue damage at blade root, arranged after load case.

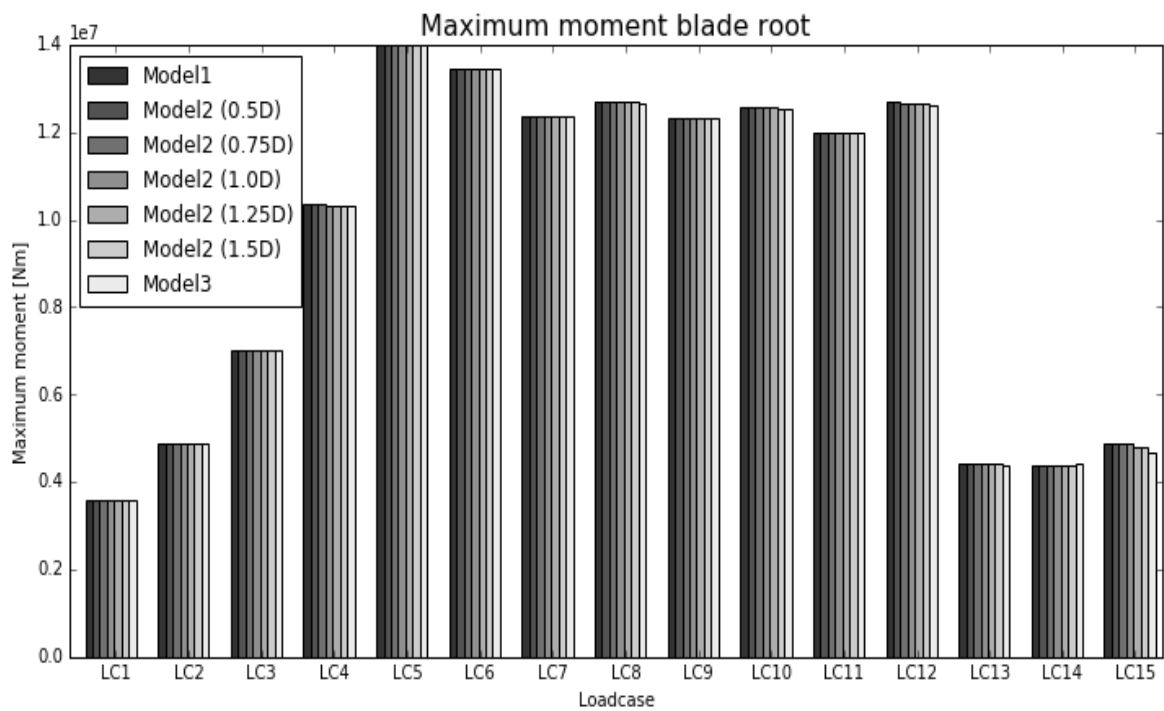


Figure 7.19: Maximum moment at blade root, arranged after load case..

7.3 Results with updated stiffness of Model 3

Model 3 and Model 2 has different damping- and stiffness characteristics, as shown in the free vibration tests of Chapter 7.1. With the impact on fatigue damage from the different soil models presented in Chapter 7.2, it has been of interest to investigate if it is stiffness- or damping characteristics of Model 3 that has caused the difference from Model 1 & 2. Results with an updated stiffness of Model 3, is presented in this subchapter.

The updated stiffness has been obtained by reducing the stiffness of Model 3 until the fundamental frequency of Model 3 matches the fundamental frequencies of Model 1 and Model 2. Since Model 3 calculates as non-linear stiffness, dependent on the load and displacement level, this calibration was done for moments around 10MNm at the mudline.

As the impact of different soil models is of little significance at the tower top and blade root, only results for the mudline and tower root will be presented. Results for fatigue damage will be presented, as this has been of main interest.

The vibration test with new Model 3 parameters is also presented.

7.3.1 Free vibration test with updated Model 3.

The free vibration test with updated parameters of Model 3, is presented in Figure 7.20. The mudline loads in the free vibration test, are representative for the mudline loads near rated conditions (load case 5,6 and 7). It should be noted that the stiffness of Model 3 is depending on load level.

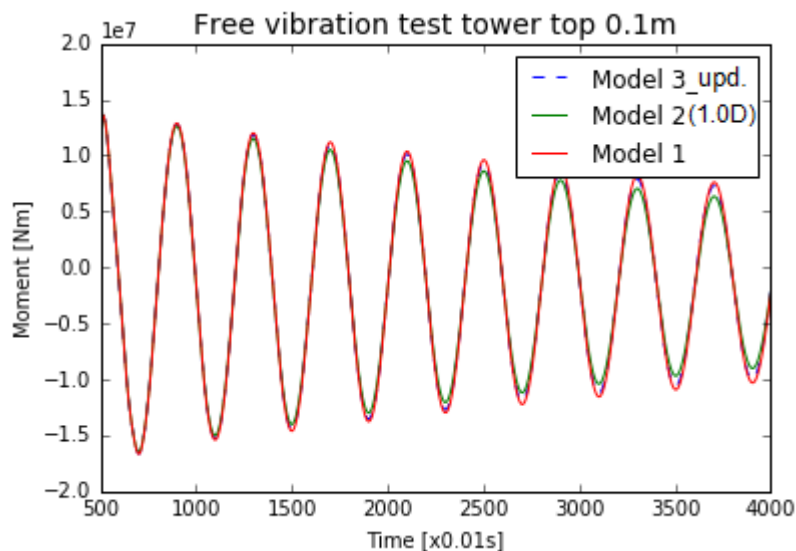


Figure 7.20: Free vibration test with new stiffness of Model 3.

Figure 7.21 is zoomed in on one of the load peaks. At this load level, Model 2 produces significantly more damping than Model 3. We see that the stiffness of Model 3, is approximately equal to that of model 1 and 2 at this load level, as load peaks coincide.

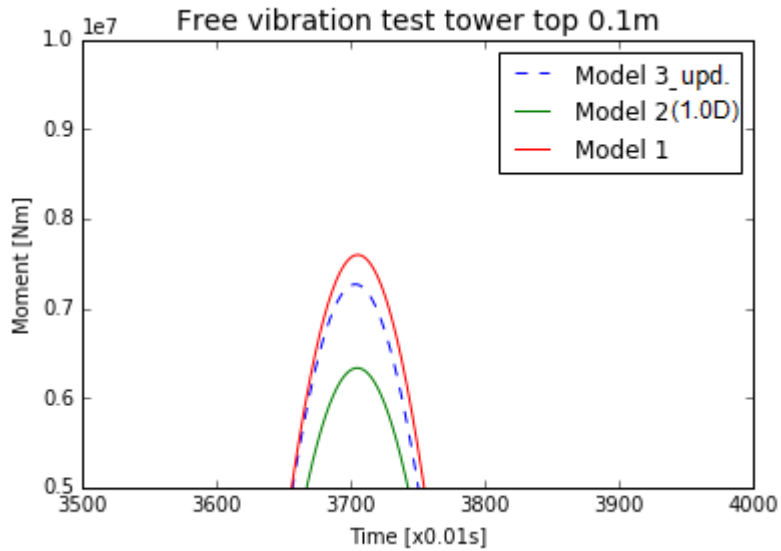


Figure 7.21: Free vibration test with new stiffness of Model 3, zoomed in.

7.3.2 Pile at mudline with updated Model 3 stiffness

The total accumulated damage at mudline, with updated parameters for Model 3, is presented in Figure 7.22. The total accumulated fatigue damage is reduced, compared with Model 1, but we see a significant difference compared with the initial Model 3 parameters.

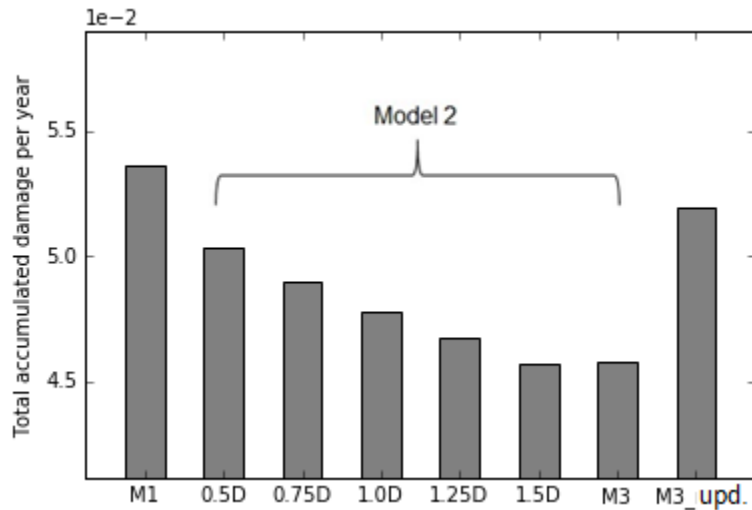


Figure 7.22: Total fatigue damage at mudline per year, with updated Model 3 stiffness.

Figure 7.23 presents the relative accumulated fatigue damage by load case, with new Model 3 parameters. Results are normalized relative to the highest value. Each load case is also probability weighed, according to Table 5.2 (p. 33).

The following trends are evident for the updated Model 3:

1. Accumulated fatigue damage is reduced in the idling cases, with respect to Model 1, that has no damping effect.
2. For operational cases, little influence on accumulated fatigue is seen, with respect to Model 1.
3. Model 3 with updated stiffness, produces consequently more fatigue damage than the Model 3 with the original parameters.

From the observed trends, the following assumptions can be made:

1. The damping effect of Model 3 in the operational cases, has little influence on fatigue damage.
2. In idling cases, the damping from Model 3 noticeably influence accumulated fatigue damage.
3. Varying the stiffness of the soil model, strongly impact the accumulated fatigue damage at the mudline. The strong impact on fatigue damage from Model 3 with the original parameters, was mainly due to stiffness characteristics. As the peak wave frequencies are between 0.11 Hz and 0.17 Hz, a higher soil stiffness, takes the tower eigen frequencies away from wave frequencies. It is assumed that this has reduced wave-tower-resonance effects for Model 3 (with the original parameters).

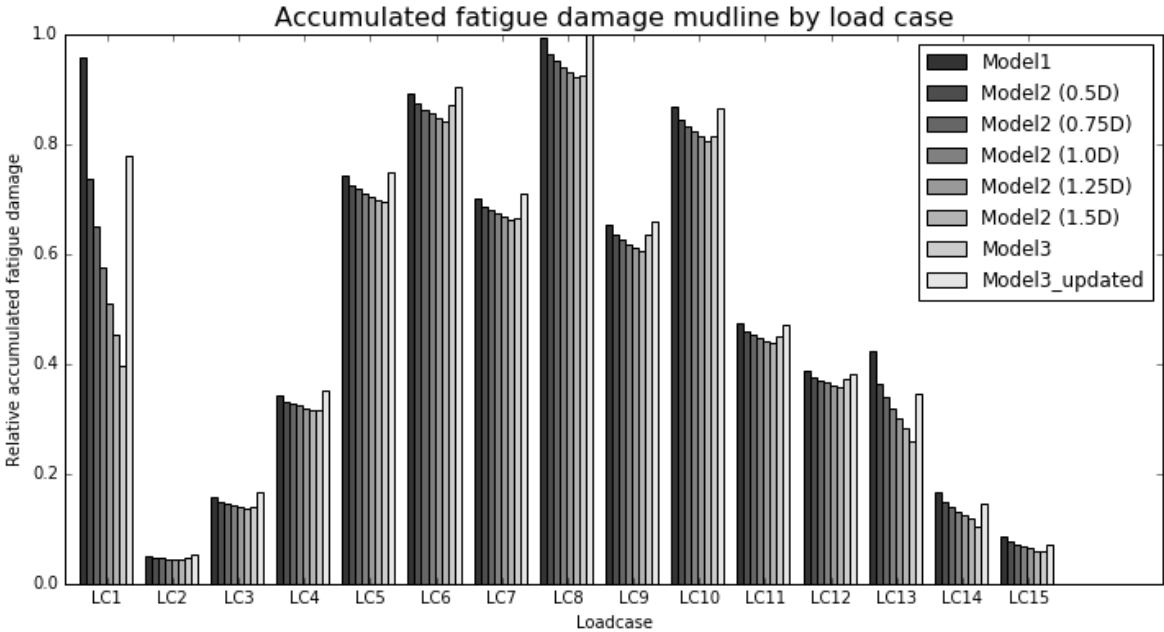


Figure 7.23: Normalized accumulated fatigue damage at mudline after load case, with new Model 3 parameters.

7.3.3 Tower root with updated Model 3 stiffness

The total accumulated damage at the tower root, with updated parameters for Model 3, is presented in Figure 7.24.

Figure 7.25 presents the relative accumulated fatigue damage by load case, with new Model 3 parameters. Results are normalized relative to the highest value. Each load case is also probability weighed, according to Table 5.2 (p. 33).

Generally, the same trends as at the mudline is observed. For load cases around rated conditions (load case 5-8), there is a small increase in accumulated fatigue damage. This can be caused by small stiffness differences between Model 1 and Model 3 (updated), but further study on this is suggested. It can be seen in Chapter 7.2 how the accumulated fatigue damage is very sensitive to Model 3 at the tower root, and small variations in stiffness can explain the observed behavior.

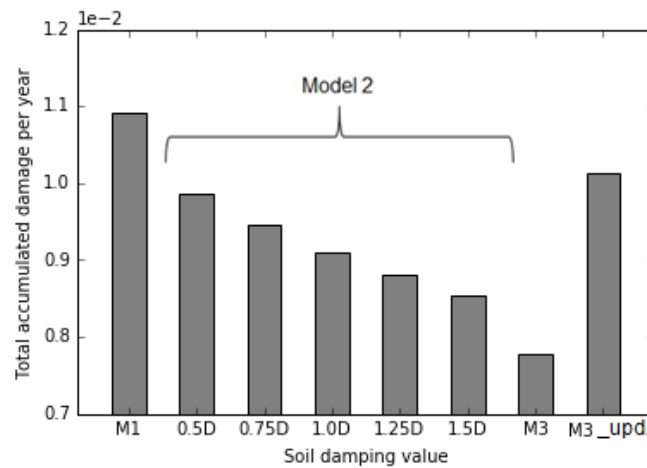


Figure 7.24: Total fatigue damage at tower root per year, with updated Model 3 stiffness.

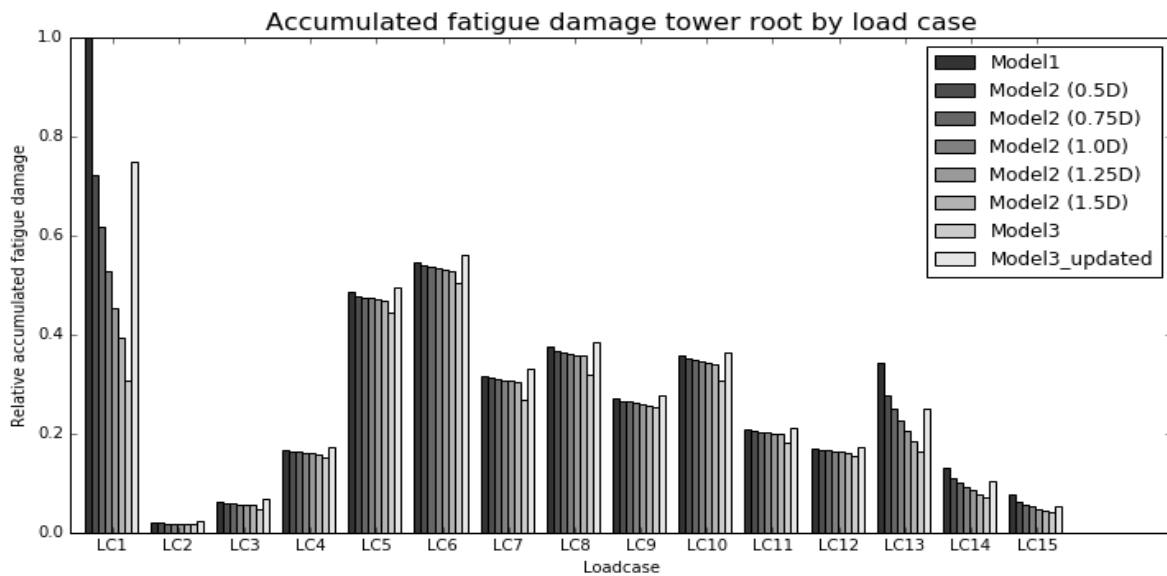


Figure 7.25: Normalized accumulated fatigue at tower root after load case., with new Model 3 parameters.

7.4 Summary of results

Table 7.1 presents a qualitative presentation of the sensitivity to soil-structure interaction model, for different positions on the OWT.

Table 7.2 presents a quantitative presentation of the sensitivity to soil-structure interaction model, for different positions on the OWT. All values are relative to Model 1, that has no soil-damping introduced. Values represent total accumulated fatigue damage for load case 1-15.

Table 7.1: Sensitivity to soil-structure interaction model according to position on structure.

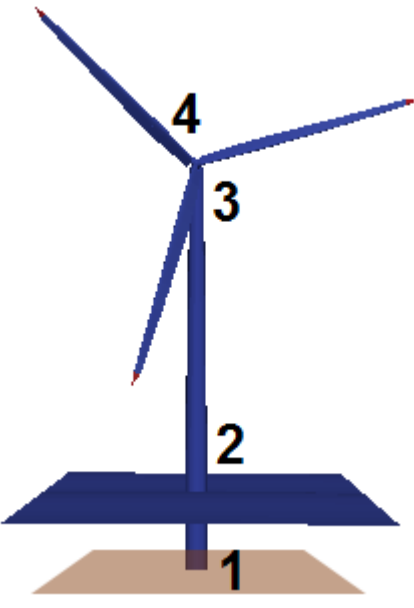
| | | |
|--|-----------------|---|
|  | Position | Fatigue damage sensitivity to soil-structure interaction model |
| | Blade root | Very small ($\approx 0\%$) |
| | Tower top | Small ($< 1\%$) |
| | Tower root | High (up to 29%) |
| | Mudline | High (up to 15%) |

Table 7.2: Numerical values for the relative accumulated fatigue damage, according to position on structure.

| | Model 1 | Model 2 | | | Model 3 | Model 3 updated stiffness |
|------------|---------|---------|------|------|---------|---------------------------|
| | | 0.5D | 1.0D | 1.5D | | |
| Mudline | 1.00 | 0.94 | 0.89 | 0.85 | 0.85 | 0.97 |
| Tower root | 1.00 | 0.90 | 0.84 | 0.78 | 0.71 | 0.93 |
| Tower top | 1.00 | 1.00 | 0.99 | 0.99 | 0.99 | 1.00 |
| Blade root | 1.00 | 1.00 | 1.00 | 1.00 | 1.00 | 1.00 |

8 Final discussion

8.1 Main findings

The results of this thesis clearly show how soil-structure interaction modelling has significant impact on fatigue damage for a bottom fixed OWT with monopile foundation. This corresponds with the findings from Damsgaard et al. (2015), where fatigue damage equivalent moments was studied for a parked rotor. With also operational cases included, the effects on fatigue damage is reduced, as aerodynamic damping dominates with an active rotor. Effects from varied soil stiffness has also become clear, but this has not been the focus of this thesis.

By modelling a wide range of environmental conditions, and calculating fatigue damage for several positions on the OWT, this thesis has given information about the effects of soil damping, in a lifetime perspective. As previous studies has focused on specific load cases, this thesis has shown how soil-structure interaction models impact the fatigue damage in a lifetime perspective, especially at lower positions of the OWT. Widespread models applied by the industry, as the p-y curve approach, neglects soil damping, thereby overestimating fatigue damage in the OWT system. This leads to potential over dimensioning of structural parts.

With a rotational dashpot damper to simulate soil damping, accumulated fatigue damage was reduced by 11% at the mudline, and 16% at the tower root. With a kinematic hardening model, with the same stiffness properties, the reduction of fatigue damage was 3% at the mudline and 7% at the tower root.

The dashpot damper brings damping as a function of angular velocity at the mudline node, thereby constantly providing damping to the system, whereas the kinematic hardening model adds damping as a function of load level. This has led to a higher effect on fatigue life by the rotational dashpot, as damping is introduced even at small load amplitudes. This has emphasized how the choice of damping model affect results. Many previous studies has used dashpot dampers to account for soil damping. The results from this thesis suggest that this approach can miscalculate the damping effect for irregular load cases, where load frequency and amplitude can have large variations.

It is believed that the kinematic hardening model gives a more realistic model for soil behavior, as hysteretic material damping, that is mainly a function of load level, dominates soil damping for bottom fixed OWT's.

With all this in mind, this thesis supports further development of soil-structure interaction models that accurately predict soil damping behavior. As the OWT industry has been depending on government subsidies, this can contribute to the important process towards a more competitive energy prices from offshore wind farms.

8.2 Uncertainties and weaknesses of the study

Several simplifications has been done, due to limitations of this project. Some of the most important ones will be discussed here.

With respect to the turbine structure, the foundation modelling should be mentioned. In the 3DFloat model, the foundation has been modelled by Euler-Bernoulli beams, with stiffness properties according

to cylindrical elements of the NREL 5MW monopile. In this setup, the transition piece, connecting the pile and the tower, has not been considered in detail. This will influence stiffness properties of the full system.

Wind and wave loads have been unidirectional in all load cases, with an exception of turbulent winds. In a real case scenario, wind and wave directions will constantly change. The approach of unidirectional wind and wave loads, has overestimated loads in the inertial x-z plane of this thesis. In a real case scenario, a wider distribution of loads around the pile and tower circumference is expected. New simulations with multidirectional wind and waves, will give more accurate estimates for fatigue damage.

Damping coefficient's for Model 2 has been chosen with a rather crude methodology, as values has been adapted from another study with a different soil profile. Yet, the aim of this thesis has not been to use the correct damping for a given soil profile, but rather to reproduce damping that could be representative for an offshore site where a monopile foundation would be installed. Still, a more comprehensive method for attaining a representative damping levels would be preferable.

8.3 Suggestions for further work

An update of the 3DFloat model is suggested with respect to the transition piece. As the transition piece is at a location of high sensitivity to soil-response, it is of interest to see how this influence the results.

In addition to this, load cases with multidirectional wind and waves, should be further investigated. As aerodynamic damping is of smaller magnitude in the side-to-side plane of the tower, relative to the fore-aft plane (especially in operational cases), it is expected that loading in this plane will have a noticeable effect on fatigue damage. Simulations with multidirectional wind and waves is therefore suggested as a continuation of this work.

More work should also be invested in parametrization of the different soil models. This thesis has shown that soil damping is important, but more work should be invested for finding soil damping models, that represents realistic soil properties. For Model 3, load-response curves has been generated from monotonic loading tests. As the loading would be cyclic at an offshore site, an update of model parameters with this in mind, will give more representative results.

Comparison with the p-y curve approach is a natural continuation of this thesis. As this is industry standard, it is of high relevance to see the results in comparison with this. The implementation of p-y curves has not yet been possible in current versions of 3DFloat. When the framework for this is fully implemented, this is suggested for further study.

9 References

- American Petroleum Institute. (2000). *Recommended Practice for Planning, Designing and Constructing Fixed Offshore Platforms - Working Stress Design*. Washington: American Petroleum Institute.
- Beuckelaers, W. (2015, June). Fatigue life calculation of monopiles for offshore wind turbines using a kinematic hardening soil model. *Ground Engineering (June, 2015)*, pp. 26-29.
- Carswell, W., Johannson, J., Løvhold, F., Arwade, S., & DeGroot, D. (2014, February). Dynamic mudline damping for offshore wind turbine monopiles. *Proceedings of the ASME 2014 33rd International Conference on Ocean, Offshore and Arctic Engineering*. San Francisco, California, USA: ASME.
- Carswell, W., Johannson, J., Løvholt, F., Arwade, S. R., Madshus, C., DeGroot, D. J., & Myers, A. T. (2015). Foundation damping and the dynamics of offshore wind turbine monopiles. *Renewable Energy (80) 2015*, pp. 724-736.
- Cassidy, M. J. (1999). *Non-Linear Analysis of Jack-Up Structures Subjected to Random Waves*, Dr. Phil. Thesis. University of Oxford.
- Chopra, A. K. (2007). *Dynamics of structures: Theory and Applications to Earthquake Engineering, 3rd ed.* Upper Saddle River: Pearson Prentice Hall.
- Damsgaard, M., Andersen, L., & Ibsen, L. (2015, May). Dynamic response sensitivity of an offshore wind turbine for varying subsoil conditions. *Ocean engineering (101) 2015*, pp. 227-234.
- Det Norske Veritas. (2014). *Design of Offshore Wind Turbine Structures, DNV-OS-J101*. Det Norske Veritas.
- Energinet.dk. (2016). *Energinet.dk*. Retrieved from <http://energinet.dk/EN/EI/Nyheder/Sider/Dansk-vindstroem-slaar-igen-rekord-42-procent.aspx>
- European Wind Energy Association. (2015). *The European offshore wind industry - key trends and statistics 2015*. Retrieved from <http://www.ewea.org/statistics/offshore-statistics/>
- Fischer, T., de Vries, W., & Schmidt, B. (2010). *Upwind Design Basis*. Stuttgart, Germany: Project UpWind.
- Gottardi, G., & Houlsby, G. T. (1995). *Model tests of circular footings on sand subjected to combined loads. Report No. 2071/95*. Oxford: Department of Engineering Science, University of Oxford.
- Hansen, M. O. (2008). *Aerodynamics of wind turbines*. London: Earthscan.
- Houlsby, G., & Cassidy, M. (2002, January). A plasticity model for the behavior of footings on sand under combined loading. *Geotechnique 52(2)*, pp. 117-129.

- Hu, P., Wang, D., & Wassidy, M. (2014). Predicting the resistance profile of a spudcan penetrating sand overlaying sand. *Canadian Geotechnical Journal* 10 (2014), 1151-1164.
- Institute, N. G. (2016, Januar 25). *Redwind project page*. Retrieved from www.ngi.no: <http://www.ngi.no/en/Project-pages/REDWIN/>
- International Energy Agency. (2014). *International Energy Agency*. Retrieved from <https://www.iea.org/Textbase/npsum/MTrenew2014sum.pdf>
- Iwan, W. D. (1967, January). On a Class of Models for the Yielding Behaviour of Continuous and Composite Systems. *Journal of applied mechanics* 34/3, pp. 612-.
- Jonkman , J., & Musial, W. (2010). *Offshore Code Comparison Collaboration (OC3) for IEA Task 23 Offshore Wind Technology and Deployment*. Golden, Colorado: National Renewable Energy Laboratory.
- Jonkman, J. (2007). *Dynamic Modelling and Load Analysis of an Offshore Floating Wind Turbine*. Golden, Colorado: National Renewable Energy Laboratory.
- Jonkman, J., Butterfield , S., Musial , W., & Scott, G. (2009). *Defenition of a 5MW-Reference wind turbine for offshore system development*. Golden, Colorado: National Renewable Energy Laboratory.
- Jonkmann, J. (2003). *Modelling of the UAE Wind turbine for Refinement of FAST_AD*. Golden, Colorado: National Renewable Energy Laboratory.
- Jung, S., Kim, S.-R., Patil, A., & Hung, L. C. (2015, September). Effect of monopile foundation modeling on structural response of a 5-MW offshore wind turbine tower. *Ocean Engineering* 109 (2015), pp. 479-488.
- Kühn, M. (1995, November). Modal analysis of the Nedwind 40 tower - comparison of measurements and caculations for the sites Oostburg and Lely. Delft: Institute For Wind Energy.
- Matha, D. (2009). *Model development and load analyses of an offshore wind turbine on a tension leg platform, with a comparison to other floating turbine concepts* . Golden, Colorado: National Renewable Energy Laboratory.
- Matlock, H. M. (1970). Correlations for design og laterally loaded piles in soft clay. *Proceedings of the Second Annual Offshore Technology Conference* (pp. 577-594). Houston, Texas: Offshore Technology Conference.
- Matlock, H. M., & Reese, L. C. (1960). Generelized solutions for laterally loaded piles. *Journals of Soil Mechanics and Foundation Engineering, ASCE* 86(5), 63-91.
- Munk, W. H. (1950). Origin and generation of waves. *Costal engineering procedings 1950*. La Jolla, California: ICCE.

- Myhr, A., Bjerkseter, C., Ågotnes, A., & Nygaard, T. (2014). Levelised cost of energy for offshore floating wind turbines in a life cycle perspective. *Renewable Energy* 66 (2014), 714-728.
- Nguyen-Sy, L. (2005). The theoretical modelling of circular shallow foundation for offshore wind turbines, Dr. Phil. Thesis. Oxford: University of Oxford.
- Page, A., & Skau, K. S. (2016). Load displacement curves for the OC3 comparison exercise (Not official). Oslo: NGL.
- Passon, P. (2006). *Derivation and description of the Soil-Pile-Interaction models for UEA-Annex XXIII Subtask 2*. Stuttgart: University of Stuttgart.
- Pradhan, D. L. (2012). Development of p-y curves for monopiles in clay using finite element model plaxis 3D foundation, M. thesis. Trondheim: NTNU.
- Randolph, M. F. (1981, June). The response of flexible piles to lateral loading. *Géotechnique* 31(2), pp. 247-259.
- Reese, L. C., & Wang, S. T. (2006, August 16). *Verification of computer program Lpile as a valid tool for design of a single pile under lateral loading*. Retrieved from www.ensoftinc.com: http://www.ensoftinc.com/main/products/pdf/Lpile-Validation_Notes.pdf
- Robertson A., J. J. (2014). Offshore Code Comparison Collaboration Continuation Within IEA Wind Task 30. San Francisco: National Renewable Energy Laboratory.
- Subhamoy, B. (2014). Challenges in Design of Foundations for offshore wind turbines. *IET Publishing ISSN 2056-4007*.
- Vorpahl, F., Schwarze, H., Fisher, T., Seidel, M., & Jonkman, J. (2013, September). Offshore wind turbine environment, loads, simulation and design. *Wiley Interdisciplinary Reviews: Energy and Environment*, September/October (2013), pp. 548-571.
- Zaaijer, M. (2006, September 11). Foundation modelling to assess dynamic behaviour of offshore wind turbines. *Applied Ocean Research* 28 (2006), pp. 45-57.

10 Appendix

10.1 Rainflow counting algorithm and fatigue damage calculations

```
import numpy as np
import pylab as plt
import scipy
import rainflow_scr as rn

#####
## Functions to calculate partial fatigue damage for welded ##
## steel structures from timeseries of stress given in Pa ##
## and two-sloped SN-curves as defined in DNV-OS-C203 Fatigue##
## Design of Offshore Steel Structures. ##
## ##
## Stress concentration factors for hot-spot stress must be ##
## included in the stress timeseries before these functions ##
## are used. ##
## ##
## Stress cycles are counted using Rainflow counting. ##
## ##
## See example_fatigue_funcs.py for example of how to use ##
## ##
## Marit Kvittem Feb 2015, ##
#####

## New turningpoints algorithm by Steffen Aasen, April 2016

def turningpoints(x): #Do not return correct turningpoints for small
amplitudes

    ## Find the amplitude at turning points of a 1D numpy array x

    dx = np.diff(x)
    Np = np.sum( dx[1:] * dx[:-1] < 0)
    ind = np.where(dx[1:] * dx[:-1] < 0)
    tp_m = x[ind]

    ## add end points
    tp = [x[0]]
    tp.extend(tp_m)
    tp.extend([x[-1]])

    return tp

def turningpoints_own2(x,amp): #Written by Steffen Aasen, April 2016

    #save indexes of turning points
    turningpoints=[]
    indexes=[]
    for i in range(1,len(x)-1):
        if x[i-1]>x[i] and x[i+1]>x[i] or x[i-1]<x[i] and x[i+1]<x[i]:
            indexes.append(i)

    #make array with turningpoints
    for element in indexes:
        if abs(x[element-1]-x[element])>amp and abs(x[element+1]-
x[element])>amp:
            turningpoints.append(x[element])
```

```

#delete points that are not turningpoints (due to numerical error)
indexes=[]

for i in range(len(turningpoints)-2):
    if turningpoints[i+1]>turningpoints[i] and
turningpoints[i+2]>turningpoints[i+1] or turningpoints[i+1]<turningpoints[i]
and turningpoints[i+2]<turningpoints[i+1]:
        indexes.append(i+1)

turningpoints_2=[]
for i in range(len(turningpoints)):
    if i not in indexes:
        turningpoints_2.append(turningpoints[i])

return turningpoints_2

def findrfc_wafo(x):
    ## Rainflow counting of 1D list of turning points x
    ## based on matlab wafo's tp2arfc4p and default values given in tp2rfc

    def_time=0.
    res0 = []
    T = len(x)
    ARFC = np.zeros((np.floor(T/2),2))
    N = -1

    res = np.zeros(max([5000,len(res0)]))

    nres = -1

    for i in range(0,T):
        nres = nres+1
        res[nres] = x[i]
        cycleFound = 1
        while cycleFound ==1 and nres >=4:
            if res[nres-1] < res[nres-2]:
                A = [res[nres-1], res[nres-2]]
            else:
                A = [res[nres-2], res[nres-1]]

            if res[nres] < res[nres-3]:
                B = [res[nres], res[nres-3]]
            else:
                B = [res[nres-3], res[nres]]

            if A[0] >= B[0] and A[1] <= B[1]:
                N=N+1
                arfc = [[res[nres-2]], [res[nres-1]]]
                ARFC[N] = [res[nres-2],res[nres-1]]
                res[nres-2] = res[nres]
                nres = nres-2
            else:
                cycleFound = 0

    ## residual
    res = res[0:nres+1]

    def res2arfc(res):
        nres = len(res)
        ARFC = []

```

```

    if nres < 2:
        return
    ## count min to max cycles, gives correct number of upcrossings
    if (res[1]-res[0]) > 0.:
        i_start = 0
    else:
        i_start=1
    I = range(i_start,nres-1,2)
    Ip1 = range(i_start+1,nres,2)
    ## def_time = 0

    for ii in range(len(I)):
        ARFC.append( [res[I[ii]], res[Ip1[ii]]] )

    ARFC = np.array(ARFC)

    return ARFC

ARFC_res = res2arfc(res)

ARFC = np.concatenate((ARFC,ARFC_res))

## make symmetric
[N,M] = np.shape(ARFC)
I = []
J=0
RFC = ARFC

for ii in range(N):
    if ARFC[ii,0] > ARFC[ii,1]:
        ## Swap variables
        RFC[ii,J],RFC[ii,J+1] = RFC[ii,J+1],RFC[ii,J]

cc = RFC

rfcamp = (RFC[:,1] - RFC[:,0])/2.

return rfcamp

def fatiguedamage_twoslope(time,stress,m1,loga1,m2,loga2,Nlim,th=25E-3,tref=25E-3,k=0.25):
    ## stress: stressvector, unit: Pa
    ## m1, loga1, m2, loga2: Parameters from table 2.2 in RP-C203
    ## Note that the parameters in RP C203 are given for stress ranges in
MPa
    ## tref, k: parameters from point 2.4 in RP-C203
    ## th: structural detail thickness
    ## Calculates fatigue damage for bilinear SN curves
    ## hist: true/false parameter, whether or not to plot histogram

    stress = stress*1.E-6

    tp = np.array(turningpoints_own2(stress,0.0)) ## Find turning points
    mm = findrfc_wafo(tp)#rn.rainflow(tp)[0]*0.5 ## Rainflow cycles as by
the routine in matlab wafo

    Nbins = len(mm)

```

```

if th<tref:
    th = tref

a1 = 10.**loga1
K1 = 2.0**m1/a1*(th/tref)**(k*m1)
beta1 = m1

a2 = 10.**loga2
K2 = 2.0**m2/a2*(th/tref)**(k*m2)
beta2 = m2

alim = (1.0/(K1*Nlim))**(1./m1)
alim2 = (1.0/(K2*Nlim))**(1./m2)

avalid = (1.0/(K2*1.0E7))**(1./m2)

if not np.round(alim,0) == np.round(alim2,0):
    print loga1
    print loga2
    print m1
    print m2
    print K1
    print K2
    print alim
    print alim2
    print 'alim not the same as alim2, check SN curve values'

dd = 0.0

amp = abs(mm)

for aa in amp:
    if aa > alim:
        dd = dd + K1*aa**beta1

    elif aa <= alim:
        if aa < avalid:
            key = True

            dd = dd + K2*aa**beta2
        else:
            dd = dd + K2*aa**beta2

D_T = dd

return D_T

```

10.2 Stress calculations at cylindrical circumference

```
def
fatigue_calculations(OD,th,Nloc,moments_file,colxm,colym,colzm,forces_file,
colxf,colyf,colzf,outputfile):
#OD = Outer diameter of tubular cross section
#th = Base material thickness
#Nloc= Number of locations for stress calculation around the circumference

    for k in range(len(dirnames)): #run fatigue calculation in each folder
        os.chdir(dirnames[k])

        #Coordinate system different from 3DFloats inertial sytem
        t=readcol(moments_file,'% ',1)
        dt=t[1]-t[0]
        Mx_col=readcol(moments_file,'% ',colxm)
        My_col=readcol(moments_file,'% ',colym)
        Mz_col=readcol(moments_file,'% ',colzm)
        Fx_col=readcol(forces_file,'% ',colxf)
        Fy_col=readcol(forces_file,'% ',colyf)
        Fz_col=readcol(forces_file,'% ',colzf)

    (Mx,My,Mz,Fx,Fy,Fz)=(np.array(Mx_col),np.array(My_col),np.array(Mz_col),np.
array(Fx_col),np.array(Fy_col),np.array(Fz_col))

        #Pick max values for moment at circumfence
        Pyth_moment=np.sqrt(My**2)

        moments_top=turningpoints(Pyth_moment)

        Max_moments=nlargest(10,moments_top)

        Avg_max_moments=sum(Max_moments)/len(Max_moments)
        moments_data[u].append(Avg_max_moments)

        #Find stdav of moments
        moments_stdav[u].append(np.std(My))

        ## Cross sectional parameters for tubular cross section
        r1 = OD/2.0 # Outer radius
        r2 = r1 - th # Inner radius
        rm = r1
        A = np.pi*(r1**2-r2**2)
        Iy = np.pi/4.0*(r1**4-r2**4) # 2nd moment of inertia
        Ix = Iy # Symmetry
        Ip = np.pi/2.0*(r1**4-r2**4) # Polar moment of inertia
        Wp = 4.0/3.0*(r1**3-r2**3) # Plastic modulus
        Sy = 0.5*Wp # 1st moment of inertia
        Sx = Sy # Symmetry
        ## Cross section locations
        yvec = []
        xvec = []
        for theta in np.arange(0,2*np.pi,2*np.pi/Nloc):
            yvec.append(-rm*np.sin(theta)) #changed to sin by
SAA
            xvec.append(-rm*np.cos(theta)) #changed to cos by
SAA

        if k==0:
            plt.figure(figsize=(3,3))
            plt.plot(xvec,yvec,'r--')
```

```

plt.axis([-4,4,-4,4])
#plt.title('Locations om tower circumference')
plt.xlabel('x[m] (wind along x-axis)')
plt.ylabel('y[m]')

Dsx = np.zeros(Nloc)
Dtxy = np.zeros(Nloc)

ii = 0
for loc in range(Nloc):
    x = xvec[loc]
    y = yvec[loc]
    cosa = -x/np.sqrt(y**2+x**2)
    sina = -y/np.sqrt(y**2+x**2)

    ## Axial stress
    sigmax = - My/Iy*x + Mx/Ix*y + Fz/A ## [Pa]
    ## Shear stress
    tauxy = 2.0/A*(-Fy*cosa+Fx*sina)+ Mz*r1/Ip #Fasthetslaere p.
53 / Stalkonstruksjoner

    dsx =
    fatiguedamage_twoslope(t,sigmax,m1,loga1,m2,loga2,Nlim,th,tref=25E-
3,k=0.25)
    dtauxy =
    fatiguedamage_twoslope(t,tauxy,m1,loga1,m2,loga2,Nlim,th,tref=25E-3,k=0.25)

    Dsx[ii] = dsx
    Dtxy[ii] = dtauxy

    ii += 1

##### Write results to fatigue_data (list) #####

#fatigue_data: [loadcase][position] on
circumference][ypos,zpos,damage,timeofsim,fatiguelife]
fatigue_data.append([])
for i in range(len(Dsx)):
    fatigue_data[k].append([])
    fatigue_data[k][i].append(yvec[i])
    fatigue_data[k][i].append(xvec[i])
    fatigue_data[k][i].append(Dsx[i]+Dtxy[i])
    fatigue_data[k][i].append(len(t)*dt)

fatigue_data[k][i].append((1/(Dsx[i]+Dtxy[i]))/(3600*24*365/(len(t)*dt)))
fatigue_data[k][i].append((Dsx[i]+Dtxy[i])*(31536000.0/len(t)*dt))

##### Write results to file #####

newfile=open(outputfile,'w')
newfile.write('%ypos[m]+'\t')
newfile.write('%zpos[m]+'\t')
newfile.write('Partial_fatigue_damage axial+'\t')
newfile.write('Partial_fatigue_damage torsion+'\t')
newfile.write('simulation_time[s]+'\t')
newfile.write('D per year+'\t')
newfile.write('fatigue_life[y]+'\n')

```

```

for i in range(len(Dsx)):
    newfile.write(str(yvec[i])+'\t')
    newfile.write(str(xvec[i])+'\t')
    newfile.write(str(Dsx[i])+'\t')
    newfile.write(str(Dtxy[i])+'\t')
    newfile.write(str(len(t)*dt)+'\t')

newfile.write(str((Dsx[i]+Dtxy[i])*(31536000.0/len(t)*dt))+'\t')
    lifetime=((1/(Dsx[i]+Dtxy[i]))/(3600*24*365/(len(t)*dt)))
    newfile.write(str(lifetime)+'\n')

newfile.close()

os.chdir('.')

print('fatigue damage calculation done on: '+str(dirnames[k])+'.
Results are written to '+outputfile)

return ('fatigue damage function done')

```

10.3 3DFloat input file

For Model 2 (D1.0), load case 6

```
!
! 3dfloat test input file for a 5MW NREL MONOPILE
! Created by:  JB de Vaal, Steffen Aasen and Tor Anders Nygaard
!   updated: 01.05.16 SAA
!
! -----
! SET ENVIRONMENT:
! -----
-----
set_environment
  gravity:          on
  buoyancy:         on
  rho_water:        1025.
  rho_air:          1.225
  nu_water:         0.00001000
  nu_air:           0.00000100
  waves:            irregular_airy_wavelets
  tshift_waves:    10.  OK
  wave_ramps:       0.    ! TAN
  wave_rampe:       100.  ! TAN
  !wave_amplitude:  1.5  OK
  !spectral_peak:   10.  OK
  wave_direction:   0.  OK
  depth:            20.  OK
  norder            -1  OK
  surface_option:   2ndorder  OK
  kinematics_option:  initial  OK
  dtwkin:           -1.    OK
  pre_computed_waves_file: off    OK
  hydro_force:      morison  ok
  current_speed:    0.    OK
  current_exponent: 0.    OK
  current_direction: 0.    OK
  !
  wind:              mean_profile
  tshift_wind:       0.    OK
  wind_speed:        12.    OK  ! is set up at line 700
  wind_ref_height:   90.
  wind_exponent:     0.14
  wind_direction:    0.
  wind_force:        drag

! -----
! SET UP AND TEST IRREGULAR WAVES:
! -----
-----
!jonswap_wavelets_constant  hs: 1.7    tp: 5.88    tstart: 25.    tcut: -1.
gamma: 2.87
depth: 20.    file: wavelets6.txt  tperiodic: 1800. ! TAN
```



```
wavelets scale_amplitude: 1. file wavelets6.txt
test_irregairy dt 1. nstep 600 x 0. 0. 0. filename waveheight.txt
wave_forces cm_morison 1.63
```

```
! -----
! MATERIALS DEFINITION:
! -----
```

```
define_material name OC4semisub rho 7850.0 e 2.1e+13 g
7.89473684211e+12
define_material name connect_mat rho 1e-08 e 2.1e+15 g 8.1e+14
define_material name wire_OC4 rho 24596.54 e 1.6353e+11 g
65119666311.8
define_material name massless1 rho 0.0001 e 210.e9 g 80.8e9
define_material name massless2 rho 0.0001 e 210.e9 g 80.8e9
define_material name massless3 rho 0.0001 e 210.e10 g
80.8e11 !Applied to Nacelle to avvoid 3f
define_material name mainshaft rho 0.0001 e 210.e9 g
1.05610143e9
define_material name mainshaft_stiff rho 0.0001 e 210.e11 g 80.8e11
!Applied to mainshaft to avvoid 3f
!define_material name mainshaft_stiff rho 1000. e 210.e11 g
80.8e11
define_material name steeltowerMassless rho 0.00001 e 2.1e+11 g
8.08e+11
define_material name steeltower2 rho 8500. e 20.1e+11 g
80.08e+10
```

```
! -----
! STRUCTURE DEFINITION:
! -----
```

```
! -----
! MONOPILE: BELOW MUDLINE TO MUDLINE DEFINITION:
! -----
```

```
!
!new_elements_beam1 nelem 11 material steeltower connect_mode
connect_none
!x1 0.0 0.0 -55.0 dcy11 6.00 tcy11 0.05
!x2 0.0 0.0 -33.0 dcy12 6.00 tcy12 0.05 btype beam
!
!new_elements_beam1 nelem 3 material steeltower connect_mode connect_1
!x1 0.0 0.0 -33.0 dcy11 6.00 tcy11 0.05
!x2 0.0 0.0 -25.0 dcy12 6.00 tcy12 0.05 btype beam
!
!new_elements_beam1 nelem 5 material steeltower connect_mode connect_1
!x1 0.0 0.0 -25.0 dcy11 6.00 tcy11 0.05
!x2 0.0 0.0 -20.0 dcy12 6.00 tcy12 0.05 btype beam
```

```
! -----
```

```

! MONOPILE: MUDLINE TO TOWER DEFINITION:
! -----
-----

new_elements_beam1 nelelem 6 material steeltower connect_mode connect_none
! TAN according to OC3 doc
x1 0.0 0.0 -20.0 dcyll1 6.00 tcyl1 0.06
x2 0.0 0.0 10.0 dcyll2 6.00 tcyl2 0.06 btype beam

! -----
-----

! TOWER DEFINITION:
! -----
-----

new_body name tower reftype inertial parent inertial axes normal

new_elements_beam1 nelelem 20 material steeltower connect_mode connect_1
! TAN according to OC3 report
x1 0.0 0.0 10.0 dcyll1 6. tcyl1 0.035
x2 0.0 0.0 87.6 dcyll2 3.87 tcyl2 0.024 btype beam

! -----
-----

! NACELLE DEFINITIONS:
! -----
-----

! yaw drive
new_body name yawdrive parent tower reftype refnode xfind 0. 0. 87.6
rotorder 123 rotation 0. 0. 0. axes normal
! yaw can be added here eg rotation 0. 0. 8.

! element to Nacelle reference point
new_elements_beam1 nelelem 1 material massless1 connect_mode connect_1
x1 0. 0. 0. dcyll1 4.0 tcyl1 1.
x2 0. 0. 1.9626 dcyll2 4.0 tcyl2 1. btype beam

! nacelle
new_body name nacelle parent yawdrive reftype refnode xfind 0. 0. 1.9626
rotorder 123 rotation 0. 5. 0. axes normal ! rotor tilt: 5 degrees

! shaft from main bearing to point mass 1
new_elements_beam1 nelelem 1 material massless3 connect_mode no_connect
x1 -3.1071 0. 0. dcyll1 2.0 tcyl1 1.
x2 -0.7968 0. 0. dcyll2 2.0 tcyl2 1. btype beam

! point mass 1 to nacelle reference point
new_elements_beam1 nelelem 1 material massless3 connect_mode connect_both
x1 -0.7968 0. 0. dcyll1 2.0 tcyl1 1. pointmass 120.e3
x2 0. 0. 0. dcyll2 2.0 tcyl2 1. btype beam

! nacelle reference point to nacelle CG
new_elements_beam1 nelelem 1 material massless3 connect_mode connect_1
x1 0. 0. 0. dcyll1 2.0 tcyl1 1.
x2 1.9072 0. 0. dcyll2 2.0 tcyl2 1. btype beam

! point mass 2 to nacelle CG
new_elements_beam1 nelelem 1 material massless3 connect_mode connect_2
x1 4.6113 0. 0. dcyll1 2.0 tcyl1 1. pointmass 120.e3
x2 1.9072 0. 0. dcyll2 2.0 tcyl2 1. btype beam

```

```

! mainbearing
new_body name mainbearing parent nacelle reftype refnode
xfind -3.1071 0. 0. rotorder 123 rotation 0. 0. 0. axes normal

! shaft from hub CG to main bearing via moment sensor

new_elements_beam1 nelem 1 material mainshaft_stiff connect_mode no_connect
! Stiffness chosen to avoid 3f
x1 -1.912 0. 0. dcyll1 2.0 tcyl1 1. pointmass 5159.11681
x2 -1.0 0. 0. dcyll2 2.0 tcyl2 1. btype beam
generator nrel5mwfloating !NB: have to define generator "nrel5mwfloating"

new_elements_beam1 nelem 1 material mainshaft_stiff connect_mode
connect_both ! Stiffness chosen to avoid 3f
x1 -1. 0. 0. dcyll1 2.0 tcyl1 1.
x2 0. 0. 0. dcyll2 2.0 tcyl2 1. btype beam

! hub
new_body name hub parent mainbearing reftype refnode xfind -1.912 0.
0. rotorder 123 rotation 0. 0. 0. axes normal

! -----
! BLADE STRUCTURAL AND AERODYNAMIC PROPERTIES
! -----
!
! blade element structural coordinate system:
!
! y out TE along flap principal axis
! z out suction side along lag principal axis
! x = y x z ! NB CAN THEREFORE BE TOWARDS TIP OR HUB
!
! structural twist is positive around x
! mass center and shear center offsets are given in blade element
structural
! coordinate system
!
! BLADE PROPERTIES
! -----
!
! distributed structural properties for blade, 5MW NREL rotor
!
r[m],eiflap[Nm**2],eiedge,gtors,ea[N],rho[kg/m],structwist[deg],flpinert[kg
m],edginert[kgm],&
! flpcgofs[m],edgcgofs[m],flpshrofs[m],edgshrofs[m]
!
blade_table blname nrel5mw
1.4999e+00 1.8110e+10 1.8114e+10 5.5644e+09 1.3943e+10 6.7893e+02 13.30818
972.86 973.04 0. 0.00017 0. 0.
1.6999e+00 1.8110e+10 1.8114e+10 5.5644e+09 1.3943e+10 6.7893e+02 13.30818
972.86 973.04 0. 0.00017 0. 0.
2.6999e+00 1.9425e+10 1.9559e+10 5.4316e+09 1.5055e+10 7.7336e+02 13.30818
1091.52 1066.38 0. -0.02309 0. 0.
3.6999e+00 1.7456e+10 1.9498e+10 4.9940e+09 1.3708e+10 7.4055e+02 13.30818
966.09 1047.36 0. 0.00344 0. 0.

```

| | | | | | | |
|------------|------------|------------|------------|------------|------------|----------|
| 4.6998e+00 | 1.5287e+10 | 1.9789e+10 | 4.6666e+09 | 1.3330e+10 | 7.4004e+02 | 13.30818 |
| 873.81 | 1099.75 | 0. | 0.04345 | 0. | 0. | |
| 5.6998e+00 | 1.0782e+10 | 1.4859e+10 | 3.4747e+09 | 9.9814e+09 | 5.9250e+02 | 13.30818 |
| 648.55 | 873.02 | 0. | 0.05893 | 0. | 0. | |
| 6.6998e+00 | 7.2297e+09 | 1.0221e+10 | 2.3235e+09 | 6.8863e+09 | 4.5027e+02 | 13.30818 |
| 456.76 | 641.49 | 0. | 0.06494 | 0. | 0. | |
| 7.6998e+00 | 6.3095e+09 | 9.1447e+09 | 1.9079e+09 | 6.0480e+09 | 4.2405e+02 | 13.30818 |
| 400.53 | 593.73 | 0. | 0.07718 | 0. | 0. | |
| 8.6998e+00 | 5.5284e+09 | 8.0632e+09 | 1.5704e+09 | 5.2795e+09 | 4.0064e+02 | 13.30818 |
| 351.61 | 547.18 | 0. | 0.08394 | 0. | 0. | |
| 9.7010e+00 | 4.9801e+09 | 6.8844e+09 | 1.1583e+09 | 4.4607e+09 | 3.8206e+02 | 13.30818 |
| 316.12 | 490.84 | 0. | 0.10174 | 0. | 0. | |
| 1.0700e+01 | 4.9368e+09 | 7.0092e+09 | 1.0021e+09 | 4.3293e+09 | 3.9965e+02 | 13.30818 |
| 303.60 | 503.86 | 0. | 0.10758 | 0. | 0. | |
| 1.1700e+01 | 4.6917e+09 | 7.1677e+09 | 8.5590e+08 | 4.4610e+09 | 4.2632e+02 | 13.30818 |
| 289.24 | 544.70 | 0. | 0.15829 | 0. | 0. | |
| 1.2700e+01 | 3.9495e+09 | 7.2717e+09 | 6.7227e+08 | 4.6253e+09 | 4.1682e+02 | 13.30818 |
| 246.57 | 569.90 | 0. | 0.22235 | 0. | 0. | |
| 1.3700e+01 | 3.3865e+09 | 7.0817e+09 | 5.4749e+08 | 5.0243e+09 | 4.0619e+02 | 13.18151 |
| 215.91 | 601.28 | 0. | 0.30756 | 0. | 0. | |
| 1.4701e+01 | 2.9337e+09 | 6.2445e+09 | 4.4884e+08 | 4.3749e+09 | 3.8142e+02 | 12.84784 |
| 187.11 | 546.56 | 0. | 0.30386 | 0. | 0. | |
| 1.5700e+01 | 2.5690e+09 | 5.0490e+09 | 3.3592e+08 | 3.4799e+09 | 3.5282e+02 | 12.19218 |
| 160.84 | 468.71 | 0. | 0.26519 | 0. | 0. | |
| 1.6700e+01 | 2.3887e+09 | 4.9485e+09 | 3.1135e+08 | 3.2615e+09 | 3.4948e+02 | 11.56072 |
| 148.56 | 453.76 | 0. | 0.25941 | 0. | 0. | |
| 1.7700e+01 | 2.2720e+09 | 4.8080e+09 | 2.9194e+08 | 3.0296e+09 | 3.4654e+02 | 11.07246 |
| 140.30 | 436.22 | 0. | 0.25007 | 0. | 0. | |
| 1.9701e+01 | 2.0501e+09 | 4.5014e+09 | 2.6100e+08 | 2.5650e+09 | 3.3933e+02 | 10.79246 |
| 124.61 | 398.18 | 0. | 0.23155 | 0. | 0. | |
| 2.1700e+01 | 1.8283e+09 | 4.2441e+09 | 2.2882e+08 | 2.1678e+09 | 3.3000e+02 | 10.23218 |
| 109.42 | 362.08 | 0. | 0.20382 | 0. | 0. | |
| 2.3700e+01 | 1.5887e+09 | 3.9953e+09 | 2.0075e+08 | 1.8811e+09 | 3.2199e+02 | 9.67221 |
| 94.36 | 335.01 | 0. | 0.19934 | 0. | 0. | |
| 2.5700e+01 | 1.3619e+09 | 3.7508e+09 | 1.7438e+08 | 1.6197e+09 | 3.1382e+02 | 9.10971 |
| 80.24 | 308.57 | 0. | 0.19323 | 0. | 0. | |
| 2.7700e+01 | 1.1024e+09 | 3.4471e+09 | 1.4447e+08 | 1.2478e+09 | 2.9473e+02 | 8.53403 |
| 62.67 | 263.87 | 0. | 0.14994 | 0. | 0. | |
| 2.9701e+01 | 8.7580e+08 | 3.1391e+09 | 1.1998e+08 | 1.0212e+09 | 2.8712e+02 | 7.93217 |
| 49.42 | 237.06 | 0. | 0.15421 | 0. | 0. | |
| 3.1700e+01 | 6.8130e+08 | 2.7342e+09 | 8.1192e+07 | 7.5893e+08 | 2.6334e+02 | 7.32134 |
| 37.34 | 196.41 | 0. | 0.13252 | 0. | 0. | |
| 3.3700e+01 | 5.3472e+08 | 2.5549e+09 | 6.9091e+07 | 6.5899e+08 | 2.5321e+02 | 6.71112 |
| 29.14 | 180.34 | 0. | 0.13313 | 0. | 0. | |
| 3.5700e+01 | 4.0890e+08 | 2.3340e+09 | 5.7454e+07 | 5.5600e+08 | 2.4167e+02 | 6.12152 |
| 22.16 | 162.43 | 0. | 0.14035 | 0. | 0. | |
| 3.7700e+01 | 3.1454e+08 | 1.8287e+09 | 4.5915e+07 | 4.1878e+08 | 2.2064e+02 | 5.54647 |
| 17.33 | 134.83 | 0. | 0.13950 | 0. | 0. | |
| 3.9701e+01 | 2.3863e+08 | 1.5841e+09 | 3.5977e+07 | 3.4208e+08 | 2.0029e+02 | 4.97147 |
| 13.30 | 116.30 | 0. | 0.15134 | 0. | 0. | |
| 4.1700e+01 | 1.7588e+08 | 1.3234e+09 | 2.7441e+07 | 2.7031e+08 | 1.7940e+02 | 4.40118 |
| 9.96 | 97.98 | 0. | 0.17418 | 0. | 0. | |
| 4.3700e+01 | 1.2601e+08 | 1.1837e+09 | 2.0903e+07 | 2.9801e+08 | 1.6509e+02 | 3.83417 |
| 7.30 | 98.93 | 0. | 0.24922 | 0. | 0. | |
| 4.5700e+01 | 1.0726e+08 | 1.0202e+09 | 1.8543e+07 | 2.3954e+08 | 1.5441e+02 | 3.33243 |
| 6.22 | 85.78 | 0. | 0.26022 | 0. | 0. | |
| 4.7700e+01 | 9.0884e+07 | 7.9781e+08 | 1.6276e+07 | 1.7713e+08 | 1.3894e+02 | 2.88971 |
| 5.19 | 69.96 | 0. | 0.22554 | 0. | 0. | |
| 4.9701e+01 | 7.6310e+07 | 7.0961e+08 | 1.4535e+07 | 1.4630e+08 | 1.2956e+02 | 2.50304 |
| 4.36 | 61.41 | 0. | 0.22795 | 0. | 0. | |

```

5.1700e+01 6.1049e+07 5.1819e+08 9.0729e+06 9.6794e+07 1.0726e+02 2.11618
3.36 45.44 0. 0.20600 0. 0.
5.3700e+01 4.9482e+07 4.5487e+08 8.0573e+06 7.9643e+07 9.8776e+01 1.72958
2.75 39.57 0. 0.21662 0. 0.
5.5700e+01 3.9359e+07 3.9512e+08 7.0783e+06 6.4663e+07 9.0248e+01 1.34158
2.21 34.09 0. 0.22784 0. 0.
5.6700e+01 3.4672e+07 3.5372e+08 6.0927e+06 5.4862e+07 8.3001e+01 0.95358
1.93 30.12 0. 0.23124 0. 0.
5.7700e+01 3.0414e+07 3.0473e+08 5.7539e+06 2.8044e+07 7.2906e+01 0.76037
1.69 20.15 0. 0.14826 0. 0.
5.8700e+01 2.6522e+07 2.8142e+08 5.3306e+06 2.5113e+07 6.8772e+01 0.57435
1.49 18.53 0. 0.15346 0. 0.
5.9200e+01 2.3837e+07 2.6171e+08 4.9352e+06 2.2218e+07 6.6264e+01 0.40435
1.34 17.11 0. 0.15382 0. 0.
5.9701e+01 1.9632e+07 1.5881e+08 4.2381e+06 1.1334e+07 5.9340e+01 0.31935
1.10 11.55 0. 0.09470 0. 0.
6.0200e+01 1.6002e+07 1.3788e+08 3.6589e+06 8.6067e+06 5.5914e+01 0.25317
0.89 9.77 0. 0.09018 0. 0.
6.0700e+01 1.2825e+07 1.1879e+08 3.1269e+06 6.4434e+06 5.2484e+01 0.21572
0.71 8.19 0. 0.08561 0. 0.
6.1200e+01 1.0083e+07 1.0163e+08 2.6432e+06 4.7679e+06 4.9114e+01 0.17820
0.56 6.82 0. 0.08035 0. 0.
6.1700e+01 7.5459e+06 8.5070e+07 2.1719e+06 3.3999e+06 4.5818e+01 0.14033
0.42 5.57 0. 0.07096 0. 0.
6.2200e+01 4.6046e+06 6.4256e+07 1.5810e+06 1.9367e+06 4.1669e+01 0.10107
0.25 4.01 0. 0.05424 0. 0.
6.2700e+01 2.4509e+05 6.6083e+06 2.5369e+05 3.8278e+05 1.1453e+01 0.06181
0.04 0.94 0. 0.05387 0. 0.
6.3001e+01 1.7458e+05 5.0128e+06 1.8655e+05 2.2568e+05 1.0319e+01 0.02295
0.02 0.68 0. 0.05181 0. 0.

```

```

aero_blade_table  blname nrel5mw      ! r/R  c/R  twist [deg]  airfoil
0.02              0.0562222222222222  13.308  Cylinder1
0.0455031746032  0.0562222222222222  13.308  Cylinder1
0.088888888888889 0.0611746031746    13.308  Cylinder1
0.132274603175   0.0661428571429    13.308  Cylinder2
0.186507936508   0.072333333333333  13.308  DU40_A17
0.251587301587   0.0738412698413    11.48   DU35_A17
0.3166666666667  0.0707619047619    10.162  DU35_A17
0.381746031746   0.0674444444444    9.011   DU30_A17
0.446825396825   0.0636031746032    7.795   DU25_A17
0.511904761905   0.0594920634921    6.544   DU25_A17
0.576984126984   0.0555873015873    5.361   DU21_A17
0.642063492063   0.0516825396825    4.188   DU21_A17
0.707142857143   0.047777777777778  3.125   NACA64_A17
0.7722222222222  0.043873015873     2.319   NACA64_A17
0.837301587302   0.0399682539683    1.526   NACA64_A17
0.891534920635   0.0367142857143    0.863   NACA64_A17
0.934920634921   0.033111111111111  0.37    NACA64_A17
0.978306349206   0.0225238095238    0.106   NACA64_A17
1.001             0.00001             0.106   NACA64_A17  ! dbg used to be
as at .978

```

```

read_airfoil
file C:\3dfloat\airfoils\Cylinder1.dat  afname  Cylinder1  thick .059
read_airfoil
file C:\3dfloat\airfoils\Cylinder2.dat  afname  Cylinder2  thick .059
read_airfoil
file C:\3dfloat\airfoils\DU40_A17.dat   afname  DU40_A17   thick .059
read_airfoil

```

```

file C:\3dfloat\airfoils\DU35_A17.dat  afname  DU35_A17  thick .059
read_airfoil
file C:\3dfloat\airfoils\DU30_A17.dat  afname  DU30_A17  thick .059
read airfoil
file C:\3dfloat\airfoils\DU25_A17.dat  afname  DU25_A17  thick .059
read_airfoil
file C:\3dfloat\airfoils\DU21_A17.dat  afname  DU21_A17  thick .059
read_airfoil
file C:\3dfloat\airfoils\NACA64_A17.dat afname  NACA64_A17  thick .059

! BLADE GEOMETRY
! -----
-----

! blade 1

! blade_1_root - body coordinate system that does not pitch
new_body name blade_1_root parent hub reftype refnode xfind -1.912 0. 0.
rotorder 321 rotation 0. -2.5 0. axes normal

! blade_1_pitching - this body has coordinate system that pitches
new_body name blade_1_pitching parent blade_1_root reftype refnode
xfind 0. 0. 0. rotorder 321 rotation 0. 0. 0. axes normal ! pitch (z axis)

! from blade root to hub CG
new_elements_beam1 nelelem 3 material massless2 connect_mode connect_2
x1 0. 0. 1.5 dcyll1 2.0 tcyl1 1. pointmass 17206.961
x2 0. 0. 0.0 dcyll2 2.0 tcyl2 1. btype beam

! from blade tip to root
new_elements_beam1 nelelem 17 material massless1 connect_mode connect_2
x1 0. 0. 63.0 dcyll1 1. tcyl1 .45
x2 0. 0. 1.5 dcyll2 3. tcyl2 .45 btype beam
blname nrel5mw scale_mass 1.057486996 frac_stiff 1.

! blade 2

! blade_2_root - body coordinate system that does not pitch
new_body name blade_2_root parent hub reftype refnode xfind -1.912 0. 0.
rotorder 321 rotation 120. -2.5 0. axes normal

! blade_2_pitching - this body has coordinate system that pitches
new_body name blade_2_pitching parent blade_2_root reftype refnode
xfind 0. 0. 0. rotorder 321 rotation 0. 0. 0. axes normal ! pitch (z axis)

! from blade root to hub CG
new_elements_beam1 nelelem 3 material massless2 connect_mode connect_2
x1 0. 0. 1.5 dcyll1 2.0 tcyl1 1. pointmass 17206.961
x2 0. 0. 0.0 dcyll2 2.0 tcyl2 1. btype beam

! from blade tip to root
new_elements_beam1 nelelem 17 material massless1 connect_mode connect_2
x1 0. 0. 63.0 dcyll1 1. tcyl1 .45
x2 0. 0. 1.5 dcyll2 3. tcyl2 .45 btype beam
blname nrel5mw scale_mass 1.057486996 frac_stiff 1.

!copy_elements

```

```

!from_body: blade_1_pitching
!to_body:   blade_2_pitching

print_b1_elements
e34.txt
34 34
1 12
1 12

print_b1_elements
e54.txt
54 54
1 12
1 12

! blade 3

! blade_3_root - body coordinate system that does not pitch
new_body name blade_3_root parent hub reftype refnode xfind -1.912 0. 0.
rotorder 321 rotation -120. -2.5 0. axes normal

! blade_3_pitching - this body has coordinate system that pitches
new_body name blade_3_pitching parent blade_3_root reftype refnode
xfind 0. 0. 0. rotorder 321 rotation 0. 0. 0. axes normal ! pitch (z axis)

! from blade root to hub CG
new_elements_beam1 nelelem 3 material massless2 connect_mode connect_2
x1 0. 0. 1.5 dcyll1 2.0 tcyl1 1. pointmass 17206.961
x2 0. 0. 0.0 dcyll2 2.0 tcyl2 1. btype beam

! from blade tip to root
new_elements_beam1 nelelem 17 material massless1 connect_mode connect_2
x1 0. 0. 63.0 dcyll1 1. tcyl1 .45
x2 0. 0. 1.5 dcyll2 3. tcyl2 .45 btype beam
blname nrel5mw scale_mass 1.057486996 frac_stiff 1.

!copy_elements
!from_body: blade_1_pitching
!to_body:   blade_3_pitching

! -----
! ROTOR WAKE MODEL AND PITCH CONTROL NODES
! -----

rotor_wake
name: rotor_1
shaft_element_body: mainbearing
shaft_element_position: -1.4 0. 0. ! expressed in body mainbearing
system
rotating_node: 1
induction: all
logfile: rotor_1.txt
nblades: 3
bladenames: blade_1_pitching
blade_2_pitching
blade_3_pitching

pitch_control_name: 5mw_floating
pitch_actuator_bodies: blade_1_pitching

```

```

blade_2_pitching
blade_3_pitching
pitch_actuator_positons: 0. 0. 0.75
                           0. 0. 0.75
                           0. 0. 0.75

! -----
! CONTROL SYSTEM PART 1: Define the generator specification
! -----
generator name: nrel5mwfloating gen_eta: 1.
scale_omega: 1.26710903694 scale_mgen: 4180074.35
omega:          mgen:          ! [rad/s] [Nm]
0.570826146749 0.0            ! constant torque above and below this
0.742097666716 0.450259926989
0.824734617833 0.556121407034
0.90737156895  0.673149455494
0.990008520067 0.801344072373
1.0             1.0
omega_eta:      eta:
0.15  0.85
0.97  0.944

! -----
! CONTROL SYSTEM PART 2: Define the pitch control specification
! -----
pitchcontrol
control_type:  iea_oc3_floating
name:          5mw_floating
scale_omega:   1.
scale_vaxial:  1.
scale_pitchcoll: -1.0
omeganom:      1.2671
ti:            10.
gain:          1.
pitchref:      0.
aux: 1. 2. 3. 4. 5. 6. 7. 8. 9. 10.

! -----
! APPLY BOUNDARY CONDITIONS
! -----

! Apply gravity to point masses for nacelle/hub system
!
apply_nodal_bc find -7.9377E-01 0.0000E+00 8.9632E+01 apply_force 0. 0. -
1176780.0 0. 0. 0. ! nacelle 120 t
apply_nodal_bc find 4.5938E+00 0.0000E+00 8.9161E+01 apply_force 0. 0. -
1176780.0 0. 0. 0. ! nacelle 120 t
apply_nodal_bc find -5.0000E+00 0.0000E+00 90.0          apply_force 0. 0. -
556821.59 0. 0. 0. ! hub (on shaft and at eccentricities)

```



```

! Soil stiffness at mudline. Coupled springs model from IEA OC3
!
add_node_stiffness find 0. 0. -20.
f_lin 0. 0. 0. 0. 0. 0.
x_lin 0. 0. -20. 0. 0. 0.
1 1 2.57481E+09
2 2 2.57481E+09
4 4 2.62912E+11
5 5 2.62912E+11
1 5 -2.25325E+10
5 1 -2.25325E+10
2 4 2.25325E+10
4 2 2.25325E+10

add_node_damping find 0. 0. -20.
1 1 0.01
2 2 0.01
4 4 934000000.0
5 5 934000000.0

!Insert node dampinge here:

! NGI Springs replaces command above

!springs                ! Define a set of springs
  name: oc3_monopile    ! Name of this set of springs.
  type: linear_yield    ! Algorithm : model4_2_1 (NGI)
  stiffness_maxforce:  ! List of springs, terminated by blank line
  1000.e6 50.e6        ! Stiffness and max (yield) force (Nm)
  1000.e6 100.e6

!add_node_stiffness
  find: 0. 0. 0.      ! Add the stiffness to this node
  f_lin: 0. 0. 0. 0. 0. 0. ! Add this steady generalized force to
the node
  x_lin: 0. 0. 0. 0. 0. 0. ! node initial reference
position/orientation
  springs_name: oc3_monopile ! refers to name in springs input
  idof_springs: 4           ! apply spring force along this DOF
  logfile: metmast1_dof4.txt ! optional logfile for force added to
the node

! -----
! CLAMP TOWER BOTTOM NODE FOR DOF 3&6
! -----

apply_nodal_bc find 0. 0. -20. apply_displ idofs 3 idofe 3 displ 0.
apply_nodal_bc find 0. 0. -20. apply_displ idofs 6 idofe 6 displ 0.

! To implement linear 'py-curves', extend the tower below ground
level/mudline, and apply linear stiffness instead of fixing the
displacement, see
! help for 'add_node_stiffness' command
!

```

```

! -----
! -----
! TOWER SHADOWING
! -----
! -----

tower_shadow type: potential
xfind: 0.    0.   10.    dcyl: 6. cdn: 1.0    ! node in tower, diameter,
drag
xfind: 0.    0.   87.6    dcyl: 3.87 cdn: 1.0    ! if linear all the way,
two nodes are enough

! -----
! -----
! APPLY MONITORS TO SENSOR SELECTED OUTPUT
! -----
! -----

! sensor 18 to 23 platform displacements swl
!
monitor_element_b1 type orientation file turb1_swl.txt nmonitor 1    find
0.0 0.0 0.5  node 1 body_name inertial
label PtfmSurge PtfmSway PtfmHeave Ptfm_xx Ptfm_xy Ptfm_xz Ptfm_yx

! sensor 48 to 50 blade 1 tip deflection
!
monitor_element_b1 type forces file UC1DU1_forces.txt nmonitor 1    find -
7.21687836487 12.5 10.0  node 2 body_name inertial
label UC1DU1Fx UC1DU1Fy UC1DU1Fz s4 s5 s6

! sensor 39 to 41 tower base forces
!
monitor_element_b1 type forces file TwrBs_forces_z.txt nmonitor 1    find
0.0 0.0 2.5  node 1 body_name tower
label s1 s2 s3 TwrBsFxt TwrBsFyt TwrBsFzt to 100    !'to' set by saa

! sensor 42 to 44 tower base moments
!
monitor_element_b1 type moments file TwrBs_moments.txt nmonitor 1    find
0.0 0.0 2.5  node 1 body_name tower
label s1 s2 s3 TwrBsMxt TwrBsMyt TwrBsMzt to 100    !'to' set by saa

! sensor 15 to 17 blade 1 tip deflection
!
monitor_element_b1 type orientation file tower_topx.txt nmonitor 1    find
0.0000E+00 0.0000E+00 8.6900E+01 node 2    body_name tower
label TTDspFA TTDspSS s3 s4 s5 s6 TTDsp_yx

! sensor 5 Wave elevation
!
monitor_element_b1 find 0. 0. 18. nmonitor 1    node 1 type
waveheight_origin

```

```

file waves_origin.txt label WaveElev

! sensor 11 to 12 blade 1 tip deflection
!
monitor_element_b1 find 0. 0. 63. nmonitor 1 node 1 type orientation
file blade_1_tipx.txt body_name blade_1_root label OoPDefl1 IPDefl1

! Elastic twist of blade tip
!
monitor_element_b1 find 0. 0. 63. nmonitor 1 node 1 type orientation
file blade_1_tiptwist.txt body_name blade_1_pitching label s1 s2 s3 s4 s5
s6 Twst_yx

! Actual pitch angle measured at blade root
!
monitor_element_b1 find 0. 0. 1.5 nmonitor 1 node 1 type orientation
file blade_1_pitch.txt body_name blade_1_root label s1 s2 s3 s4 s5 s6
Pitch_yx

! sensor 24 to 26 blade 1 forces at 0% span (1.5 m)
!

monitor_element_b1 find 0. 0. 1.25 nmonitor 1 node 1 type forces ! dbg
file blade_1_root_force_hub_n1.txt body_name blade_1_root label s1 s2 s3
RootFxc1 RootFyc1 RootFzc1

monitor_element_b1 find 0. 0. 1.25 nmonitor 1 node 1 type moments !
dbg
file blade_1_root_moment_hub_n1.txt body_name blade_1_root label s1 s2 s3
RootMxc1 RootMyx1 RootMzc1

! sensor 27 to 29 blade 1 moments at 0% span (1.5 m)
!
monitor_element_b1 find 0. 0. 3.305 nmonitor 1 node 2 type moments !
dbg
file blade_1_root_moment.txt body_name blade_1_root label blade_mx
blade_my blade_mz ! elem system

! sensor 30 to 32 low speed shaft moments TAN May 20, 2013
!
monitor_element_b1 find 1.162 0. 0. nmonitor 1 node 2 type moments !
dbg
file lsshft_torque.txt body_name hub label s1 s2 s3 RotTorq

monitor_element_b1 find 1.662 0. 0. nmonitor 1 node 2 type moments !
dbg
file lsshft_bend.txt body_name hub label s1 s2 s3 s4 LSSGagMya LSSGagMza

! sensor 33 to 35 tower top forces
!
!TAN 20/5-2013 Express in system following tower top

monitor_element_b1 find 0. 0. 0. nmonitor 1 node 1 type forces
file tower_top_force.txt body_name yawdrive label s1 s2 s3 YawBrFxp
YawBrFyp YawBrFzp

```

```

! sensor 36 to 38 tower top forces
!
!TAN 20/5-2013 Express in system following tower top

monitor_element_b1 find 0. 0. 0. nmonitor 1 node 1 type moments
file tower_top_moment.txt body_name yawdrive label s1 s2 s3 YawBrMxp
YawBrMyp YawBrMzp

monitor_element_b1 type wind_fixed find 0. 0. 90. nmonitor 1 node 2
file wind.txt body_name inertial label WindVxi WindVyi WindVzi

! Mudline forces and moments
!
monitor_element_b1 type forces file mudline_forces.txt nmonitor 1 find
0.0 0.0 -17. node 1 body_name inertial
label s1 s2 s3 fx_mud fy_mud fz_mud

monitor_element_b1 type moments file mudline_moments.txt nmonitor 1 find
0.0 0.0 -17. node 1 body_name inertial
label s1 s2 s3 mx_mud my_mud mz_mud

!
monitor_element_b1 type orientation file turb1_mud.txt nmonitor 1 find
0.0 0.0 -20. node 1 body_name inertial
label surge_mud sway_mud heave_mud mud_xx mud_xy mud_xz mud_yx

monitor_element_b1 find 0. 0. -20. nmonitor 1 node 1 type gather
file IFE_3Dfloat_sensors.txt label oc4_gather toffset 1.
sensors:
nfact: 1 source: WindVxi scale: 1. unit: [m/s] ! header
as source label
nfact: 1 source: WindVyi scale: 1. unit: [m/s] !
nfact: 1 source: WindVzi scale: 1. unit: [m/s] !
nfact: 1 source: WaveElev scale: 1. unit: [m] !
nfact: 1 source: GenPwr_1 scale: .000944 unit: [kW] header:
GenPwr
nfact: 1 source: GenTq_1 scale: 1.030927835e-5 unit: [kNm] !
1./97.e3 header: GenTq
nfact: 1 source: Azimuth_1 scale: 57.295779513082323 unit: [deg]
header: Azimuth ! 180./rpi
nfact: 1 source: RotSpeed_1 scale: 9.549296585513721 unit: [rpm]
header: RotSpeed ! 30./pi
nfact: 1 source: RotSpeed_1 scale: 926.2817687948309 unit: [rpm]
header: GenSpeed ! 30.*97./rpi
nfact: 1 source: PtfmSurge scale: 1. unit: [m] !
nfact: 1 source: PtfmSway scale: 1. unit: [m] !
nfact: 1 source: PtfmHeave scale: 1. unit: [m] !
nfact: 1 source: OoPDefl1 scale: 1. unit: [m] !
nfact: 1 source: IPDefl1 scale: 1. unit: [m] !
nfact: 1 source: Twst_yx scale: -57.295779513082323 unit: [deg]
header: TwstDefl1
nfact: 1 source: BldPitch1_1 scale: -57.295779513082323 unit: [deg]
header: BldPitch1 !
nfact: 1 source: TTDspFA scale: 1. unit: [m] !
nfact: 1 source: TTDspSS scale: 1. unit: [m] !

```

```

nfact: 1 source: TTDsp_yx      scale: 57.295779513082323  unit: [deg]
header: TTDspTwst
nfact: 1 source: RootFxc1     scale: .001                unit: [kN]
nfact: 1 source: RootFyc1     scale: .001                unit: [kN]
nfact: 1 source: RootFzc1     scale: -.001               unit: [kN]
nfact: 1 source: RootMxc1     scale: -.001               unit: [kNm]
nfact: 1 source: RootMyc1     scale: -.001               unit: [kNm]
nfact: 1 source: RootMzc1     scale: -.001               unit: [kNm] !
nfact: 1 source: RotTorq      scale: -.001               unit: [kNm] !
nfact: 1 source: blade_mx     scale: -.001               unit: [kNm] !
nfact: 1 source: blade_my     scale: -.001               unit: [kNm] !
nfact: 1 source: blade_mz     scale: -.001               unit: [kNm] !
nfact: 1 source: LSSGagMya    scale: .001                unit: [kNm] !
nfact: 1 source: LSSGagMza    scale: .001                unit: [kNm] !
nfact: 1 source: YawBrFxp     scale: -.001               unit: [kN]  ! Nacelle
coord.syst.
nfact: 1 source: YawBrFyp     scale: -.001               unit: [kN]  !
nfact: 1 source: YawBrFzp     scale: .001                unit: [kN]  !
nfact: 1 source: YawBrMxp     scale: .001                unit: [kNm] !
nfact: 1 source: YawBrMyp     scale: .001                unit: [kNm] !
nfact: 1 source: YawBrMzp     scale: .001                unit: [kNm] !
nfact: 1 source: TwrBsFxt     scale: -.001               unit: [kN]  ! Tower
base coord.sys.
nfact: 1 source: TwrBsFyt     scale: -.001               unit: [kN]  !
nfact: 1 source: TwrBsFzt     scale: .001                unit: [kN]  !
nfact: 1 source: TwrBsMxt     scale: .001                unit: [kNm] !
nfact: 1 source: TwrBsMyt     scale: .001                unit: [kNm] !
nfact: 1 source: TwrBsMzt     scale: .001                unit: [kNm] !
nfact: 1 source: fx_mud       scale: -.001               unit: [kN]  !
nfact: 1 source: fy_mud       scale: -.001               unit: [kN]  !
nfact: 1 source: fz_mud       scale: .001                unit: [kN]  !
nfact: 1 source: mx_mud       scale: .001                unit: [kNm] !
nfact: 1 source: my_mud       scale: .001                unit: [kNm] !
nfact: 1 source: mz_mud       scale: .001                unit: [kNm] !

```

```

! -----
! SET UP WIND INCLUDING TURBULENCE
! -----

```

```

! Wind settings ! TAN LC 6, Table 1 "Effects of soil stiffness scaling ..
!
wind_transient
0.      0.01    0.
100.    12.0    0.    !old value:    ! TAN

```

```

turbulence_box      turbulence   file      turbulence_info
c:\3dfloat\turbulence\turbulence_case_6_9320_u.txt
turb_tstart: 100.  turb_intens: 0.146      reference_node:  0. 0. 0.
reference_height    90.
turbulence_scaling target_turbulence_intensity

```

```

! -----
! RUN DESIRED SOLUTION SETTINGS
! -----

```

```

! Take one step to assemble all matrices
! -----
monitor element_b1 type plot nmonitor 100
file turb1.plot

!set material damping
damping type ratio2rayl ratio_1 0.51 ratio_2 0.51 omega_1 0.1 omega_2
1.

! set solver settings
newmark dt: 0.01 nassemble: 1 nnewton: 50 nsubmin: 2 rwilson: 0.9
relax: 0.0 resid_newton: 1e-8 nmonitor: 10

!-----
!EIGEN ANALYSIS
!-----
! eigen frequency analysis
! short step to assemble matrices and apply added mass

!newmark dt 0.000000001 nassemble 1 nnewton: 1 nsubmin: 0 rwilson: 0.9
relax: 0.0 resid_newton: 0.00000001 nmonitor: 1

!step nstep 1 method new_gen_alpha

!eigen_analysis amplitude 20. nfreq 20 filename plotall

!end
!-----

!take one step
step nstep 1 method step9

! time = 0.01sec

step nstep 499 method step9

! time = 5.00sec

damping type ratio2rayl ratio_1 0.00 ratio_2 0.01 omega_1 0.0 omega_2
1.57

step nstep 178500 method step9

!time 1790s

! Tecplot

monitor_element_b1 type tecplot file turb1.dat nmonitor 20

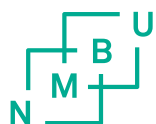
step nstep 1000 method step9

!time 1800s, 30min

print_solution
solution.txt

END

```

Norges miljø- og biovitenskapelig universitet
Noregs miljø- og biovitenskapelige universitet
Norwegian University of Life Sciences

Postboks 5003
NO-1432 Ås
Norway